

## Supporting Information

### **Modulating the photolysis of aryl azides in supramolecular host to develop photoactivatable fluorophores**

Xujun Qiu,<sup>1‡</sup> Eric Pohl,<sup>2‡</sup> André Jung,<sup>3</sup> Qianyu Cai,<sup>1</sup> Haopu Su,<sup>1</sup> Olaf Fuhr,<sup>4,5</sup> Ute Schepers,<sup>1,2\*</sup> and Stefan Bräse<sup>1,3\*</sup>

<sup>1</sup>Institute of Organic Chemistry (IOC), Karlsruhe Institute of Technology (KIT), Kaiserstrasse 12, 76131 Karlsruhe, Germany.

<sup>2</sup>Institute of Functional Interfaces (IFG), Karlsruhe Institute of Technology (KIT), Kaiserstrasse 12, 76131 Karlsruhe, Germany.

<sup>3</sup>Institute of Biological and Chemical Systems – Functional Molecular Systems (IBCS-FMS), Karlsruhe Institute of Technology (KIT), Kaiserstrasse 12, 76131 Karlsruhe, Germany.

<sup>4</sup>Institute of Nanotechnology (INT), Karlsruhe Institute of Technology (KIT), Kaiserstrasse 12, 76131 Karlsruhe, Germany.

<sup>5</sup>Karlsruhe Nano Micro Facility (KNMF), Karlsruhe Institute of Technology (KIT), Kaiserstrasse 12, 76131 Karlsruhe, Germany.

\*Corresponding Authors: Stefan Bräse, E-mail: [braese@kit.edu](mailto:braese@kit.edu). Ute Schepers, E-mail: [ute.schepers@kit.edu](mailto:ute.schepers@kit.edu)

## Table of Contents

Table of Contents .....	2
General Remarks .....	2
Experimental Procedures .....	6
Supplementary Data and Characterization .....	12
Additional Data and Characterization .....	55
References .....	64

## General Remarks

### Materials and Methods

The starting materials, solvents, and reagents were purchased from ABCR, ACROS, ALFA AESAR, APOLLO SCIENTIFIC, CARBOLUTION, CHEMPUR, FLUKA, FLUOROCHEM, MERCK, RIEDEL-DE HAËN, SIGMA ALDRICH, STREM, TCI, or THERMO FISHER SCIENTIFIC and used without further purification unless stated otherwise. Solvents of technical quality were purified by distillation or with the solvent purification system MB SPS5 (acetonitrile, dichloromethane, diethyl ether, tetrahydrofuran, toluene) from MBRAUN. Solvents of p.a. quality were purchased from ACROS, FISHER SCIENTIFIC, SIGMA ALDRICH, Roth, or RIEDEL-DE HAËN and were used without further purification.

Solvents were evaporated under reduced pressure at 45 °C using a rotary evaporator. For solvent mixtures, each solvent was measured volumetrically.

Flash column chromatography was performed using MERCK silica 60 (0.040 × 0.063 mm, 230–400 mesh ASTM) and quartz sand (glowed and purified with hydrochloric acid).

### Reaction Monitoring

All reactions were monitored by thin-layer chromatography (TLC) using silica-coated aluminum plates (MERCK, silica 60, F254). UV active compounds were detected with a UV-lamp at 254 nm and 366 nm excitation.

GC-MS (gas chromatography-mass spectrometry) measurements were performed on an AGILENT TECHNOLOGIES model 6890N (electron impact ionization), equipped with an AGILENT 19091S-433 column (5% phenyl methyl siloxane, 30 m, 0.25 µm) and a 5975B VL MSD detector with a turbopump. Helium was used as a carrier gas.

### Liquid Chromatography – Mass Spectrometry (LC-MS)

Liquid Chromatography – Mass Spectrometry (LC–MS) was performed using a THERMOFISHER UltiMate 3000 system containing a degasser, pump, autosampler, column compartment and diode array detector coupled with an ISQTM EM Single Quadrupole Mass Spectrometer system with ESI-source. The flow rate was 0.45 mL/min on a stationary KINETEX XB-C18 column (2.1 mm × 100 mm, 2.6 μm particle size).

#### **Preparative Reversed Phase High Performance Liquid Chromatography (RP-HPLC)**

Preparative Reversed Phase High Performance Liquid Chromatography (RP-HPLC) was performed on the Puriflash™ 4125 system from INTERCHIM. A VDSpher® C18-M-SE precolumn (10 μm, 40 x 16 mm) followed by a VDSpher® C18-M-SE separation column (10 μm, 250 x 20 mm, VDS OPTILAB) was used as the stationary phase. A linear gradient of acetonitrile and double distilled water, both supplemented with 0.1% trifluoroacetic acid (TFA), at a flow rate of 15 mL/min served as the mobile phase.

#### **Nuclear Magnetic Resonance Spectroscopy (NMR)**

NMR spectra were recorded on a BRUKER Avance 500 NMR instrument at 500 MHz for <sup>1</sup>H NMR, 126 MHz for <sup>13</sup>C NMR, and 470 MHz for <sup>19</sup>F NMR.

The NMR spectra were recorded at room temperature in deuterated solvents acquired from EURISOTOP, SIGMA ALDRICH, or DEUTERO.

#### **Infrared Spectroscopy (IR)**

The infrared spectra were recorded with a BRUKER, Alpha P instrument. All samples were measured by attenuated total reflection (ATR). The positions of the absorption bands are given in wavenumbers  $\tilde{\nu}$  in  $\text{cm}^{-1}$  and were measured in the range from  $3600 \text{ cm}^{-1}$  to  $500 \text{ cm}^{-1}$ .

Characterization of the absorption bands was done in dependence of the absorption strength with the following abbreviations: vs (very strong, 0–9%), s (strong, 10–39%), m (medium, 40–69%), w (weak, 70–89%), vw (very weak, 90–100%).

#### **Mass Spectrometry (MS)**

ESI (electro spray ionization) experiments were recorded on a Q-Exactive (Orbitrap) mass spectrometer (THERMO FISHER SCIENTIFIC, San Jose, CA, USA) equipped with a HESI II probe to record high resolution. The tolerated error is  $\pm 5$  ppm of the molecular mass. The spectra were interpreted by molecular peaks  $[\text{M}]^+$ , peaks of protonated molecules  $[\text{M}+\text{H}]^+$  and characteristic fragment peaks and indicated with their mass-to-charge ratio ( $m/z$ ).

MALDI-ToF-MS (Matrix Assisted Laser Desorption Ionization Time of Flight Mass Spectrometry) was recorded on an Axima Confidence spectrometer (model: TO-6071R00) equipped with Shimadzu Biotech Launchpad™ software (version 2.9.3.20110624) from Shimadzu Biotech. A wavelength  $\lambda = 337 \text{ nm}$  nitrogen laser was used to desorb and ionize the samples. The target was a 384-spot Shimadzu Kratos Analytical Standard sample plate

(DE1580TA) from Shimadzu Biotech. Samples to be analyzed were applied directly to the target or dissolved in a mixture of acetonitrile and double-distilled water. A saturated 1:1 mixture of 2,5-dihydroxybenzoic acid and  $\alpha$ -cyano-4-hydroxycinnamic acid (Universal MALDI Matrix, Sigma-Aldrich®) dissolved in a 1:1 mixture of acetonitrile and double-distilled water served as the matrix. Co-crystallization of the matrix and sample was carried out in room air. For measurement, the sample was fired approximately 100 times at a frequency of 50 Hz, and the results were averaged. The protonated molecular ion peak  $[M+H]^+$ , as well as the pseudomolecular ion peaks with sodium  $[M+Na]^+$  and potassium  $[M+K]^+$ , if present, were reported.

### Absorption Spectroscopy

UV/Vis spectra were recorded on an Agilent Cary 100 Bio Varian UV/vis spectrometer.

### Photoreaction

Photoreaction was carried out under the irradiation of 405 nm LEDs (M405L4 - 405 nm, 1000 mW (Min) Mounted LED, 1000 mA, THORLABS) with stirring. The samples were positioned in the center of an aluminum block (10 cm  $\times$  5 cm  $\times$  10 cm) with stirring underneath. The LED was mounted on top of the aluminum block, with the samples placed directly below the LED at a distance of 5 cm.

### Photoluminescence Measurements in Water

Emission spectra were recorded either on a Horiba Duetta™ fluorescence spectrometer equipped with a 75 W xenon arc lamp or on a JASCO FP-8300 fluorescence spectrometer equipped with a 450 W xenon arc lamp. Absolute fluorescence quantum yields were measured at a Quantaaurus QY C11347 from Hamamatsu.

### Crystallographic Information

Single crystals of  $C_{24}H_{22}ClN_5O_2$  (**Az-1** $\bullet$ 2H<sub>2</sub>O) and  $C_{24}H_{25}ClN_5O_{2.5}$  (**AZ-2** $\bullet$ 2.5H<sub>2</sub>O) were obtained by slowly evaporating of aqueous solution of **Az-1** and **Az-2**. A suitable crystal was selected and studied on a Stoe StadiVari diffractometer with Dectris Eiger 4M detector at 180 K using Ga-K $\alpha$  radiation ( $\lambda = 1.34143 \text{ \AA}$ ) generated by a Excilium Metal-Jet D2 X-ray source. Using Olex2<sup>[1]</sup> the structure was solved with the ShelXT<sup>[2]</sup> structure solution program using Intrinsic Phasing and refined with the ShelXL<sup>[3]</sup> refinement package using Least Squares minimization. Refinement was performed with anisotropic temperature factors for all non-hydrogen atoms; hydrogen atoms were calculated on idealized positions. Crystallographic data and structure refinement details are summarized in table S1 and S2.

Crystallographic data for compound **Az-1** $\bullet$ 2H<sub>2</sub>O and **AZ-2** $\bullet$ 2.5H<sub>2</sub>O reported in this paper have been deposited with the Cambridge Crystallographic Data Centre as supplementary information with deposition numbers CCDC-2351099 and 2351100.

### Density Functional Theory (DFT) calculation

Quantum chemical calculations were performed using Density Functional Theory DFT within Gaussian 16<sup>[4]</sup>. The ground state was optimized at the PBE0<sup>[5]</sup> / 6-31+G(d,p)<sup>[6]</sup> level of theory. The excited state calculations were performed using Time-Dependent DFT (TD-DFT) at the same level of theory. Solvent effects of water were included utilizing the polarizable continuum model (PCM).

All computations were managed by the Silico software suite<sup>[7]</sup>, which incorporates a number of open source libraries, including cclib<sup>[8]</sup> for file parsing and Openbabel / pybel<sup>[9,10]</sup> for file conversion. 3D density plots were rendered using VMD 1.9.3<sup>[11]</sup> and tachyon<sup>[12]</sup>. Emission spectra were simulated with the MultiWfm software package<sup>[13]</sup>.

### **Cytotoxicity test**

100  $\mu$ l of a  $1 \times 10^5$  Cells/mL HeLa suspension were seeded into each well of a 96-Well-Plate and incubated overnight (37°C, 5% CO<sub>2</sub>). Following the incubation cell media was removed and the cells were treated with different concentrations (50  $\mu$ M, 5  $\mu$ M and 0,5  $\mu$ M) of the **Az-1, Az-2, Az-3, Cb-1, Cb-2, Cb-3** and their complex with CB7 for a duration of 24 h. After 24 h exposure 10  $\mu$ L MTT was added to each well and incubated for 3 h at 37 °C and 5 % CO<sub>2</sub>. The reaction was stopped by addition of 100  $\mu$ L of stop solution (Promega). Following 24 h of incubation, the absorption of the formazan was observed at 595 nm using the Spectramax3000 plate reader.

### **Cell imaging**

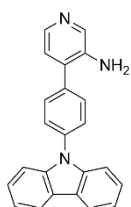
200  $\mu$ L of a  $10 \times 10^4$  cells/mL HeLa solution were added per well of an 8-well ibidi® slide and incubated overnight (37 °C, 5% CO<sub>2</sub>). Following incubation, the cells were treated with 125 nM MitoTracker™Red for 30 min. Afterwards the cells were washed with DPBS -/- followed by the addition of 5  $\mu$ M **Az-1, Az-2, Az-3, Cb-1, Cb-2, Cb-3** and their complex with CB7. The cells were incubated for 3 h at 37 °C and 5 % CO<sub>2</sub>. After incubation the cells were washed with DPBS -/- and fresh media was added. Microscopy was performed using the confocal fluorescence microscope Leica Stellaris 5.0 using the following excitation wavelengths: for **Az-1, Az-2, Az-3, Cb-1, Cb-2, Cb-3** and their complex with CB7 405 nm, for MitoTracker™ Red: 560 nm).

## Experimental Procedures

General procedure for Suzuki coupling:

To a 50 mL reaction vial, (3.00 mmol, 1.00 equiv.) boronic acid derivatives, (0.623 g, 3.60 mmol, 1.20 equiv.) 4-bromopyridin-3-amine, (0.173 g, 0.150 mmol, 0.05 equiv.) tetrakis(triphenylphosphine)palladium(0), and (0.955 g, 4.50 mmol, 1.50 equiv.) tripotassium phosphate were dissolved in the 1,4-dioxane (20 mL) and water (5 mL) mixture. After degassing and charging with inert gas, the reaction mixtures were reacting at 105 °C for 16 hours. After cooling down, the reaction mixture was suspended in a mixture of 1.5 N aqueous solution of NaOH (20 mL) and CH<sub>2</sub>Cl<sub>2</sub> (30 mL). The aqueous phase was extracted with CH<sub>2</sub>Cl<sub>2</sub> (3 × 30 mL). The combined organic phases were dried over Na<sub>2</sub>SO<sub>4</sub> and evaporated under reduced pressure. After purifying by column chromatography using DCM/MeOH 19:1, the pyridine aniline products were obtained.

### 4-(4-(9H-carbazol-9-yl)phenyl)pyridin-3-amine



Brown viscose (1.11 g, 3.31 mmol, 95%).

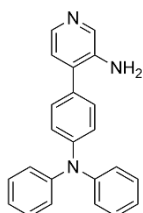
<sup>1</sup>H NMR (500 MHz, CDCl<sub>3</sub>, ppm)  $\delta$  = 8.24 (s, 1H, *H*<sub>Ar</sub>), 8.17 (d, *J* = 7.8 Hz, 2H, *H*<sub>Ar</sub>), 8.14 (d, *J* = 4.9 Hz, 1H, *H*<sub>Ar</sub>), 7.72 (d, *J* = 1.9 Hz, 4H, *H*<sub>Ar</sub>), 7.50 (d, *J* = 8.2 Hz, 2H, *H*<sub>Ar</sub>), 7.48–7.41 (m, 2H, *H*<sub>Ar</sub>), 7.36–7.29 (m, 2H, *H*<sub>Ar</sub>), 7.15 (d, *J* = 4.9 Hz, 1H, *H*<sub>Ar</sub>), 3.94 (s, 2H, NH<sub>2</sub>).

<sup>13</sup>C NMR (126 MHz, CDCl<sub>3</sub>, ppm)  $\delta$  = 140.7 (2C, *C*<sub>Ar</sub>), 140.5 (1C, *C*<sub>Ar</sub>), 139.9 (1C, *C*<sub>Ar</sub>), 138.5 (1C, *C*<sub>Ar</sub>), 137.9 (1C, *C*<sub>Ar</sub>), 136.0 (1C, *C*<sub>Ar</sub>), 132.8 (1C, *C*<sub>Ar</sub>), 130.1 (2C, *C*<sub>Ar</sub>), 127.7 (2C, *C*<sub>Ar</sub>), 126.2 (2C, *C*<sub>Ar</sub>), 124.3 (2C, *C*<sub>Ar</sub>), 123.7 (2C, *C*<sub>Ar</sub>), 120.6 (1C, *C*<sub>Ar</sub>), 120.4 (2C, *C*<sub>Ar</sub>), 109.8 (2C, *C*<sub>Ar</sub>).

ESI-MS for [C<sub>23</sub>H<sub>17</sub>N<sub>3</sub>+H]<sup>+</sup>: Calc. *m/z* = 336.1496, found *m/z* = 336.1487.

IR (ATR,  $\tilde{\nu}$ ) = 3471 (vs), 3443 (vs), 3397 (vs), 3390 (vs), 3370 (vs), 3293 (vs), 3189 (vs), 3055 (vs), 3045 (vs), 3022 (vs), 2998 (vs), 2985 (vs), 2854 (vs), 2812 (vs), 2720 (vs), 2709 (vs), 2681 (vs), 2662 (vs), 2630 (s), 2588 (s), 2578 (s), 1622 (vs), 1607 (vs), 1593 (vs), 1515 (vs), 1494 (s), 1476 (vs), 1449 (vs), 1420 (vs), 1407 (vs), 1328 (s), 1318 (vs), 1227 (vs), 745 (vs), 718 (vs) cm<sup>-1</sup>.

### 4-(4-(diphenylamino)phenyl)pyridin-3-amine



Brown viscose (1.06 g, 3.14 mmol, 91%).

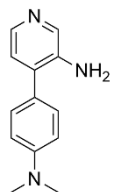
<sup>1</sup>H NMR (500 MHz, CD<sub>3</sub>CN, ppm)  $\delta$  = 8.08 (s, 1H, *H*<sub>Ar</sub>), 7.91 (d, *J* = 4.9 Hz, 1H, *H*<sub>Ar</sub>), 7.38–7.35 (m, 2H, *H*<sub>Ar</sub>), 7.34–7.30 (m, 4H, *H*<sub>Ar</sub>), 7.12–7.07 (m, 8H, *H*<sub>Ar</sub>), 7.00 (d, *J* = 4.9 Hz, 1H, *H*<sub>Ar</sub>), 4.24 (s, 2H, NH<sub>2</sub>).

<sup>13</sup>C NMR (126 MHz, CD<sub>3</sub>CN, ppm)  $\delta$  = 148.6 (1C, *C*<sub>Ar</sub>), 148.5 (2C, *C*<sub>Ar</sub>), 141.8 (1C, *C*<sub>Ar</sub>), 140.1 (1C, *C*<sub>Ar</sub>), 138.9 (1C, *C*<sub>Ar</sub>), 133.2 (1C, *C*<sub>Ar</sub>), 131.8 (1C, *C*<sub>Ar</sub>), 130.5 (4C, *C*<sub>Ar</sub>), 130.2 (2C, *C*<sub>Ar</sub>), 125.5 (4C, *C*<sub>Ar</sub>), 124.7 (1C, *C*<sub>Ar</sub>), 124.4 (2C, *C*<sub>Ar</sub>), 124.2 (2C, *C*<sub>Ar</sub>).

ESI-MS for [C<sub>23</sub>H<sub>19</sub>N<sub>3</sub>+H]<sup>+</sup>: Calc. *m/z* = 338.1652, found *m/z* = 338.1645.

IR (ATR,  $\tilde{\nu}$ ) = 3453 (m), 3446 (m), 3436 (m), 3357 (m), 3313 (s), 3195 (s), 3189 (s), 3182 (s), 3176 (s), 3100 (m), 3085 (m), 3057 (s), 3033 (s), 1610 (m), 1587 (vs), 1513 (vs), 1483 (vs), 1423 (m), 1410 (m), 1325 (s), 1315 (s), 1269 (vs), 1228 (m), 817 (m), 753 (m), 733 (m), 694 (vs), 509 (m)  $\text{cm}^{-1}$ .

#### 4-(4-(dimethylamino)phenyl)pyridin-3-amine



Brown viscose (1.21 g, 5.67 mmol, 98%).

$^1\text{H}$  NMR (500 MHz,  $\text{CDCl}_3$ , ppm)  $\delta$  = 8.12 (s, 1H,  $H_{\text{Ar}}$ ), 8.03 (d,  $J$  = 4.9 Hz, 1H,  $H_{\text{Ar}}$ ), 7.39–7.35 (m, 2H,  $H_{\text{Ar}}$ ), 7.02 (d,  $J$  = 4.9 Hz, 1H,  $H_{\text{Ar}}$ ), 6.83–6.79 (m, 2H,  $H_{\text{Ar}}$ ), 3.81 (s, 2H,  $\text{NH}_2$ ), 3.01 (s, 6H,  $\text{CH}_3$ ).

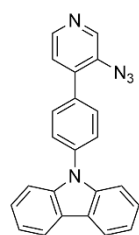
$^{13}\text{C}$  NMR (126 MHz,  $\text{CDCl}_3$ , ppm)  $\delta$  = 150.4 (1C,  $C_{\text{Ar}}$ ), 140.4 (1C,  $C_{\text{Ar}}$ ), 140.1 (1C,  $C_{\text{Ar}}$ ), 138.0 (1C,  $C_{\text{Ar}}$ ), 134.3 (1C,  $C_{\text{Ar}}$ ), 129.3 (2C,  $C_{\text{Ar}}$ ), 124.4 (1C,  $C_{\text{Ar}}$ ), 124.2 (1C,  $C_{\text{Ar}}$ ), 112.7 (2C,  $C_{\text{Ar}}$ ), 40.5 (2C,  $\text{CH}_3$ ).

ESI-MS for  $[\text{C}_{13}\text{H}_{15}\text{N}_3+\text{H}]^+$ : Calc.  $m/z$  = 214.1339, found  $m/z$  = 214.1335.

IR (ATR,  $\tilde{\nu}$ ) = 3415 (vs), 3294 (vs), 3142 (vs), 3060 (vs), 3041 (vs), 2998 (vs), 2982 (vs), 2970 (s), 2947 (s), 2916 (s), 2897 (vs), 2884 (vs), 2857 (s), 2816 (s), 2805 (s), 1610 (vs), 1587 (s), 1520 (vs), 1495 (vs), 1483 (vs), 1448 (vs), 1418 (vs), 1406 (s), 1331 (s), 1319 (vs), 1301 (vs), 809 (vs)  $\text{cm}^{-1}$ .

Aryl azides were synthesized from the method previously used<sup>[14]</sup>.

#### 9-(4-(3-azidopyridin-4-yl)phenyl)-9H-carbazole



*p*-Toluenesulfonic acid monohydrate (0.851 g, 4.47 mmol, 1.50 equiv.) was dissolved in acetonitrile/water (20/5.0 mL) at 25 °C. Once dissolved, tert-butyl nitrite (0.461 g, 4.47 mmol, 1.50 equiv.) was added, followed by 4-(4-(9H-carbazol-9-yl)phenyl)pyridin-3-amine (1.00 g, 2.98 mmol, 1.00 equiv.) portion-wise. The reaction mixture was stirred for 3h at rt. After which, a solution of sodium azide (0.582 g, 8.95 mmol, 3.00 equiv.) in water (5.0 mL) was added dropwise. The resulting reaction mass was stirred for another 3 hours at 25 °C. After the complete conversion was achieved, the reaction mixture was extracted with ethyl acetate (3 × 20 ml). The combined organic layers were dried over sodium sulfate. After the removal of the solvent, the crude solid was purified by chromatography (EtOAc:DCM=2:3) resulting 9-(4-(3-azidopyridin-4-yl)phenyl)-9H-carbazole (0.98 g, 2.71 mmol, 91%) as a yellow solid.

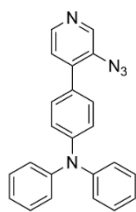
$^1\text{H}$  NMR (500 MHz,  $\text{CDCl}_3$ , ppm)  $\delta$  = 8.66 (s, 1H,  $H_{\text{Ar}}$ ), 8.51 (d,  $J$  = 4.9 Hz, 1H,  $H_{\text{Ar}}$ ), 8.17 (dt,  $J$  = 7.8, 0.9 Hz, 2H,  $H_{\text{Ar}}$ ), 7.78–7.74 (m, 2H,  $H_{\text{Ar}}$ ), 7.72–7.68 (m, 2H,  $H_{\text{Ar}}$ ), 7.51 (d,  $J$  = 8.2 Hz, 2H,  $H_{\text{Ar}}$ ), 7.44 (ddd,  $J$  = 8.3, 7.0, 1.2 Hz, 2H,  $H_{\text{Ar}}$ ), 7.40 (d,  $J$  = 4.9 Hz, 1H,  $H_{\text{Ar}}$ ), 7.32 (td,  $J$  = 7.5, 7.1, 1.0 Hz, 2H,  $H_{\text{Ar}}$ ).

$^{13}\text{C}$  NMR (126 MHz,  $\text{CDCl}_3$ , ppm)  $\delta$  = 146.3 (1C,  $C_{\text{Ar}}$ ), 141.6 (1C,  $C_{\text{Ar}}$ ), 140.7 (2C,  $C_{\text{Ar}}$ ), 139.6 (1C,  $C_{\text{Ar}}$ ), 138.5 (1C,  $C_{\text{Ar}}$ ), 134.3 (1C,  $C_{\text{Ar}}$ ), 134.3 (1C,  $C_{\text{Ar}}$ ), 130.8 (2C,  $C_{\text{Ar}}$ ), 127.0 (2C,  $C_{\text{Ar}}$ ), 126.2 (2C,  $C_{\text{Ar}}$ ), 124.8 (1C,  $C_{\text{Ar}}$ ), 123.7 (2C,  $C_{\text{Ar}}$ ), 120.6 (2C,  $C_{\text{Ar}}$ ), 120.4 (2C,  $C_{\text{Ar}}$ ), 109.9 (2C,  $C_{\text{Ar}}$ ).

ESI-MS for  $[\text{C}_{23}\text{H}_{15}\text{N}_5+\text{H}]^+$ : Calc.  $m/z$  = 362.1327, found  $m/z$  = 362.1322.

IR (ATR,  $\tilde{\nu}$ ) = 3052 (vs), 3046 (vs), 2981 (s), 2128 (vs), 2104 (vs), 1519 (vs), 1489 (s), 1478 (s), 1448 (vs), 1311 (vs), 1300 (vs), 1223 (vs), 742 (vs), 721 (vs)  $\text{cm}^{-1}$ .

#### 4-(3-azidopyridin-4-yl)-N,N-diphenylaniline



p-Toluenesulfonic acid monohydrate (0.846 g, 4.45 mmol, 1.50 equiv.) was dissolved in acetonitrile/water (20/5.0 mL) at 25 °C. Once dissolved, tert-butyl nitrite (0.458 g, 4.45 mmol, 1.50 equiv.) was added, followed by 4-(4-(diphenylamino)phenyl)pyridin-3-amine (1.00 g, 2.96 mmol, 1.00 equiv.) portion-wise. The reaction mixture was stirred for 3h at rt. After which, a solution of sodium azide (0.578 g, 8.89 mmol, 3.00 equiv.) in water (5.0 mL) was added dropwise. The resulting reaction mass was stirred for another 3 hours at 25 °C. After the complete conversion was achieved, the reaction mixture was extracted with ethyl acetate (3 × 20 ml). The combined organic layers were dried over sodium sulfate. After the removal of the solvent, the crude solid was purified by chromatography (EtOAc: DCM=2:3) resulting 4-(3-azidopyridin-4-yl)-N,N-diphenylaniline (0.99 g, 2.72 mmol, 92%) as a yellow solid.

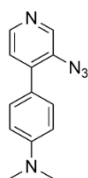
$^1\text{H}$  NMR (500 MHz,  $\text{CDCl}_3$ , ppm)  $\delta$  = 8.55 (s, 1H,  $H_{\text{Ar}}$ ), 8.40 (d,  $J$  = 5.0 Hz, 1H,  $H_{\text{Ar}}$ ), 7.40–7.36 (m, 2H,  $H_{\text{Ar}}$ ), 7.32–7.26 (m, 5H,  $H_{\text{Ar}}$ ), 7.17–7.14 (m, 4H,  $H_{\text{Ar}}$ ), 7.13–7.06 (m, 4H,  $H_{\text{Ar}}$ ).

$^{13}\text{C}$  NMR (126 MHz,  $\text{CDCl}_3$ , ppm)  $\delta$  = 148.7 (1C,  $C_{\text{Ar}}$ ), 147.4 (2C,  $C_{\text{Ar}}$ ), 146.3 (1C,  $C_{\text{Ar}}$ ), 141.7 (1C,  $C_{\text{Ar}}$ ), 140.2 (1C,  $C_{\text{Ar}}$ ), 133.9 (1C,  $C_{\text{Ar}}$ ), 130.0 (2C,  $C_{\text{Ar}}$ ), 129.6 (4C,  $C_{\text{Ar}}$ ), 128.4 (1C,  $C_{\text{Ar}}$ ), 125.3 (4C,  $C_{\text{Ar}}$ ), 124.5 (1C,  $C_{\text{Ar}}$ ), 123.8 (2C,  $C_{\text{Ar}}$ ), 122.1 (2C,  $C_{\text{Ar}}$ ).

ESI-MS for  $[\text{C}_{23}\text{H}_{17}\text{N}_5+\text{H}]^+$ : Calc.  $m/z$  = 364.1557, found  $m/z$  = 364.1552.

IR (ATR,  $\tilde{\nu}$ ) = 3084 (vs), 3052 (vs), 3035 (vs), 2980 (vs), 2106 (vs), 1585 (vs), 1482 (vs), 1266 (vs)  $\text{cm}^{-1}$ .

#### 4-(3-azidopyridin-4-yl)-N,N-dimethylaniline



p-Toluenesulfonic acid monohydrate (1.34 g, 7.03 mmol, 1.50 equiv.) was dissolved in acetonitrile/water (20/5.0 mL) at 25 °C. Once dissolved, tert-butyl nitrite (0.725 g, 7.03 mmol, 1.50 equiv.) was added, followed by 4-(4-(dimethylamino)phenyl)pyridin-3-amine (1.00 g, 4.69 mmol, 1.00 equiv.) portion-wise. The reaction mixture was stirred for 3h at rt. After which, a solution of sodium azide (0.914 g, 14.1 mmol, 3.00 equiv.) in water (5.0 mL) was added dropwise. The resulting reaction mass was stirred for another 3 hours at 25 °C. After the complete conversion was achieved, the reaction mixture was extracted with ethyl acetate (3 × 20 ml). The combined organic layers were dried over sodium sulfate. After the removal of the solvent, the crude solid was purified by chromatography (MeOH: DCM=1:19) resulting 4-(3-azidopyridin-4-yl)-N,N-dimethylaniline (1.06 g, 4.43 mmol, 94%) as a yellow solid.

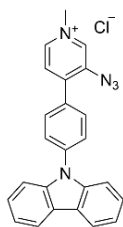
$^1\text{H}$  NMR (500 MHz,  $\text{CDCl}_3$ , ppm)  $\delta$  = 8.52 (s, 1H,  $H_{\text{Ar}}$ ), 8.36 (d,  $J$  = 5.0 Hz, 1H,  $H_{\text{Ar}}$ ), 7.47–7.43 (m, 2H,  $H_{\text{Ar}}$ ), 7.25 (d,  $J$  = 5.0 Hz, 1H,  $H_{\text{Ar}}$ ), 6.80–6.76 (m, 2H,  $H_{\text{Ar}}$ ), 3.02 (s, 6H,  $\text{CH}_3$ ).

$^{13}\text{C}$  NMR (126 MHz,  $\text{CDCl}_3$ , ppm)  $\delta$  = 150.8 (1C,  $C_{\text{Ar}}$ ), 146.2 (1C,  $C_{\text{Ar}}$ ), 141.5 (1C,  $C_{\text{Ar}}$ ), 140.8 (1C,  $C_{\text{Ar}}$ ), 133.7 (2C,  $C_{\text{Ar}}$ ), 130.1 (1C,  $C_{\text{Ar}}$ ), 124.3 (1C,  $C_{\text{Ar}}$ ), 122.7 (1C,  $C_{\text{Ar}}$ ), 111.9 (2C,  $C_{\text{Ar}}$ ), 40.4 (2C,  $\text{CH}_3$ ).

ESI-MS for  $[\text{C}_{13}\text{H}_{13}\text{N}_5+\text{H}]^+$ : Calc.  $m/z$  = 240.1244, found  $m/z$  = 240.1237.

IR (ATR,  $\tilde{\nu}$ ) = 3048 (m), 3033 (s), 2997 (s), 2980 (s), 2971 (s), 2945 (s), 2941 (s), 2909 (s), 2890 (s), 2864 (s), 2817 (s), 2126 (vs), 2097 (vs), 2076 (vs), 1610 (s), 1584 (s), 1527 (s), 1483 (s), 1446 (s), 1410 (s), 1363 (s), 1300 (vs), 1288 (vs), 1261 (s), 808 (m)  $\text{cm}^{-1}$ .

#### 4-(4-(9H-carbazol-9-yl)phenyl)-3-azido-1-methylpyridin-1-ium chloride (AZ-1)



9-(4-(3-azidopyridin-4-yl)phenyl)-9H-carbazole (0.20 g, 0.553 mmol, 1.00 equiv.) was dissolved in acetonitrile (10 mL), and methyl iodide (0.118 g, 0.830 mmol, 1.50 equiv.) was added dropwise at room temperature with stirring. The resulting reaction mixture was left overnight at 40 °C. The precipitation was collected by filtration and washed with acetonitrile. After dissolving in 10 mL water, (0.451 g, 2.77 mmol, 5.00 equiv.) ammonium hexafluorophosphate was added, which resulted in a precipitate. The precipitate was collected by filtration and washed with water, and dried. After dissolving the solid in 10 mL acetonitrile, (0.769 g, 2.77 mmol, 5.00 equiv.) tetrabutylammonium chloride was added, which resulted in a precipitate. The precipitate was collected by filtration and washed with acetonitrile, and dried. The desired product 4-(4-(9H-carbazol-9-yl)phenyl)-3-azido-1-methylpyridin-1-ium chloride was obtained as a pale yellow solid (0.192 g, 0.466 mmol, 84%).

$^1\text{H}$  NMR (500 MHz,  $\text{DMSO-}d_6$ , ppm)  $\delta$  = 9.37 (s, 1H,  $H_{Ar}$ ), 8.89 (d,  $J$  = 5.4 Hz, 1H,  $H_{Ar}$ ), 8.31–8.28 (m, 3H,  $H_{Ar}$ ), 8.08–8.03 (m, 2H,  $H_{Ar}$ ), 7.93–7.89 (m, 2H,  $H_{Ar}$ ), 7.53–7.45 (m, 4H,  $H_{Ar}$ ), 7.34 (ddd,  $J$  = 7.9, 6.3, 1.7 Hz, 2H,  $H_{Ar}$ ), 4.42 (s, 3H,  $\text{CH}_3$ ).

$^{13}\text{C}$  NMR (126 MHz,  $\text{DMSO-}d_6$ , ppm)  $\delta$  = 144.9 (1C,  $C_{Ar}$ ), 141.1 (1C,  $C_{Ar}$ ), 139.7 (2C,  $C_{Ar}$ ), 139.1 (1C,  $C_{Ar}$ ), 138.7 (1C,  $C_{Ar}$ ), 138.0 (1C,  $C_{Ar}$ ), 131.5 (2C,  $C_{Ar}$ ), 131.1 (1C,  $C_{Ar}$ ), 127.8 (1C,  $C_{Ar}$ ), 126.6 (2C,  $C_{Ar}$ ), 126.5 (2C,  $C_{Ar}$ ), 123.1 (2C,  $C_{Ar}$ ), 120.7 (2C,  $C_{Ar}$ ), 120.6 (2C,  $C_{Ar}$ ), 109.7 (2C,  $C_{Ar}$ ), 47.6 (1C,  $\text{CH}_3$ ).

ESI-MS for  $[\text{C}_{24}\text{H}_{18}\text{N}_5]^+$ : Calc.  $m/z$  = 376.1557, found  $m/z$  = 376.1548.

IR (ATR,  $\tilde{\nu}$ ) = 3378 (vs), 3368 (vs), 3364 (vs), 3353 (vs), 3344 (vs), 3331 (vs), 3320 (vs), 3311 (vs), 3300 (vs), 3291 (vs), 3284 (vs), 3269 (vs), 3264 (vs), 3250 (vs), 3239 (vs), 3154 (s), 3131 (s), 3086 (s), 3067 (s), 3043 (s), 3020 (s), 3013 (s), 2970 (vs), 2932 (s), 2915 (s), 2911 (s), 2898 (s), 2814 (s), 2118 (vs), 1598 (vs), 1505 (vs), 1477 (s), 1448 (vs), 1326 (vs), 1315 (s)  $\text{cm}^{-1}$ .

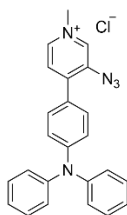
Additional information on the chemical synthesis is available *via* the Chemotion repository:

<https://dx.doi.org/10.14272/reaction/SA-FUHFF-UHFFFADPSC-IJEBCCZWNN-UHFFFADPSC-NUHFF-MUHFF-NUHFF-ZZZ>

Additional information on the analysis of the target compound is available *via* the Chemotion repository:

<https://dx.doi.org/10.14272/IJEBCCZWNNYQIP-UHFFFAOYSA-M.1>

### 3-azido-4-(4-(diphenylamino)phenyl)-1-methylpyridin-1-ium chloride (Az-2)



4-(3-azidopyridin-4-yl)-N,N-diphenylaniline (0.20 g, 0.550 mmol, 1.00 equiv.) was dissolved in acetonitrile (10 mL), and methyl iodide (0.117 g, 0.826 mmol, 1.50 equiv.) was added dropwise at room temperature with stirring. The resulting reaction mixture was left overnight at 40 °C. The precipitation was collected by filtration and washed with acetonitrile. After dissolving in 10 mL water, (0.449 g, 2.75 mmol, 5.00 equiv.) ammonium hexafluorophosphate was added, which resulted in a precipitate. The precipitate was collected by filtration and washed with water, and dried. After dissolving the solid in 10 mL acetonitrile, (0.765 g, 2.75 mmol, 5.00 equiv.) tetrabutylammonium chloride was added, which resulted in a precipitate. The precipitate was collected by filtration and washed with acetonitrile, and dried. The desired product 3-azido-4-(4-(diphenylamino)phenyl)-1-methylpyridin-1-ium chloride was obtained as a yellow solid (0.203 g, 0.491 mmol, 89%).

$^1\text{H}$  NMR (500 MHz, DMSO- $d_6$ , ppm)  $\delta$  = 9.18 (s, 1H,  $H_{Ar}$ ), 8.71 (d,  $J$  = 6.3 Hz, 1H,  $H_{Ar}$ ), 8.09 (d,  $J$  = 6.4 Hz, 1H,  $H_{Ar}$ ), 7.74–7.67 (m, 2H,  $H_{Ar}$ ), 7.45–7.37 (m, 4H,  $H_{Ar}$ ), 7.20 (td,  $J$  = 7.3, 1.2 Hz, 2H,  $H_{Ar}$ ), 7.18–7.14 (m, 4H,  $H_{Ar}$ ), 7.01–6.95 (m, 2H,  $H_{Ar}$ ), 4.32 (s, 3H,  $\text{CH}_3$ ).

$^{13}\text{C}$  NMR (126 MHz, DMSO- $d_6$ , ppm)  $\delta$  = 149.9 (1C,  $C_{Ar}$ ), 145.9 (2C,  $C_{Ar}$ ), 145.2 (1C,  $C_{Ar}$ ), 140.7 (1C,  $C_{Ar}$ ), 138.2 (1C,  $C_{Ar}$ ), 136.9 (1C,  $C_{Ar}$ ), 131.2 (2C,  $C_{Ar}$ ), 130.0 (4C,  $C_{Ar}$ ), 126.6 (1C,  $C_{Ar}$ ), 125.7 (4C,  $C_{Ar}$ ), 124.9 (2C,  $C_{Ar}$ ), 124.0 (1C,  $C_{Ar}$ ), 119.6 (2C,  $C_{Ar}$ ), 47.1 (1C,  $\text{CH}_3$ ).

ESI-MS for  $[\text{C}_{24}\text{H}_{20}\text{N}_5]^+$ : Calc.  $m/z$  = 378.1714, found  $m/z$  = 378.1704.

IR (ATR,  $\tilde{\nu}$ ) = 3851 (m), 3646 (m), 3479 (vs), 3440 (vs), 3405 (vs), 3265 (s), 3254 (s), 3196 (s), 3123 (m), 3061 (s), 3035 (s), 3019 (s), 3011 (s), 2991 (s), 2980 (s), 2951 (s), 2923 (s), 2128 (vs), 1585 (vs), 1488 (vs), 1483 (vs), 1472 (vs), 1448 (s), 1329 (vs), 1306 (s), 1270 (vs), 1194 (vs), 1180 (vs), 1173 (s), 754 (s), 695 (s)  $\text{cm}^{-1}$ .

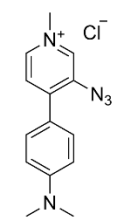
Additional information on the chemical synthesis is available *via* the Chemotion repository:

<https://dx.doi.org/10.14272/reaction/SA-FUHFF-UHFFFADPSC-VNRJBELPCO-UHFFFADPSC-NUHFF-MUHFF-NUHFF-ZZZ>

Additional information on the analysis of the target compound is available *via* the Chemotion repository:

<https://dx.doi.org/10.14272/VNRJBELPCOZABG-UHFFFAOYSA-M.1>

### 3-azido-4-(4-(dimethylamino)phenyl)-1-methylpyridin-1-ium chloride (Az-3)



4-(3-azidopyridin-4-yl)-N,N-dimethylaniline (0.20 g, 0.836 mmol, 1.00 equiv.) was dissolved in acetonitrile (10 mL), and methyl iodide (0.178 g, 1.25 mmol, 1.50 equiv.) was added dropwise at room temperature with stirring. The resulting reaction mixture was left overnight at 40 °C. The precipitation was collected by filtration and washed with acetonitrile. After dissolving in 10 mL water, (0.681 g, 4.18 mmol, 5.00 equiv.) ammonium hexafluorophosphate was added, which resulted in a precipitate. The precipitate was collected by filtration and washed with water, and dried. After dissolving the solid in 10 mL acetonitrile, (1.16 g, 4.18 mmol, 5.00 equiv.) tetrabutylammonium chloride was added, which

resulted in a precipitate. The precipitate was collected by filtration and washed with acetonitrile, and dried. The desired product 3-azido-4-(4-(dimethylamino)phenyl)-1-methylpyridin-1-ium chloride was obtained as an orange solid (0.224 g, 0.773 mmol, 92%).

$^1\text{H}$  NMR (500 MHz, , DMSO- $d_6$ , ppm)  $\delta$  = 9.06 (d,  $J$  = 1.4 Hz, 1H,  $H_{Ar}$ ), 8.60 (dd,  $J$  = 6.6, 1.4 Hz, 1H,  $H_{Ar}$ ), 8.05 (d,  $J$  = 6.5 Hz, 1H,  $H_{Ar}$ ), 7.80–7.73 (m, 2H,  $H_{Ar}$ ), 6.88–6.81 (m, 2H,  $H_{Ar}$ ), 4.27 (s, 3H,  $\text{CH}_3$ ), 3.04 (s, 6H,  $\text{CH}_3$ ).

$^{13}\text{C}$  NMR (126 MHz, , DMSO- $d_6$ , ppm)  $\delta$  = 152.0 (1C,  $C_{Ar}$ ), 145.7 (1C,  $C_{Ar}$ ), 140.4 (1C,  $C_{Ar}$ ), 137.8 (1C,  $C_{Ar}$ ), 135.9 (1C,  $C_{Ar}$ ), 131.2 (2C,  $C_{Ar}$ ), 125.4 (1C,  $C_{Ar}$ ), 118.3 (1C,  $C_{Ar}$ ), 111.6 (2C,  $C_{Ar}$ ), 46.7 (1C,  $\text{CH}_3$ ), 39.6 (2C,  $\text{CH}_3$ ).

ESI-MS for  $[\text{C}_{11}\text{H}_8\text{N}_4+\text{H}]^+$ : Calc.  $m/z$  = 254.1401, found  $m/z$  = 254.1397.

IR (ATR,  $\tilde{\nu}$ ) = 3851 (m), 3646 (m), 3046 (m), 2119 (vs), 1779 (m), 1771 (m), 1746 (vs), 1585 (vs), 1503 (vs), 1470 (s), 1440 (s), 1381 (s), 1337 (s), 1315 (vs), 1272 (m), 1172 (vs), 1131 (vs), 1068 (s), 1025 (m), 944 (m), 899 (m), 818 (s), 788 (s), 767 (s), 744 (s), 702 (s), 687 (s), 667 (s), 640 (m), 631 (m), 512 (m)  $\text{cm}^{-1}$ .

Additional information on the chemical synthesis is available *via* the Chemotion repository:

<https://dx.doi.org/10.14272/reaction/SA-FUHFF-UHFFFADPSC-SZCWTGKVOH-UHFFFADPSC-NUHFF-MUHFF-NUHFF-ZZZ>

Additional information on the analysis of the target compound is available *via* the Chemotion repository:

<https://dx.doi.org/10.14272/SZCWTGKVOHZBBE-UHFFFAOYSA-M.1>

#### For the synthesis of **Cb-1**, **Cb-2**, and **Cb-3**

**Az-1** (5.00 mg, 0.01 mmol 1.00 equiv.) and cucurbit[7]uril (14.1 mg, 0.02 mmol, 1.00 equiv.) were separately dissolved with water (10 ml) in quartz flasks, and the reaction solution was irradiated of 405 nm LEDs at 25 °C. After 2 h, amantadine (5.51 mg, 0.03 mmol, 3.00 equiv.) was added to the reaction mixture. After stirring for 0.5 hour, water was removed, and the resulting mixture was injected into the preparative reversed-phase high-performance liquid chromatography using acetonitrile and double distilled water supplemented with 0.1% trifluoroacetic acid as eluent. **Cb-1** was collected and dried as a brown solid (4.13 mg, 0.01 mmol, 89%). **Cb-2** and **Cb-3** were obtained using the same method as brown solids (92% for **Cb-2**, and 86% for **Cb-3**)

## Supplementary Data and Characterization

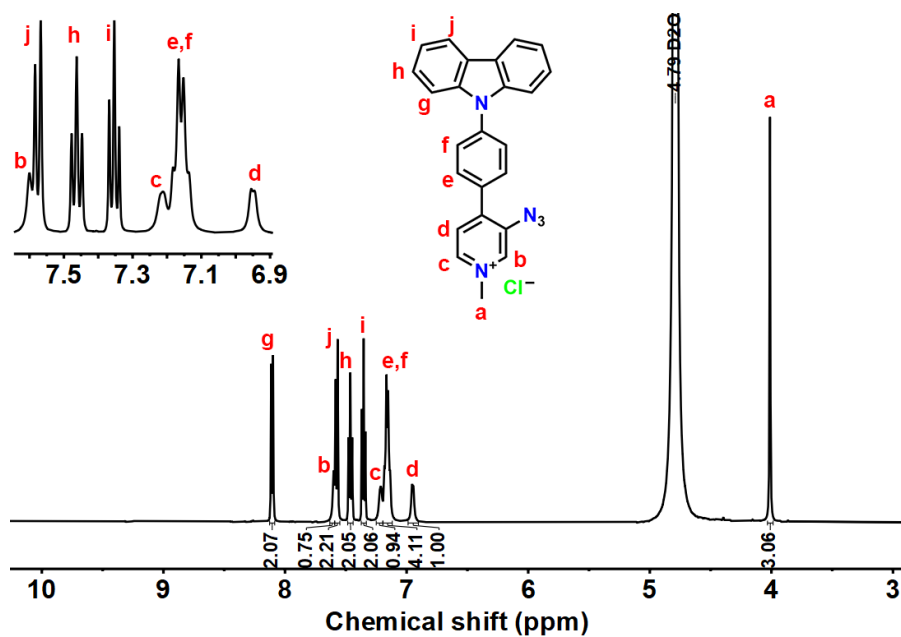


**Figure S1.**  $^1\text{H}$  NMR of 4-(4-(9H-carbazol-9-yl)phenyl)-3-azido-1-methylpyridin-1-ium chloride (AZ-1, 0.5 mM), 500 MHz,  $\text{D}_2\text{O}$ .

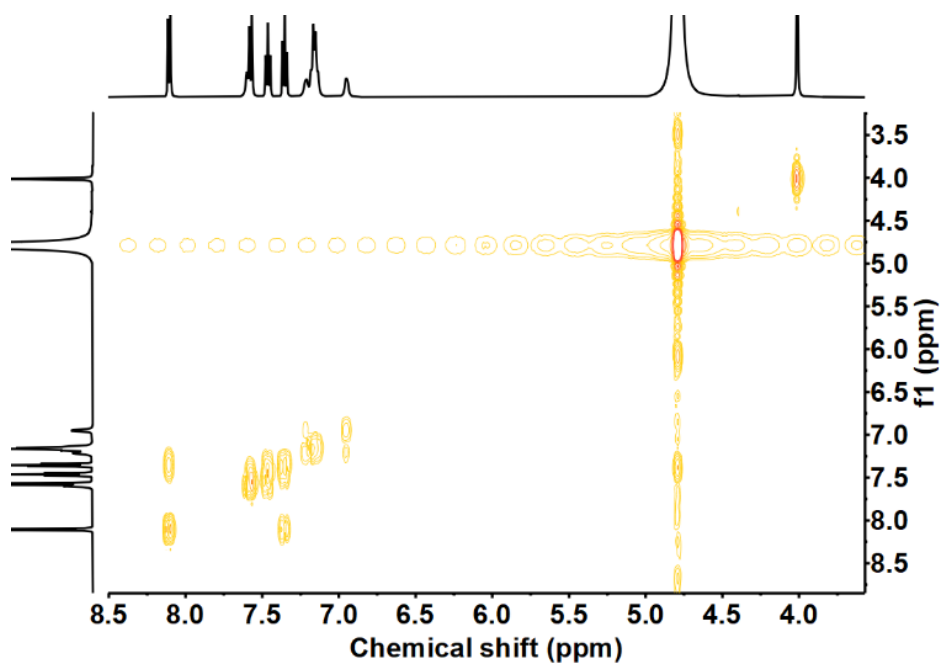


**Figure S2.**  $^1\text{H}$ - $^1\text{H}$  COSY NMR of 4-(4-(9H-carbazol-9-yl)phenyl)-3-azido-1-methylpyridin-1-ium chloride (AZ-1, 0.5 mM), 500 MHz,  $\text{D}_2\text{O}$ .

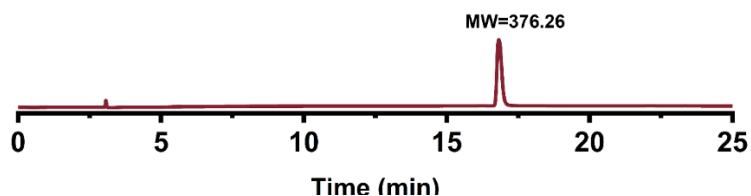


**Figure S3.** LC-MS of 4-(4-(9H-carbazol-9-yl)phenyl)-3-azido-1-methylpyridin-1-ium chloride (**AZ-1**).

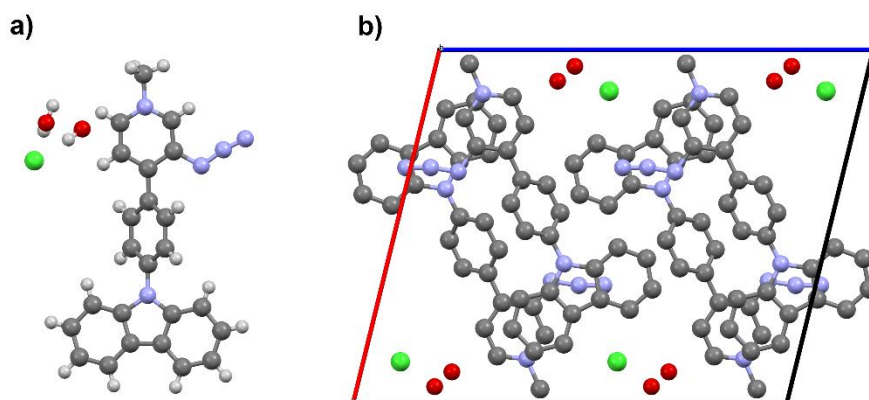


**Figure S4.** Crystal structure of a) **Az-1**•2H<sub>2</sub>O; b) **Az-1**•2H<sub>2</sub>O in packing model.

**Table S1** Crystal data and structure refinement for **Az-1**•2H<sub>2</sub>O.

Identification code	<b>Az-1</b> •2H <sub>2</sub> O
Empirical formula	C <sub>24</sub> H <sub>22</sub> ClN <sub>5</sub> O <sub>2</sub>
Formula weight	447.91
Temperature/K	180
Crystal system	monoclinic
Space group	<i>P</i> 2 <sub>1</sub> / <i>c</i>
<i>a</i> /Å	16.3613(4)
<i>b</i> /Å	6.89670(10)
<i>c</i> /Å	19.5442(5)
$\alpha$ /°	90
$\beta$ /°	103.785(2)
$\gamma$ /°	90
Volume/Å <sup>3</sup>	2141.83(8)
<i>Z</i>	4
$\rho_{\text{calc}}$ /cm <sup>3</sup>	1.389
$\mu$ /mm <sup>-1</sup>	1.211
<i>F</i> (000)	936.0
Crystal size/mm <sup>3</sup>	0.15 × 0.04 × 0.03
Radiation	Ga K $\alpha$ ( $\lambda$ = 1.34143)

$2\theta$  range for data collection/ $^{\circ}$  8.106 to 124.968  
 Index ranges  $-21 \leq h \leq 21, -8 \leq k \leq 3, -25 \leq l \leq 25$   
 Reflections collected 20376  
 Independent reflections 5117 [ $R_{\text{int}} = 0.0157, R_{\text{sigma}} = 0.0118$ ]  
 Data/restraints/parameters 5117/0/296  
 Goodness-of-fit on  $F^2$  1.082  
 Final R indexes [ $I \geq 2\sigma(I)$ ]  $R_1 = 0.0536, wR_2 = 0.1603$   
 Final R indexes [all data]  $R_1 = 0.0612, wR_2 = 0.1663$   
 Largest diff. peak/hole /  $e \text{ \AA}^{-3}$  0.61/-0.80  
 CCDC number 2351099

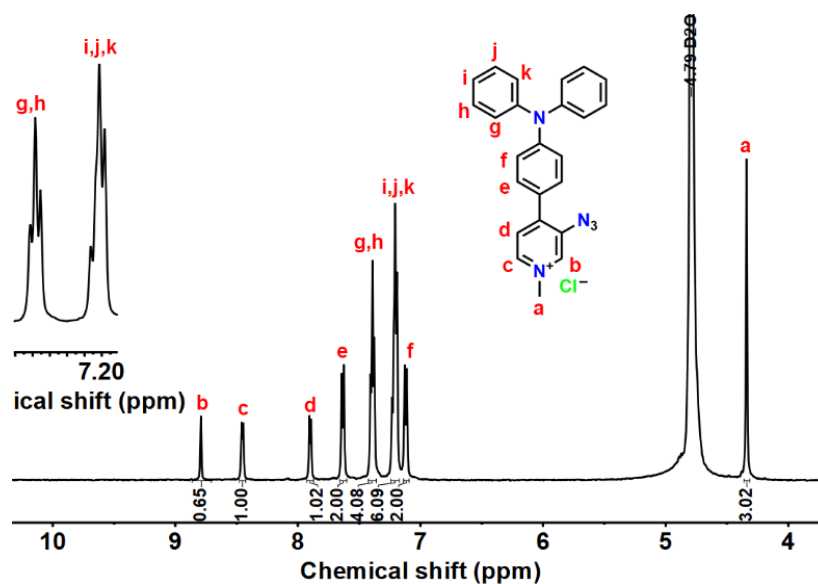


**Figure S5.**  $^1\text{H}$  NMR of 3-azido-4-(4-(diphenylamino)phenyl)-1-methylpyridin-1-ium chloride (**Az-2**, 0.5 mM), 500 MHz,  $\text{D}_2\text{O}$ .

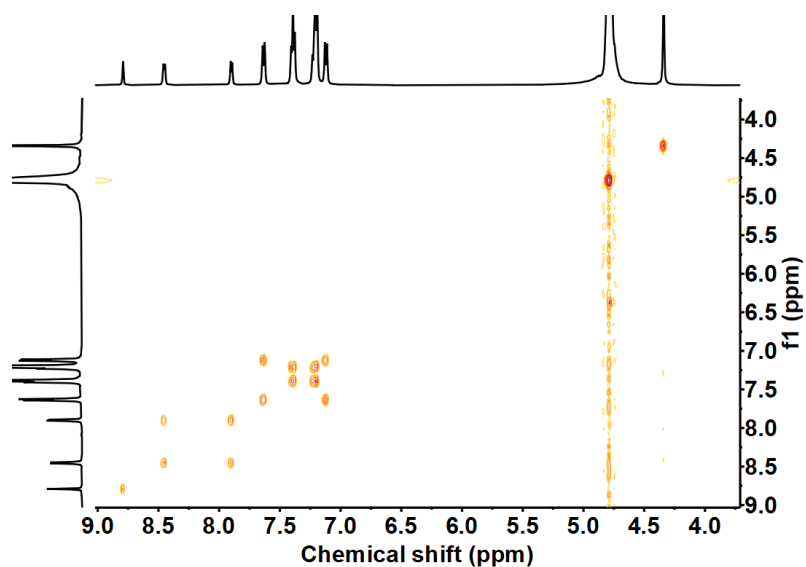


**Figure S6.**  $^1\text{H}$ - $^1\text{H}$  COSY NMR of 3-azido-4-(4-(diphenylamino)phenyl)-1-methylpyridin-1-ium chloride (**AZ-2**, 0.5 mM), 500 MHz,  $\text{D}_2\text{O}$ .

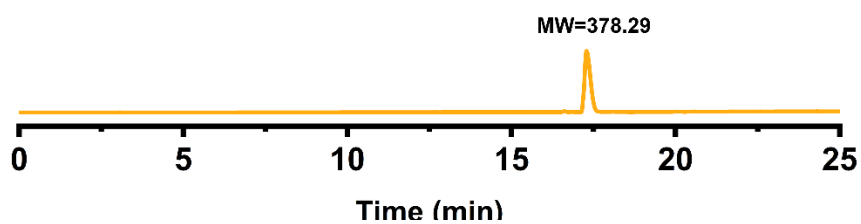


**Figure S7.** LC-MS of 3-azido-4-(4-(diphenylamino)phenyl)-1-methylpyridin-1-ium chloride (**AZ-2**).

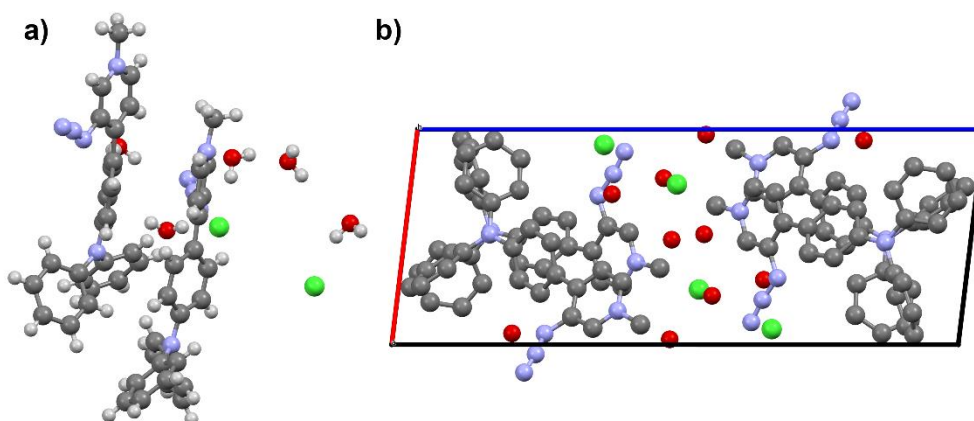


**Figure S8.** Crystal structure of a) **AZ-2**•2.5 $\text{H}_2\text{O}$ ; b) **2AZ-2**•2.5 $\text{H}_2\text{O}$  in packing model.

**Table S2** Crystal data and structure refinement for **2AZ-2**•5 $\text{H}_2\text{O}$ .

Identification code	<b>AZ-2</b> •2.5 $\text{H}_2\text{O}$
Empirical formula	$\text{C}_{24}\text{H}_{25}\text{ClN}_5\text{O}_{2.5}$

Formula weight	458.94
Temperature/K	180
Crystal system	triclinic
Space group	<i>P</i> 1
a/Å	9.5693(2)
b/Å	10.1473(2)
c/Å	24.8566(6)
$\alpha$ /°	101.497(2)
$\beta$ /°	93.876(2)
$\gamma$ /°	103.476(2)
Volume/Å <sup>3</sup>	2283.56(9)
Z	4
$\rho_{\text{calc}}$ /cm <sup>3</sup>	1.335
$\mu$ /mm <sup>-1</sup>	1.153
F(000)	964.0
Crystal size/mm <sup>3</sup>	0.12 × 0.1 × 0.03
Radiation	Ga K $\alpha$ ( $\lambda$ = 1.34143)
2 $\theta$ range for data collection/°	6.36 to 124.998
Index ranges	-5 ≤ h ≤ 12, -13 ≤ k ≤ 11, -32 ≤ l ≤ 32
Reflections collected	37773
Independent reflections	10827 [ $R_{\text{int}}$ = 0.0269, $R_{\text{sigma}}$ = 0.0219]
Data/restraints/parameters	10827/0/603
Goodness-of-fit on F <sup>2</sup>	1.063
Final R indexes [ $I \geq 2\sigma(I)$ ]	$R_1$ = 0.0691, $wR_2$ = 0.2164
Final R indexes [all data]	$R_1$ = 0.0822, $wR_2$ = 0.2283
Largest diff. peak/hole / e Å <sup>-3</sup>	0.91/-0.91
CCDC number	2351100

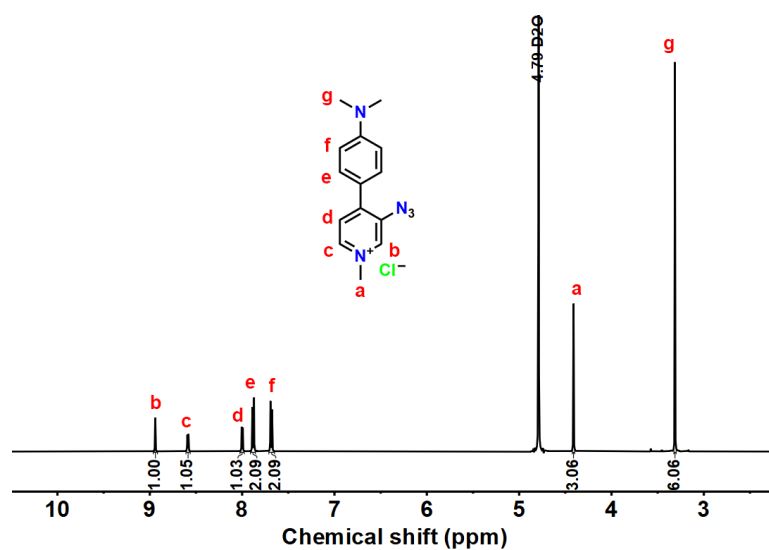


**Figure S9.**  $^1\text{H}$  NMR of 3-azido-4-(4-(dimethylamino)phenyl)-1-methylpyridin-1-ium chloride (**Az-3**, 0.5 mM), 500 MHz,  $\text{D}_2\text{O}$ .

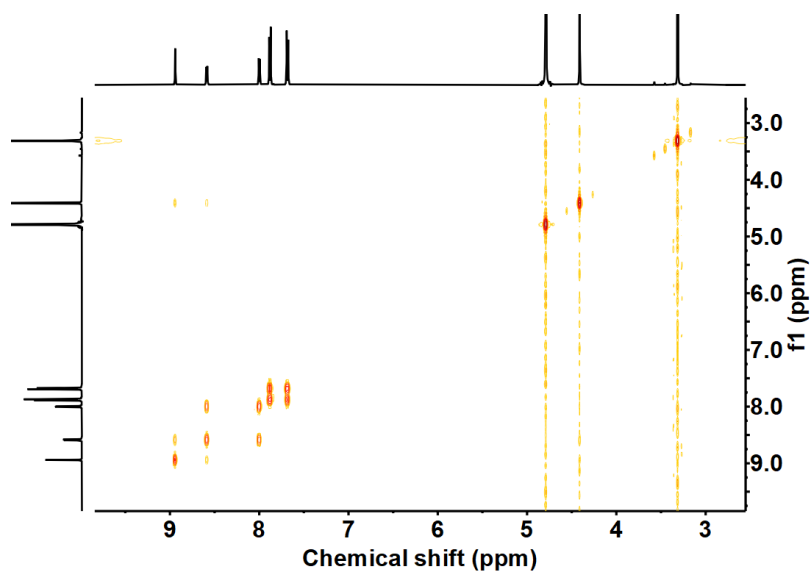


**Figure S10.**  $^1\text{H}$ - $^1\text{H}$  COSY NMR of 3-azido-4-(4-(dimethylamino)phenyl)-1-methylpyridin-1-ium chloride (**Az-3**, 0.5 mM), 500 MHz,  $\text{D}_2\text{O}$ .

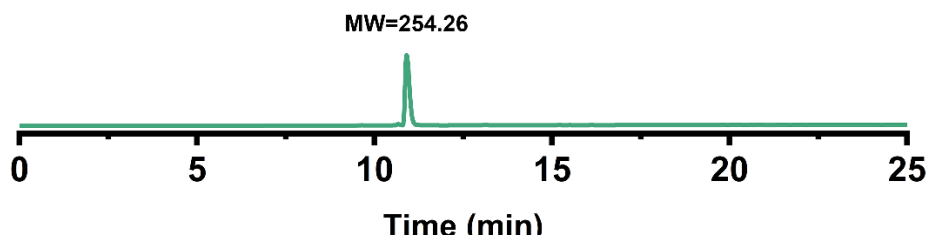


**Figure S11.** LC-MS of 3-azido-4-(4-(dimethylamino)phenyl)-1-methylpyridin-1-ium chloride (**AZ-3**).

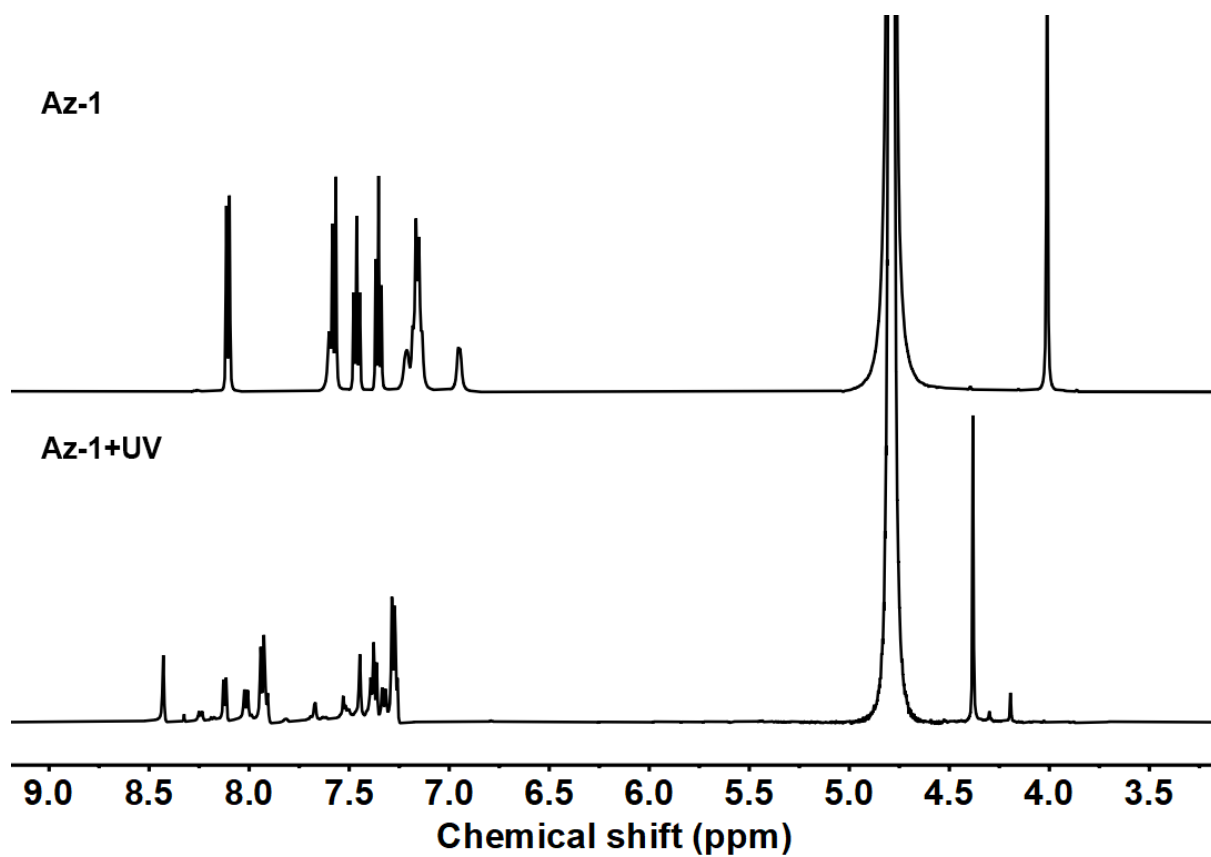


**Figure S12.** <sup>1</sup>H NMR spectra of photolysis of aryl azide **Az-1** (0.5 mM) in D<sub>2</sub>O (4.79 ppm) at 25 °C, 500 MHz.

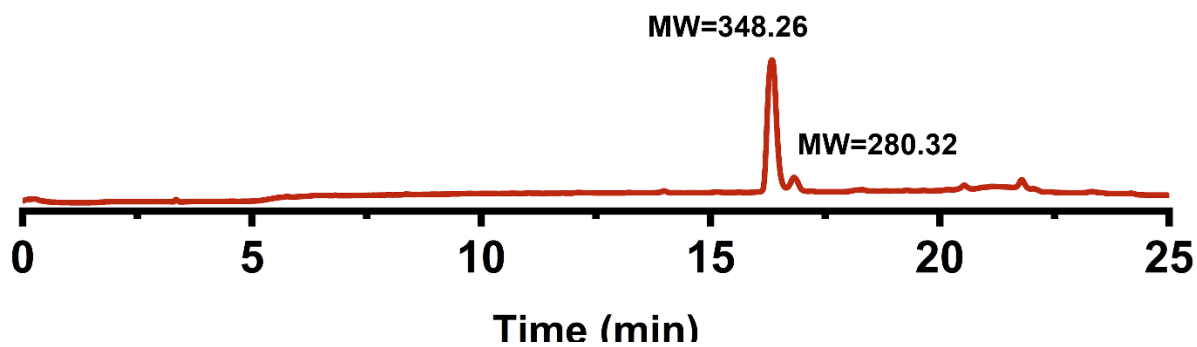


**Figure S13.** LC-MS of photolysis of aryl azide **Az-1** after photoreaction.

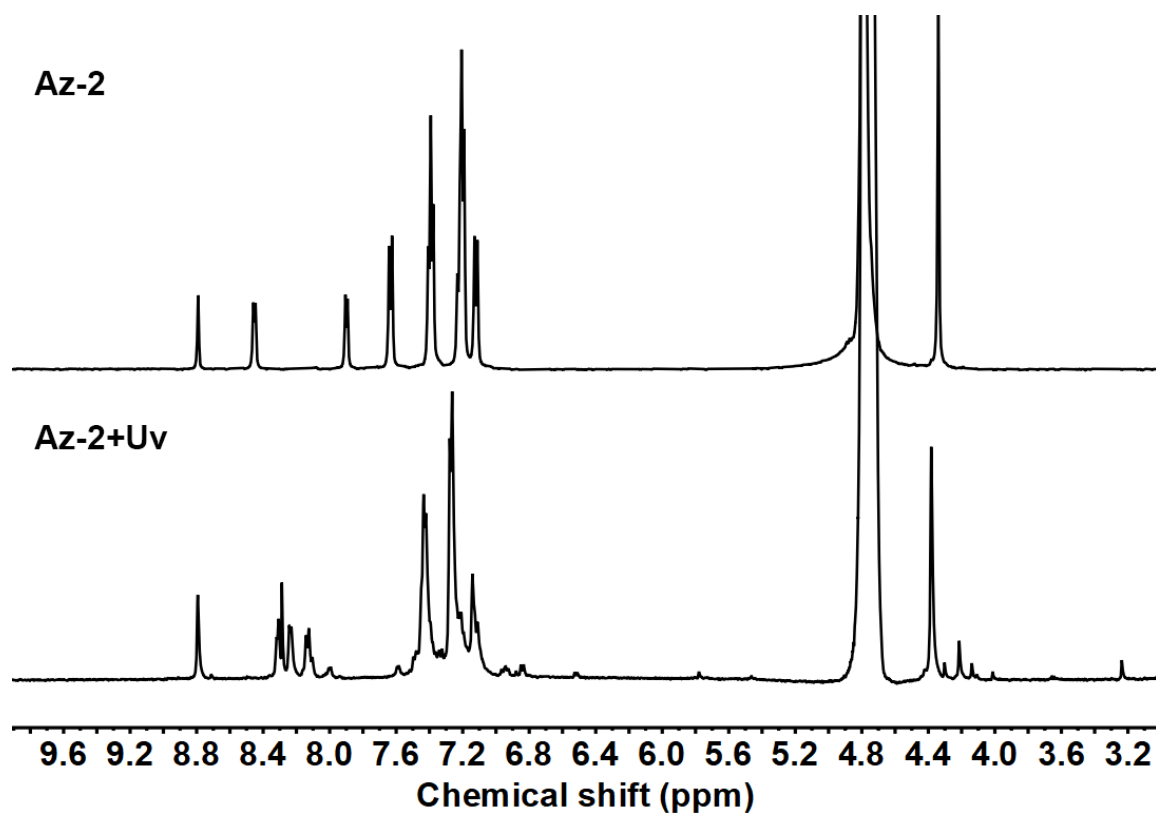


**Figure S14.** <sup>1</sup>H NMR spectra of photolysis of aryl azide **Az-2** (0.5 mM) in D<sub>2</sub>O (4.79 ppm) at 25 °C, 500 MHz.

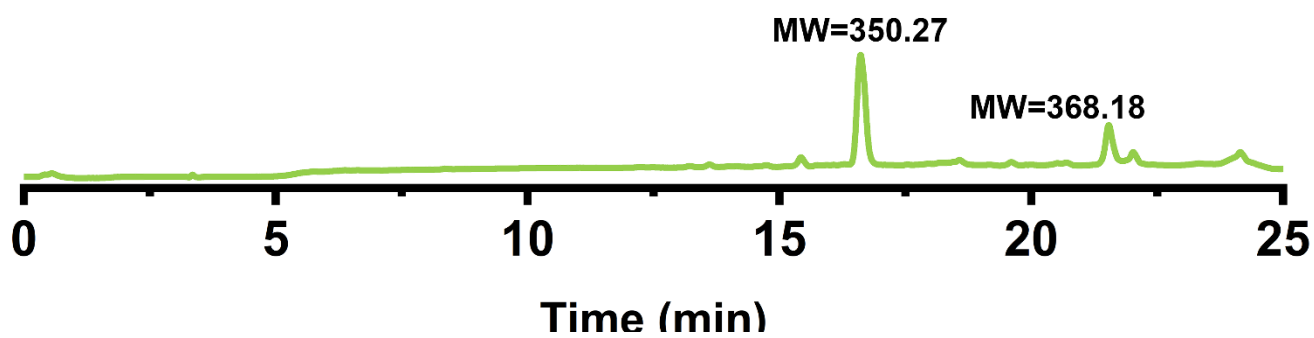


**Figure S15.** LC-MS of photolysis of aryl azide **Az-2** after photoreaction.

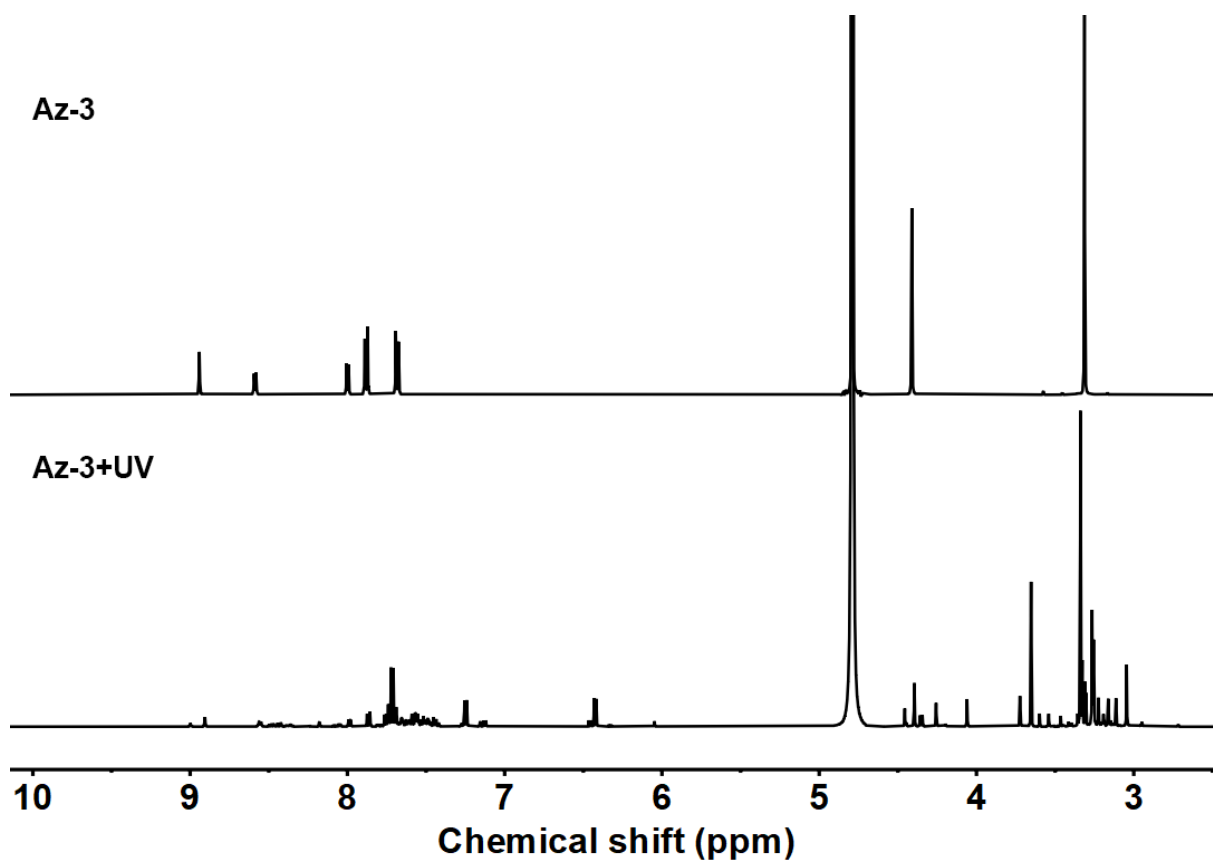


Figure S16. <sup>1</sup>H NMR spectra of photolysis of aryl azide **Az-3** (0.5 mM) in D<sub>2</sub>O (4.79 ppm) at 25 °C, 500 MHz.

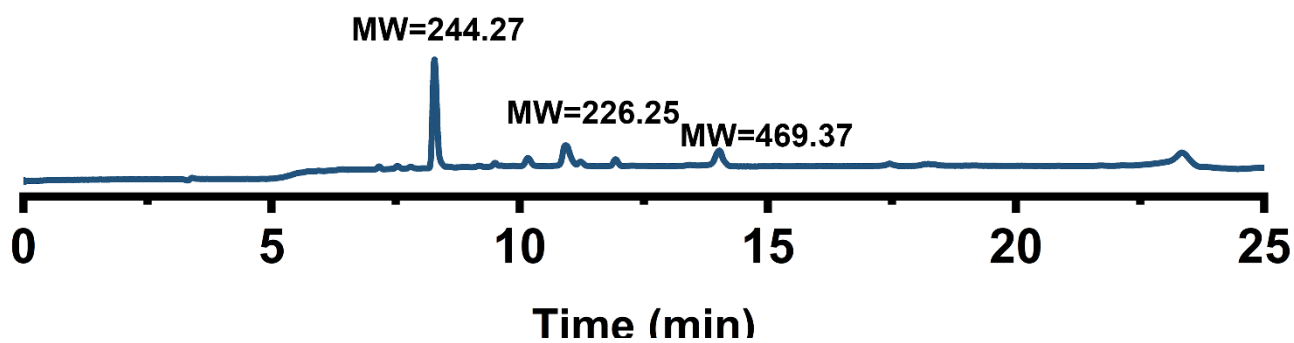
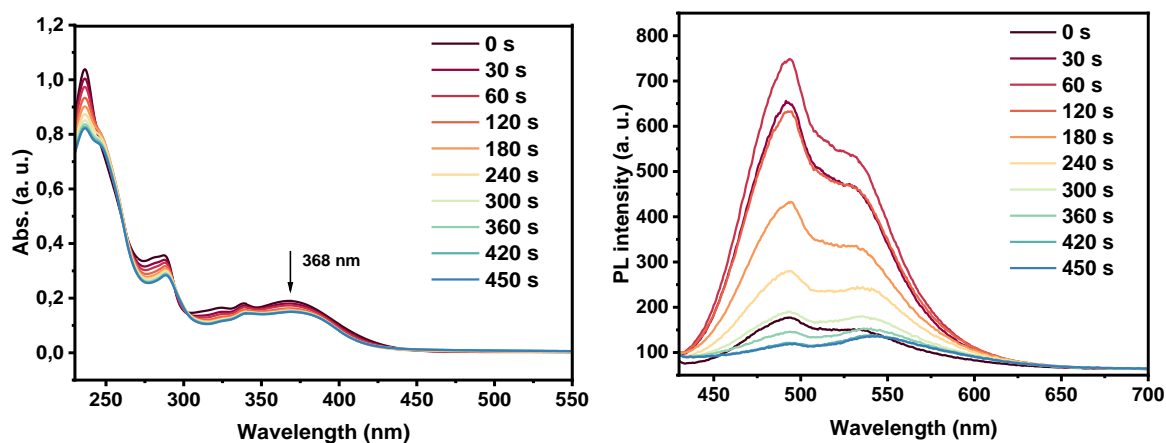
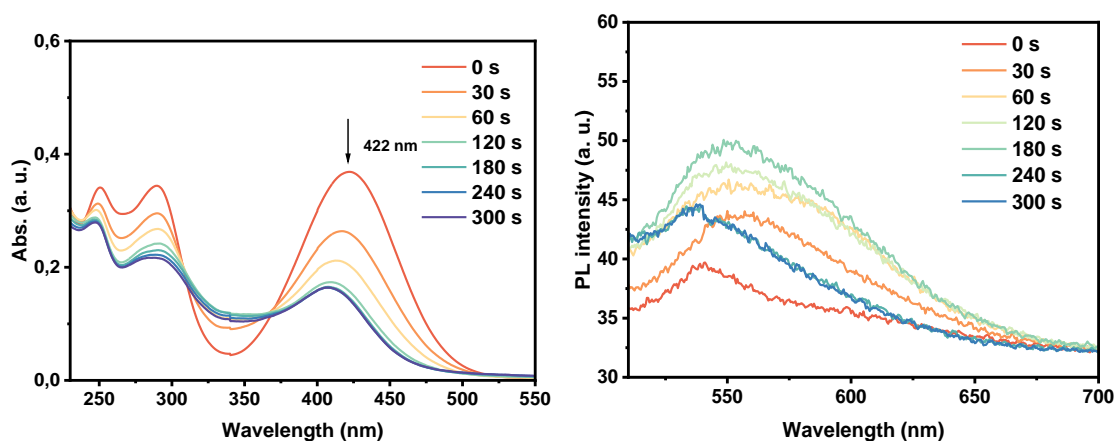


Figure S17. LC-MS of photolysis of aryl azide **Az-3** after photoreaction.



**Figure S18.** UV (left) and emission (right) spectra of photolysis of aryl azide **Az-1** (0.5 mM) after different reaction times in Milli Q water at 25 °C. The reaction mixture was diluted with Milli Q water to  $2 \times 10^{-4}$  M for UV and emission measurements ( $\lambda_{\text{ex}} = 369$  nm, Ex bandwidth = 5 nm, Em bandwidth = 5 nm).



**Figure S19.** UV (left) and emission (right) spectra of photolysis of aryl azide **Az-2** (0.5 mM) after different reaction times in Milli Q water at 25 °C. The reaction mixture was diluted with Milli Q water to  $2 \times 10^{-4}$  M for UV and emission measurements ( $\lambda_{\text{ex}} = 422$  nm, Ex bandwidth = 5 nm, Em bandwidth = 5 nm).

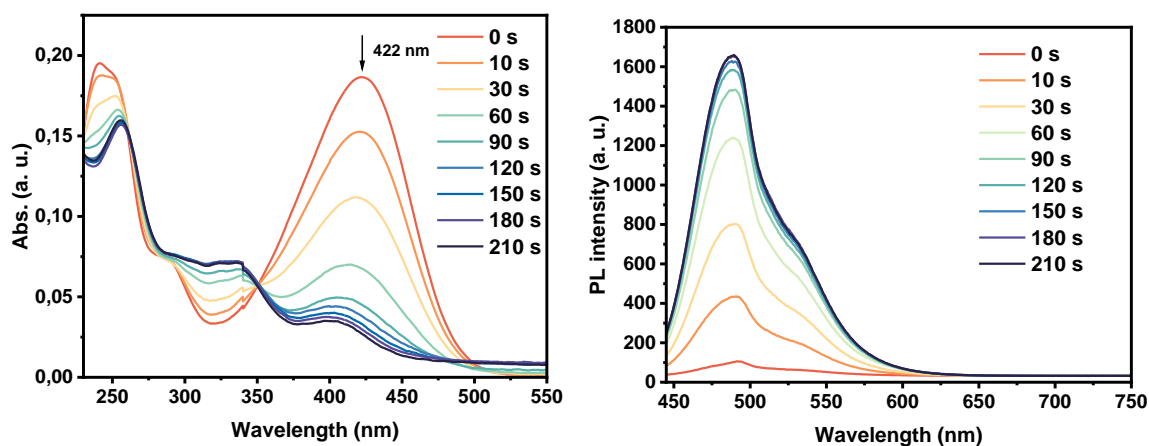


**Figure S20.** UV (left) and emission (right) spectra of photolysis of aryl azide **Az-3** (0.5 mM) after different reaction times in Milli Q water at 25 °C. The reaction mixture was diluted with Milli Q water to  $2 \times 10^{-4}$  M for UV and emission measurements ( $\lambda_{\text{ex}} = 422$  nm, Ex bandwidth = 5 nm, Em bandwidth = 5 nm).

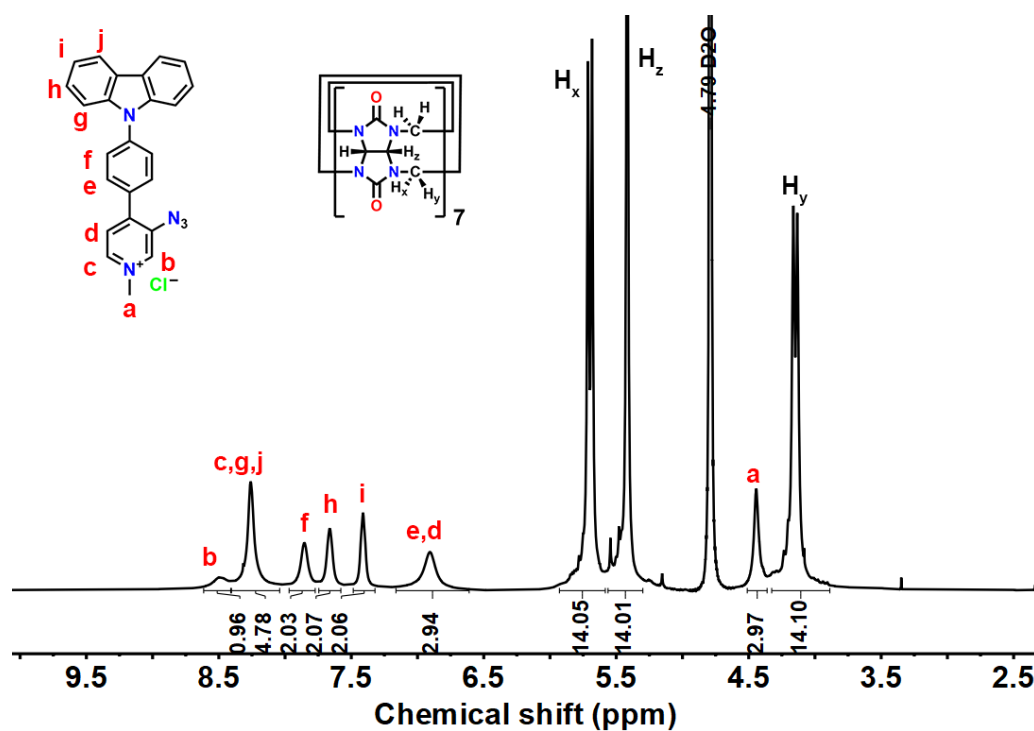


**Figure S21.**  $^1\text{H}$  NMR spectra of aryl azide **Az-1**+CB7 in 1:1 molar ratio (0.5 mM) in  $\text{D}_2\text{O}$  at 25 °C, 500 MHz.

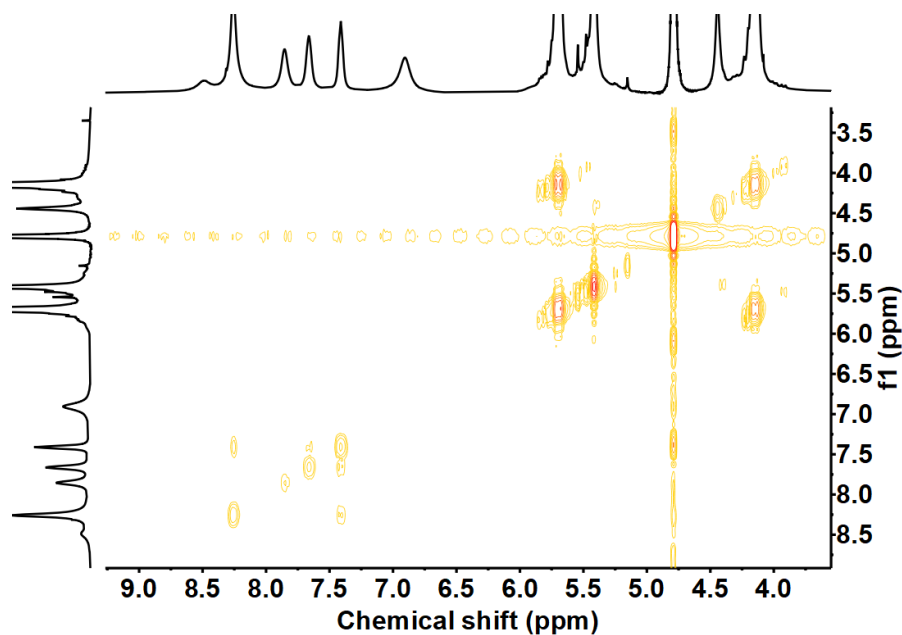


**Figure S22.**  $^1\text{H}$ - $^1\text{H}$  COSY NMR spectra of aryl azide **Az-1**+CB7 in 1:1 molar ratio (0.5 mM) in  $\text{D}_2\text{O}$  (4.79 ppm) at 25 °C, 500 MHz.

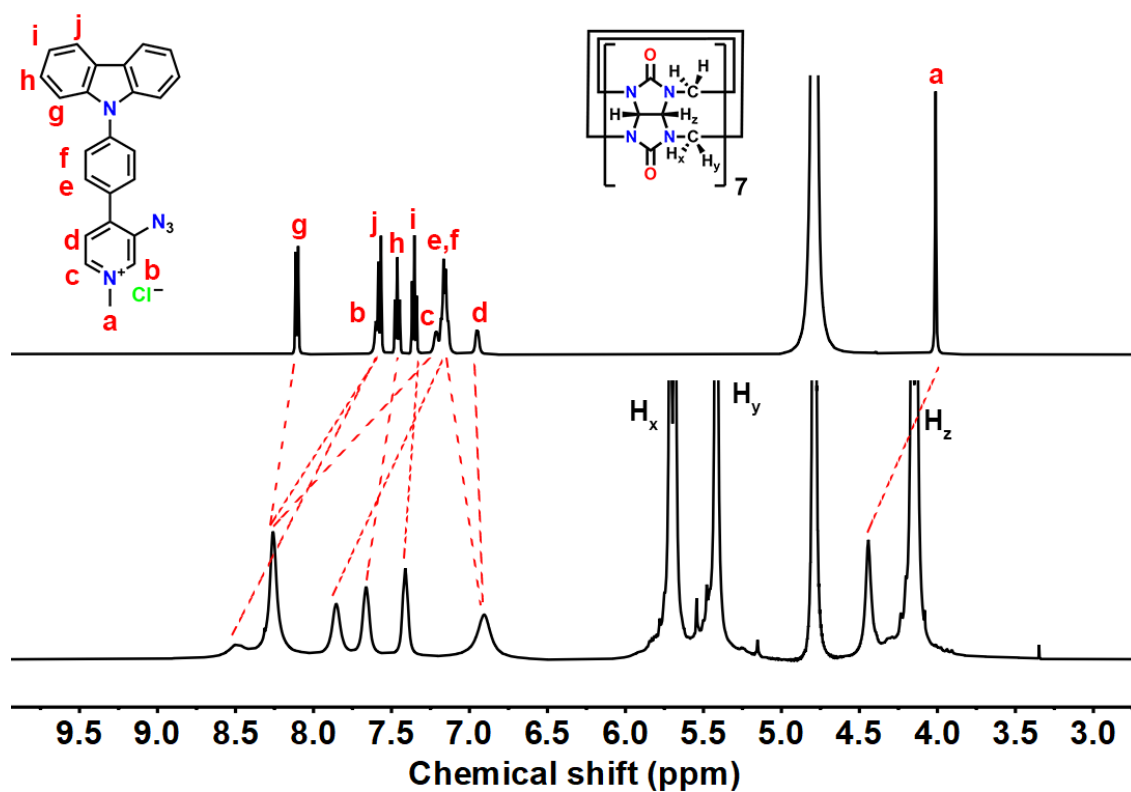


**Figure S23.**  $^1\text{H}$  NMR spectra of aryl azide **Az-1** (top) and **Az-1+CB7** (down) in 1:1 molar ratio (0.5 mM) in  $\text{D}_2\text{O}$  (4.79 ppm) at 25 °C, 500 MHz.

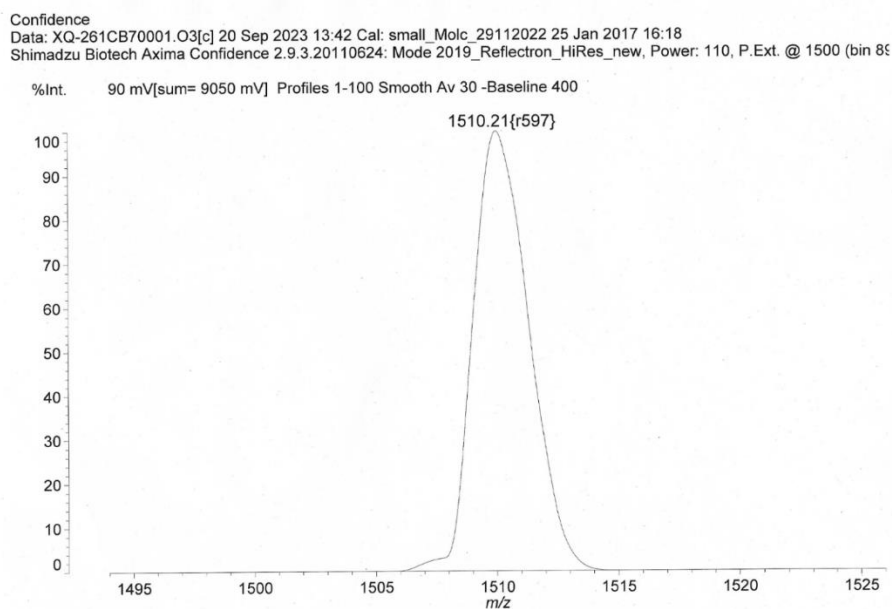


**Figure S24.** MALDI-MS spectra of aryl azide **Az-1+CB7** in 1:1 molar ratio in Milli Q water at 25 °C.

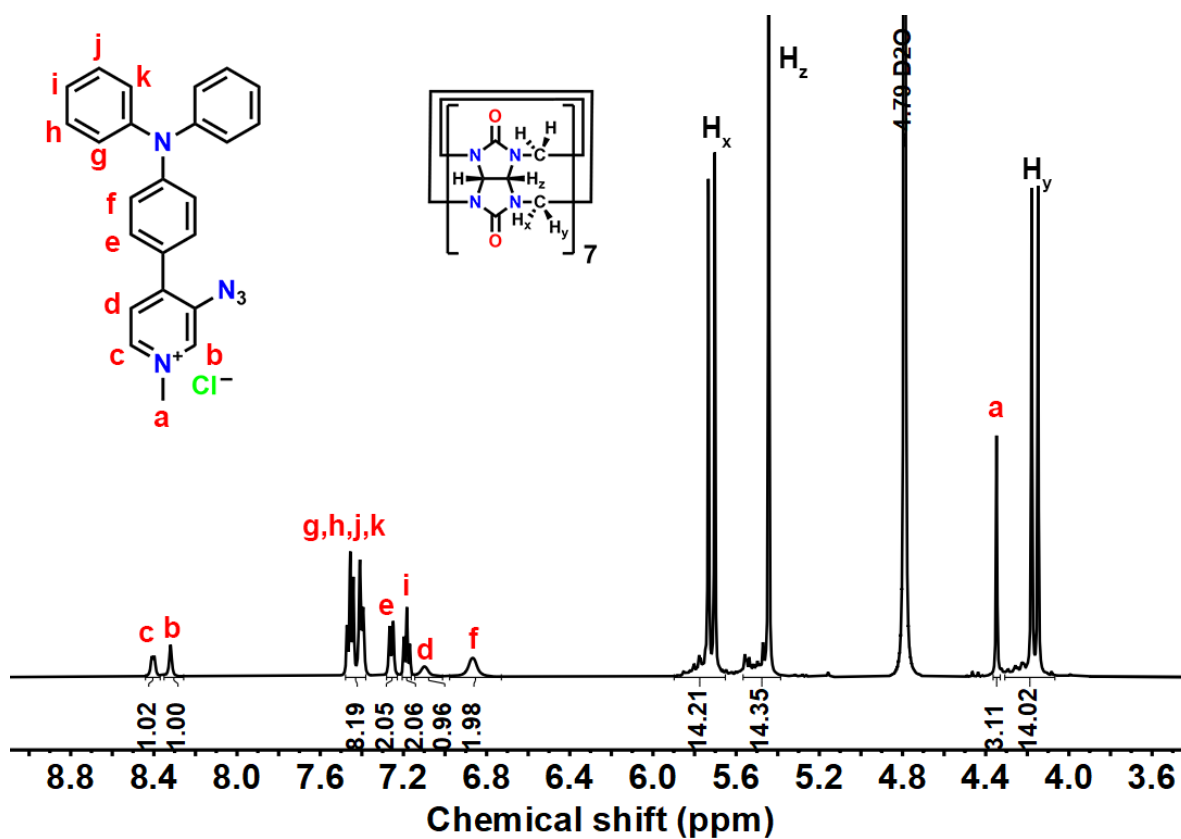


**Figure S25.**  $^1\text{H}$  NMR spectra of aryl azide **Az-2**+CB7 in 1:1 molar ratio (0.5 mM) in  $\text{D}_2\text{O}$  at 25 °C, 500 MHz.

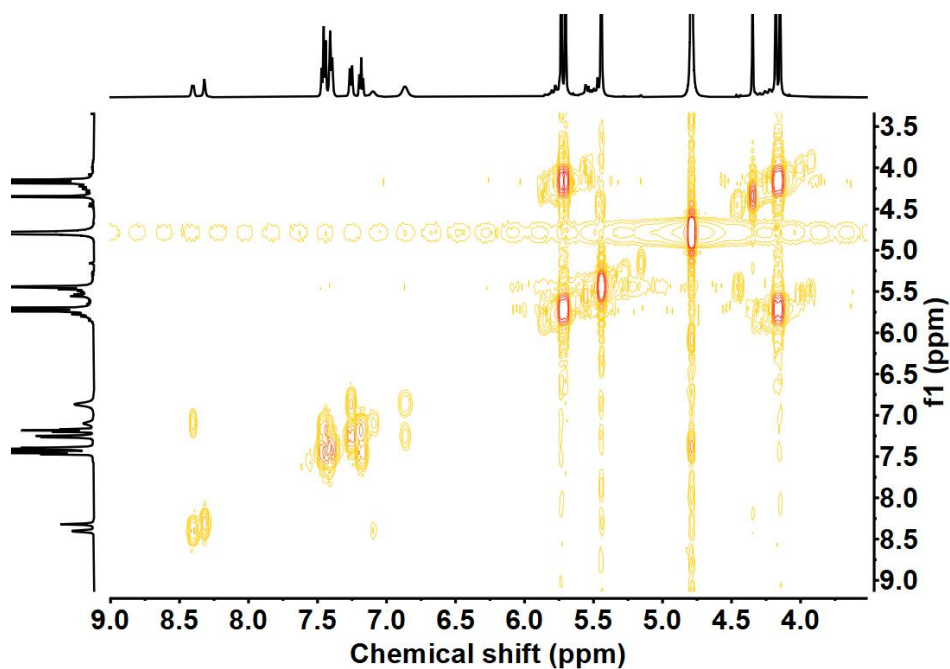


**Figure S26.**  $^1\text{H}$ - $^1\text{H}$  COSY NMR spectra of aryl azide **Az-2**+CB7 in 1:1 molar ratio (0.5 mM) in  $\text{D}_2\text{O}$  (4.79 ppm) at 25 °C, 500 MHz.

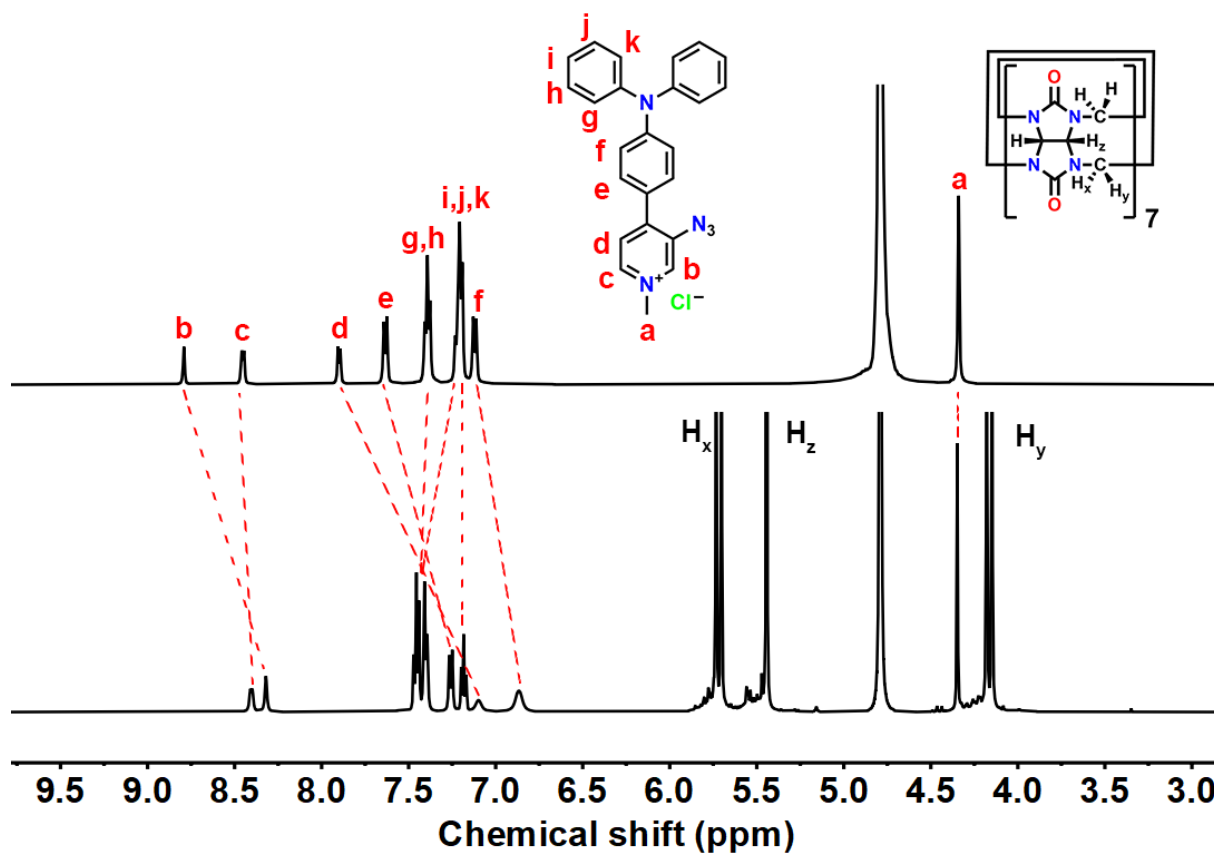


**Figure S27.**  $^1\text{H}$  NMR spectra of aryl azide **Az-2** (top) and **Az-2**+**CB7** (down) in 1:1 molar ratio (0.5 mM) in  $\text{D}_2\text{O}$  (4.79 ppm) at 25 °C, 500 MHz.

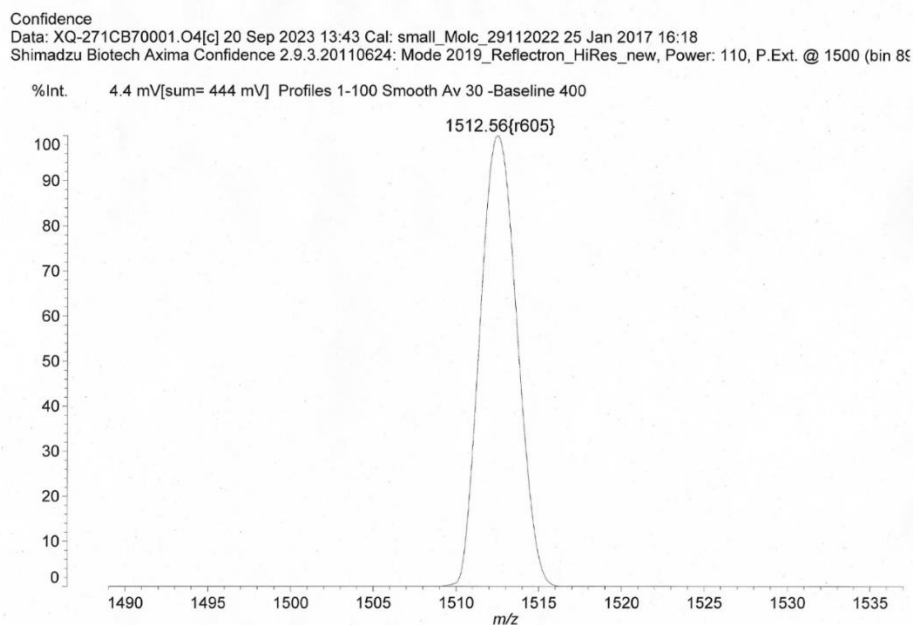


**Figure S28.** MALDI-MS spectra of aryl azide **Az-2**+**CB7** in 1:1 molar ratio in Milli Q water at 25 °C.

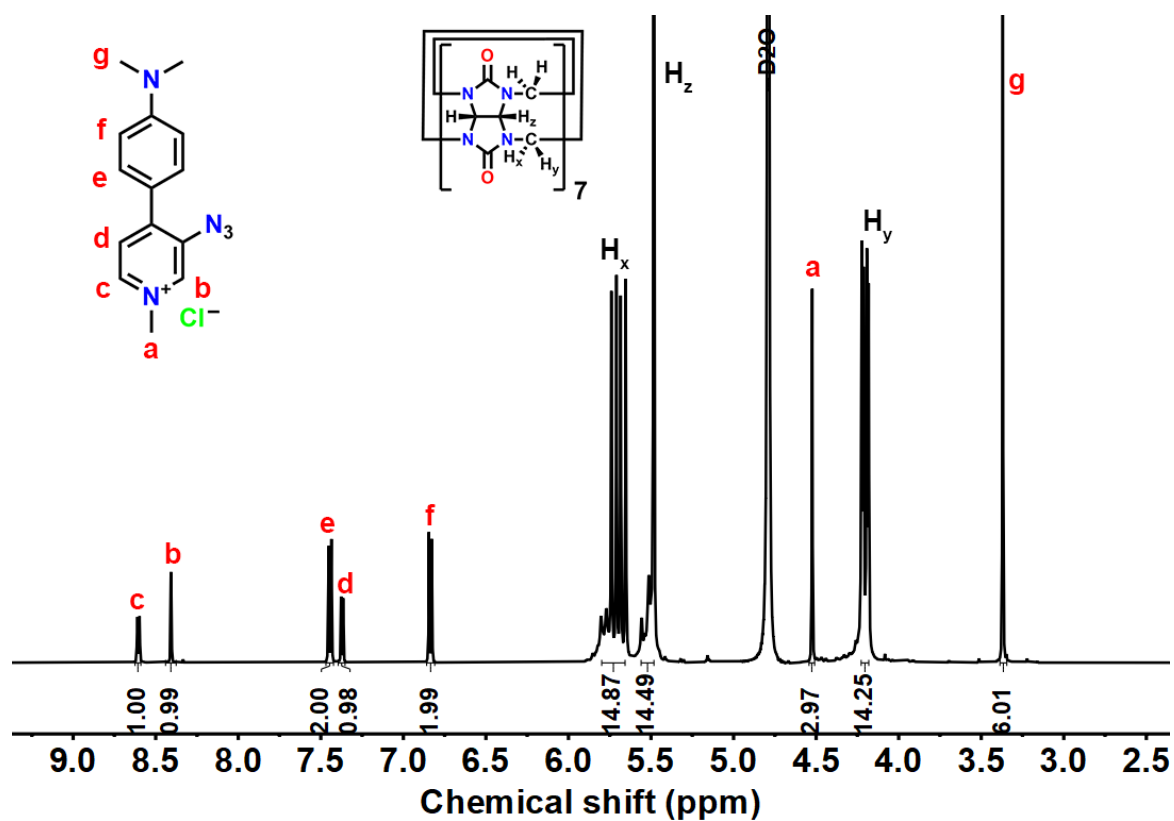


Figure S29.  $^1\text{H}$  NMR spectra of aryl azide **Az-3**+CB7 in 1:1 molar ratio (0.5 mM) in  $\text{D}_2\text{O}$  at 25 °C, 500 MHz.

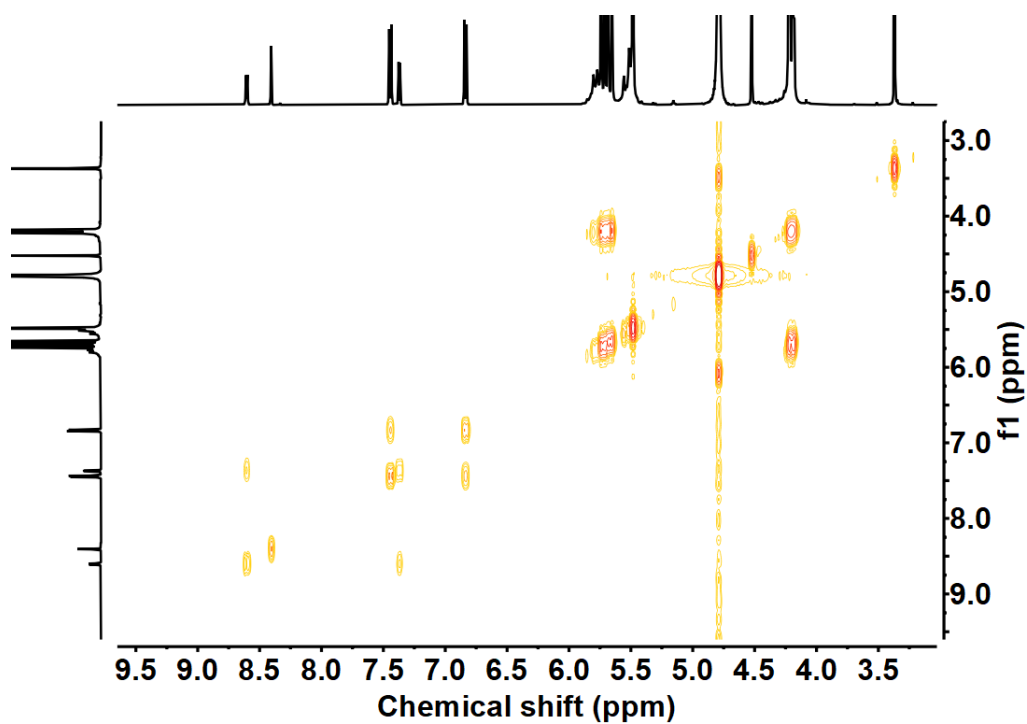
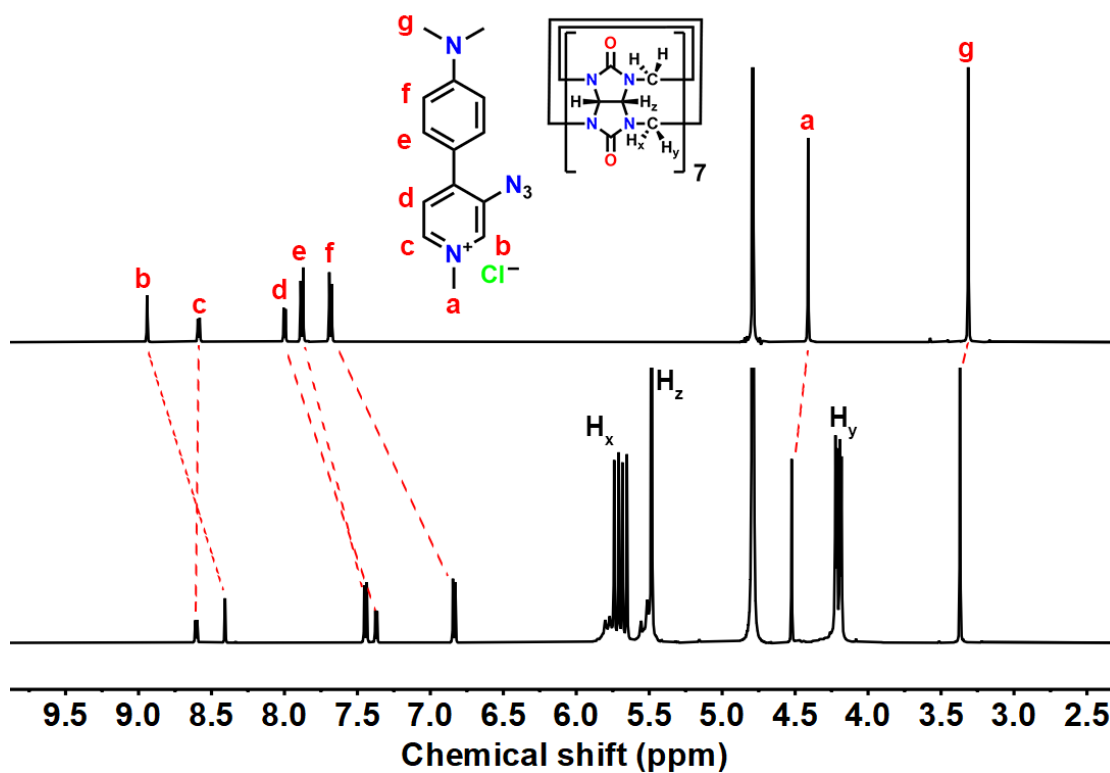
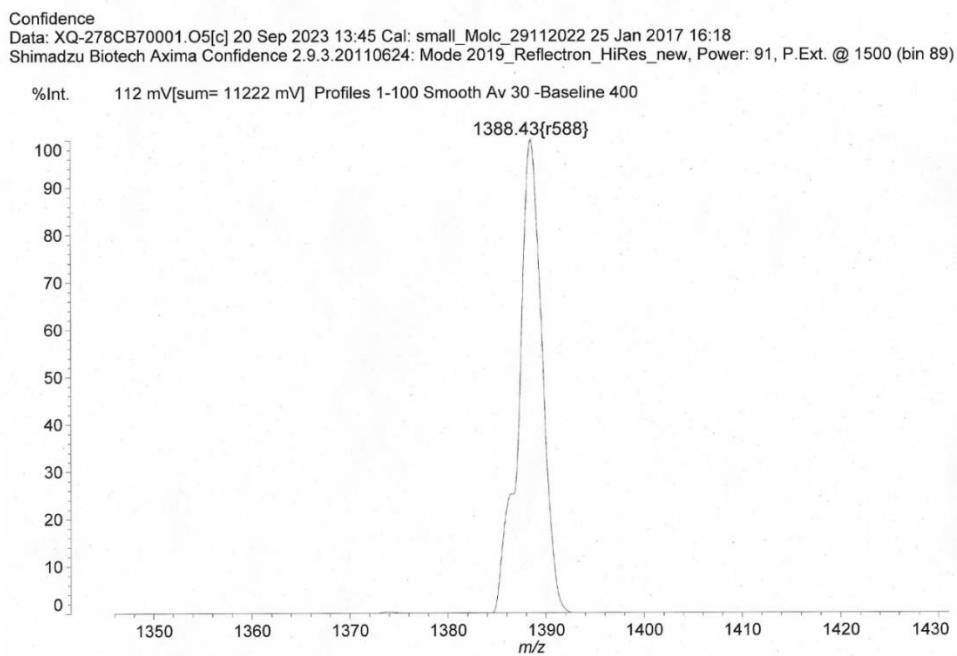


Figure S30.  $^1\text{H}$ - $^1\text{H}$  COSY NMR spectra of aryl azide **Az-3**+CB7 in 1:1 molar ratio (0.5 mM) in  $\text{D}_2\text{O}$  at 25 °C, 500 MHz.



**Figure S31.** <sup>1</sup>H NMR spectra of aryl azide **Az-3** (top) and **Az-3+CB7** (down) in 1:1 molar ratio (0.5 mM) in D<sub>2</sub>O (4.79 ppm) at 25 °C, 500 MHz.



**Figure S32.** MALDI-MS spectra of aryl azide **Az-3+CB7** in 1:1 molar ratio in Milli Q water at 25 °C.

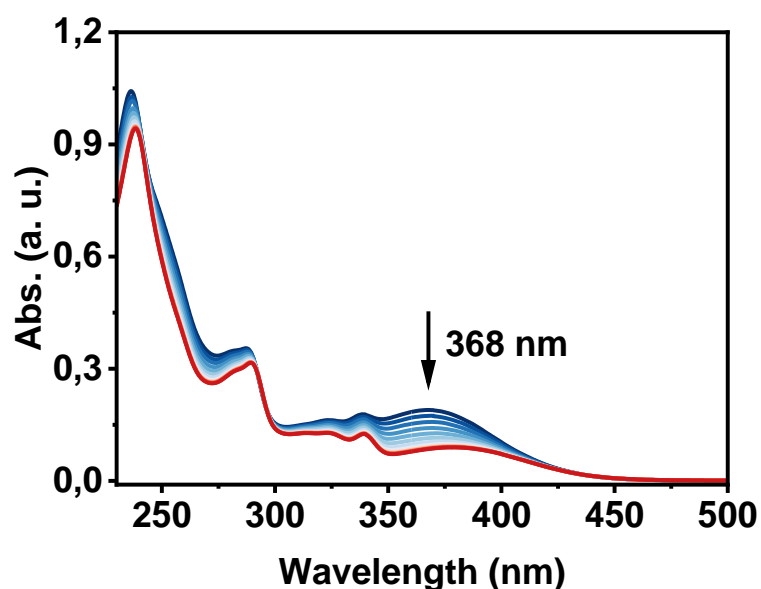


**Figure S33.** UV-vis titration spectra of **Az-1** ( $[Az-1] = 20 \mu M$ ) upon addition of **CB7** ( $[CB7] = 0-49 \mu M$ ) in Milli Q water at 25 °C.

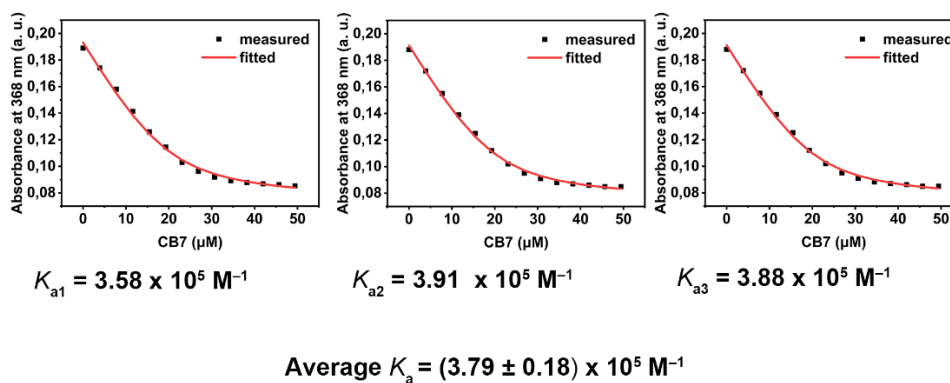


**Figure S34.** UV absorbance changes of **Az-1** at 368 nm upon increasing concentration of **CB7** in Milli Q water. The binding constant value was determined by a non-linear curve fitting. The black squares depict the acquired data. The fit according to a 1:1 binding model is shown as red line. The error was calculated from 3 replica experiments as the standard deviation.

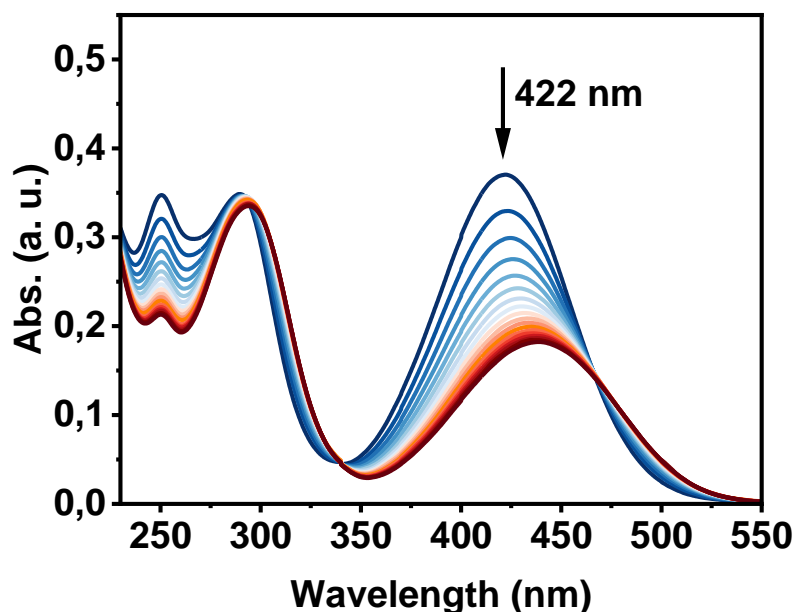


**Figure S35.** UV-vis titration spectra of **Az-2** ( $[\text{Az-2}] = 20 \mu\text{M}$ ) upon addition of **CB7** ( $[\text{CB7}] = 0\text{--}64 \mu\text{M}$ ) in Milli Q water at  $25 \text{ }^\circ\text{C}$ .

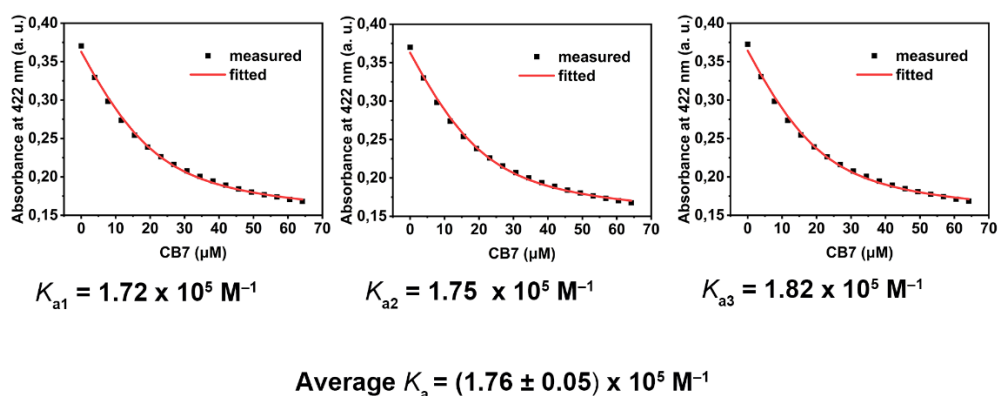


**Figure S36.** UV absorbance changes of **Az-2** at 422 nm upon increasing concentration of **CB7** in Milli Q water. The binding constant value was determined by a non-linear curve fitting. The black squares depict the acquired data. The fit according to a 1:1 binding model is shown as red line. The error was calculated from 3 replica experiments as the standard deviation.

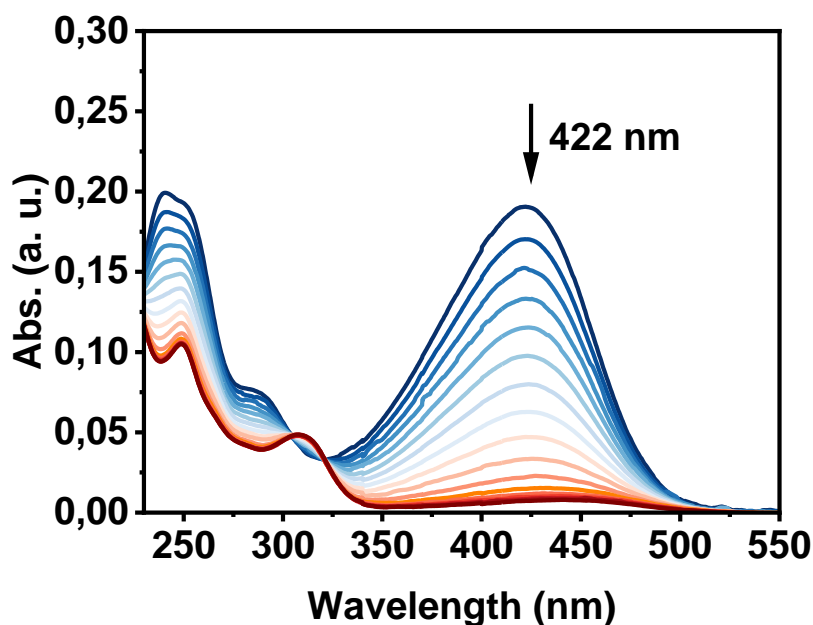


**Figure S37.** UV-vis titration spectra of Az-3 ([Az-3] = 20  $\mu\text{M}$ ) upon addition of CB7 ([CB7] = 0–38  $\mu\text{M}$ ) in Milli Q water at 25  $^{\circ}\text{C}$ .

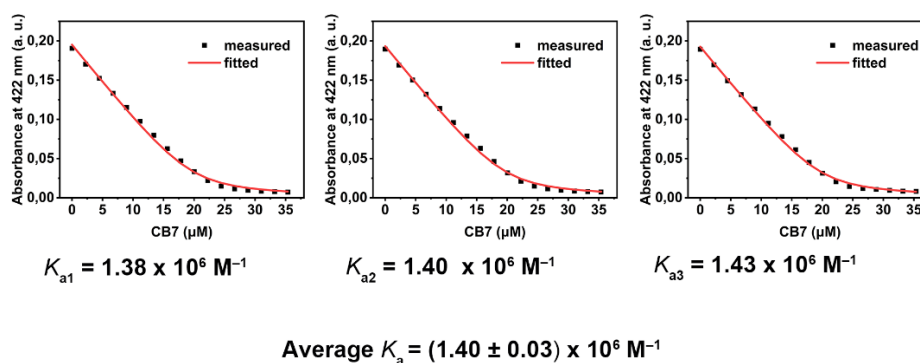


**Figure S38.** UV absorbance changes of Az-3 at 422 nm upon increasing concentration of CB7 in Milli Q water. The binding constant value was determined by a non-linear curve. The black squares depict the acquired data. The fit according to a 1:1 binding model is shown as red line. The error was calculated from 3 replica experiments as the standard deviation.

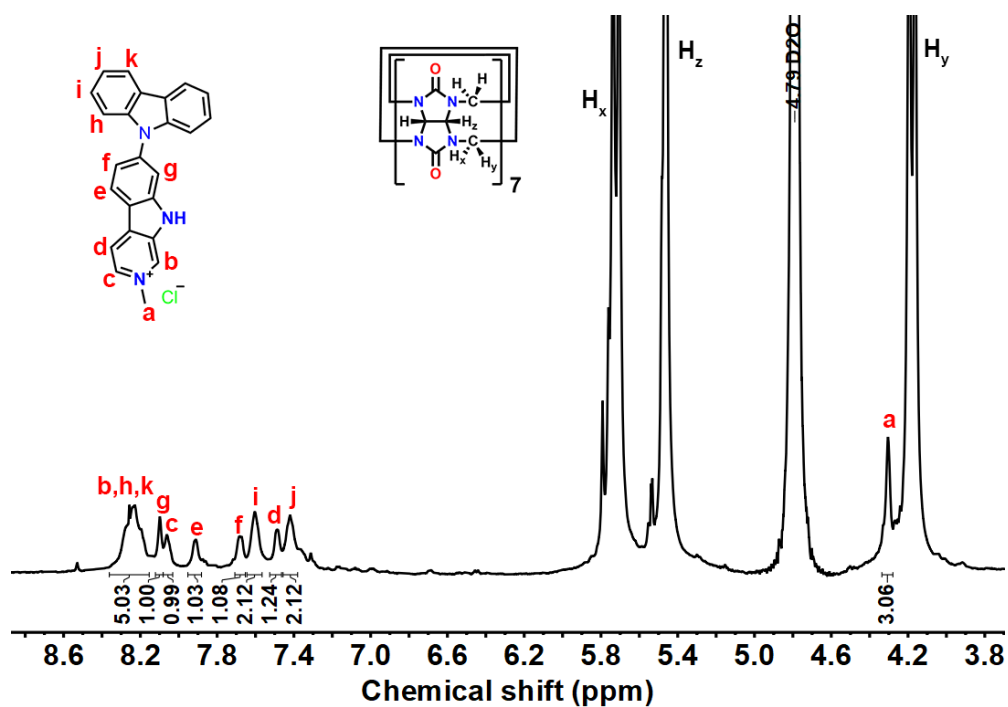


**Figure S39.**  $^1\text{H}$  NMR spectra of photolysis product carbazole **Cb-1•CB7** (0.5 mM) in  $\text{D}_2\text{O}$  at 25 °C, 500 MHz.

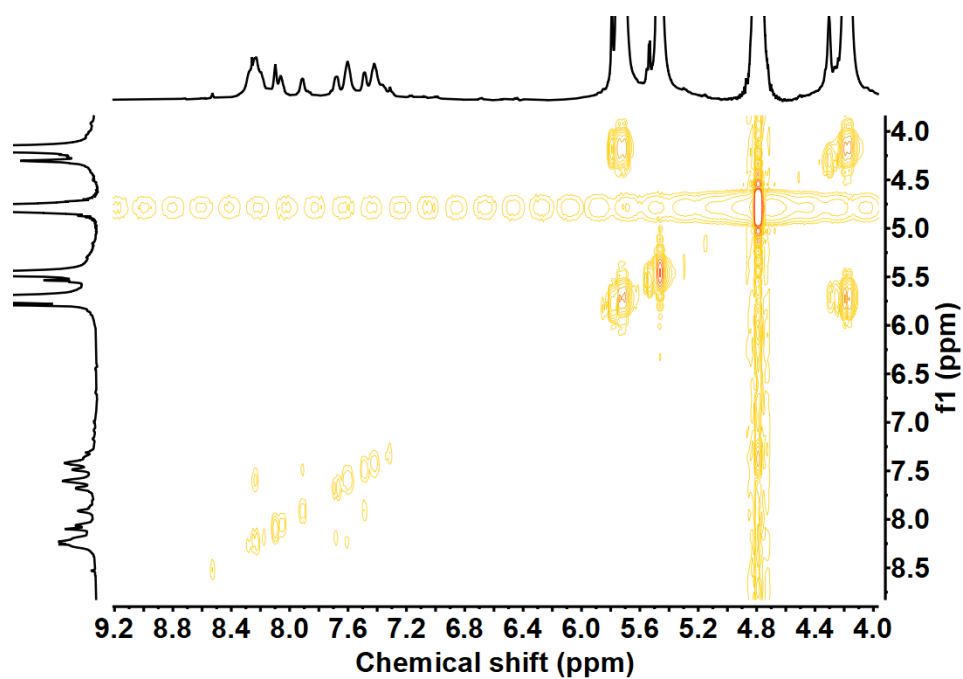


**Figure S40.**  $^1\text{H}$ - $^1\text{H}$  COSY NMR spectra of photolysis product carbazole **Cb-1•CB7** (0.5 mM) in  $\text{D}_2\text{O}$  (4.79 ppm) at 25 °C, 500 MHz.

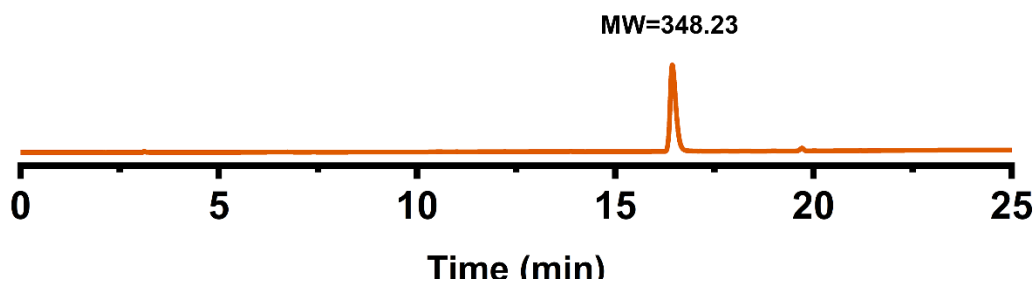


Figure S41. LC-MS of photolysis of aryl azide **Az-1**•CB7 after photoreaction.

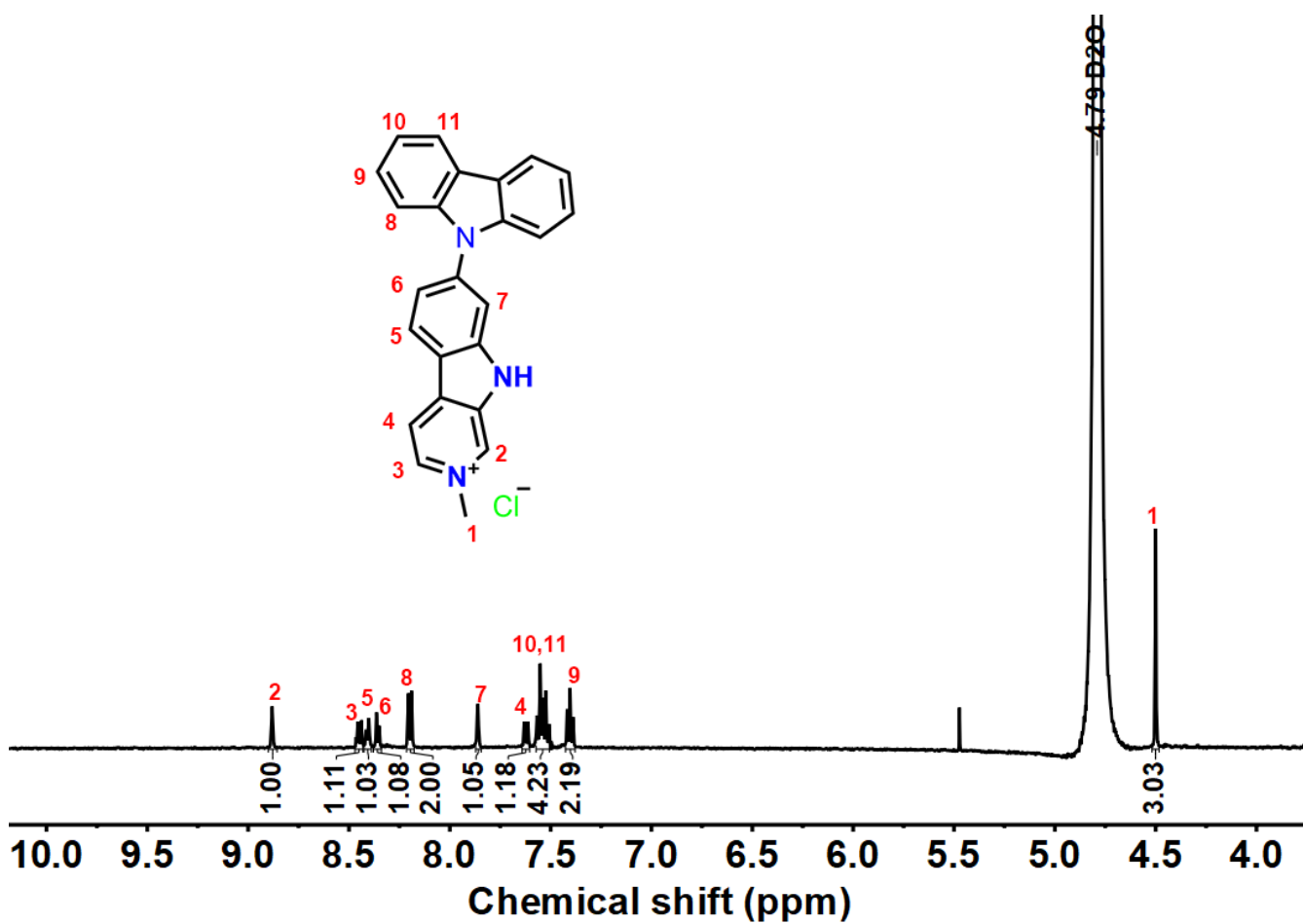
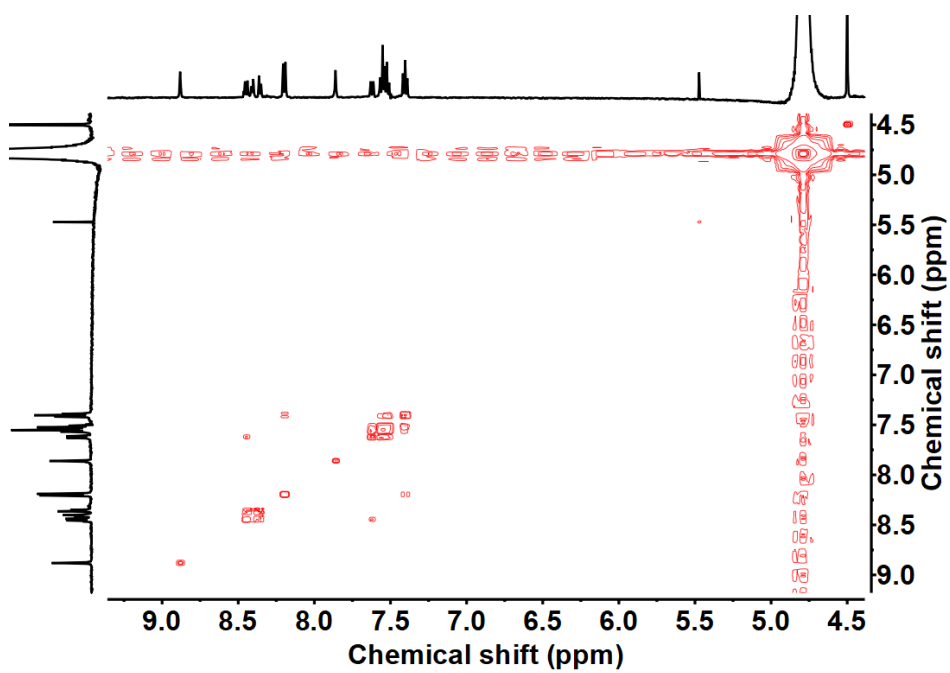
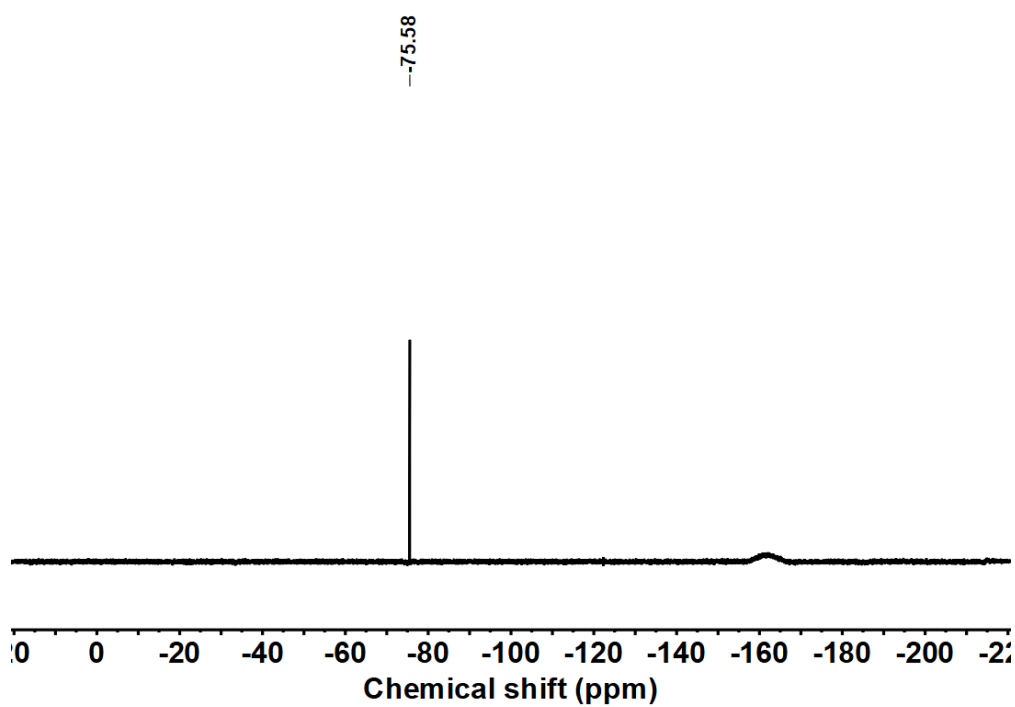


Figure S42. <sup>1</sup>H NMR spectra of photolysis product carbazole **Cb-1** (0.5 mM) in D<sub>2</sub>O at 25 °C, 500 MHz.



**Figure S43.**  $^1\text{H}$ - $^1\text{H}$  COSY NMR spectra of photolysis product carbazole **Cb-1** (0.5 mM) in  $\text{D}_2\text{O}$  (4.79 ppm) at 25 °C, 500 MHz.



**Figure S44.**  $^{19}\text{F}$  NMR spectra of photolysis product carbazole **Cb-1** (0.5 mM) in  $\text{D}_2\text{O}$  at 25 °C, 470 MHz.

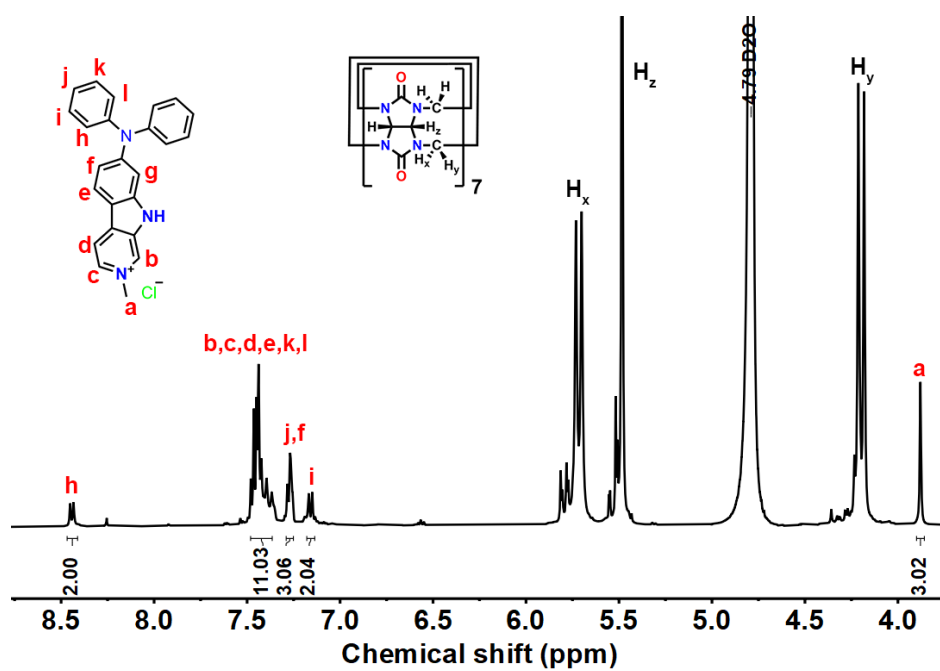


**Figure S45.** <sup>1</sup>H NMR spectra of photolysis product carbazole **Cb-2•CB7** (0.5 mM) in D<sub>2</sub>O (4.79 ppm) at 25 °C, 500 MHz.

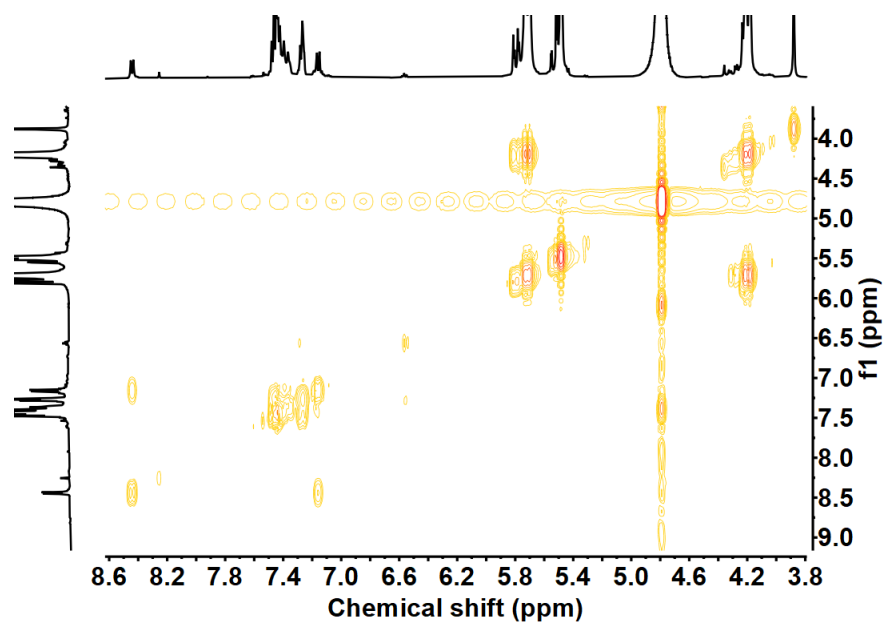


**Figure S46.** <sup>1</sup>H-<sup>1</sup>H COSY NMR spectra of photolysis product carbazole **Cb-2•CB7** (0.5 mM) in D<sub>2</sub>O (4.79 ppm) at 25 °C, 500 MHz.

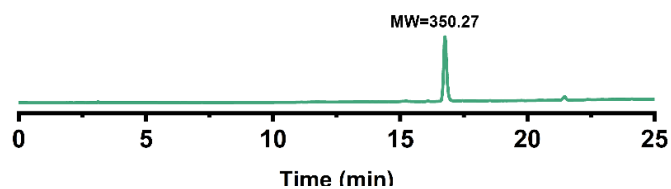


Figure S47. LC-MS of photolysis of aryl azide **Az-2**•CB7 after photoreaction.

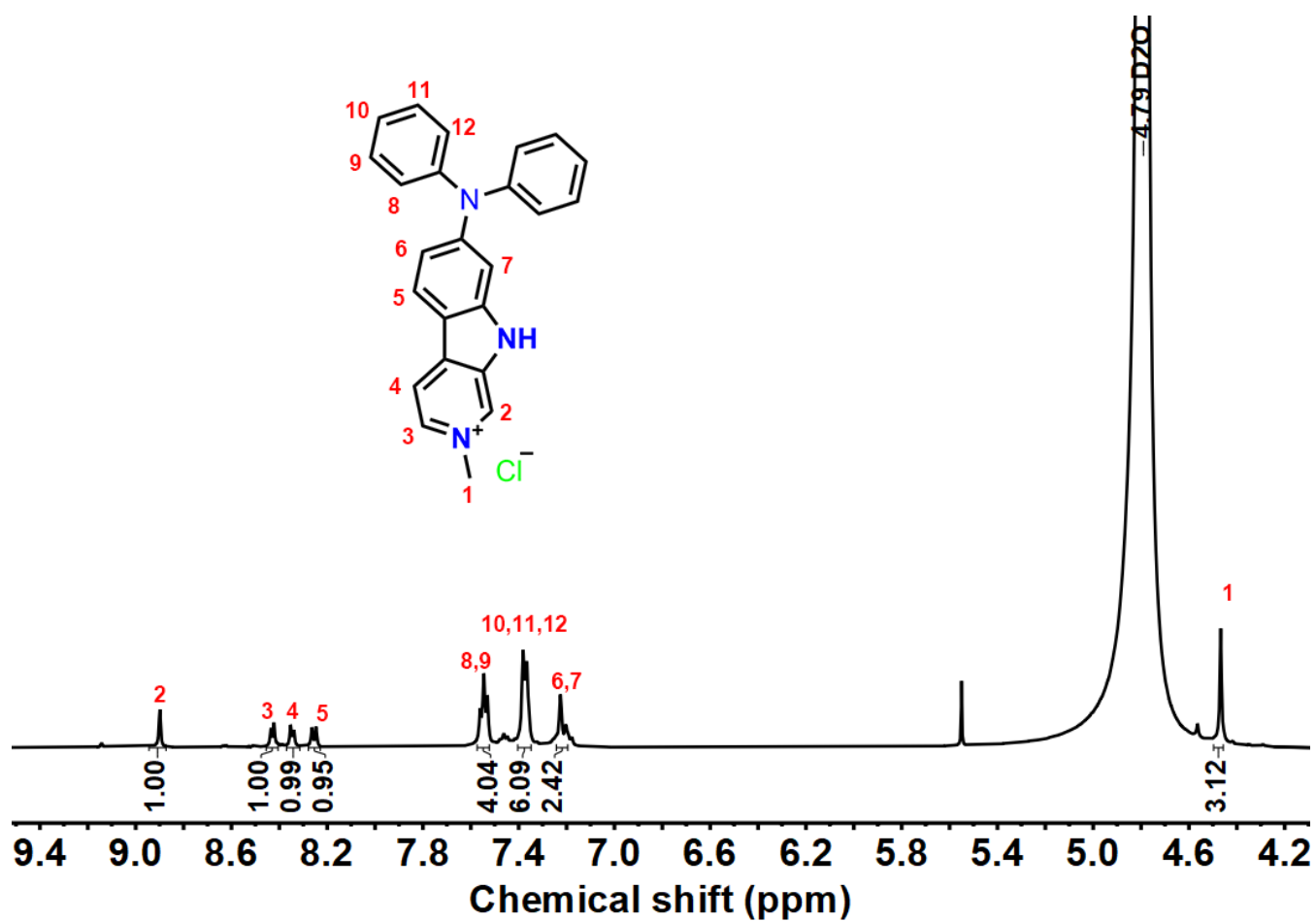
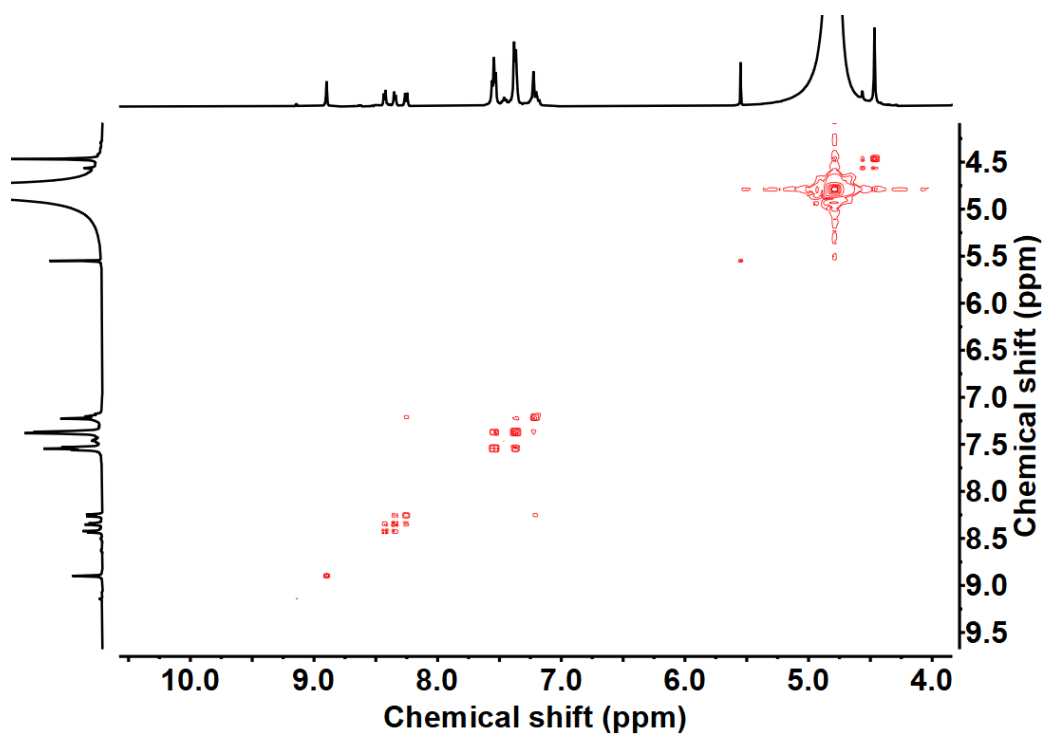
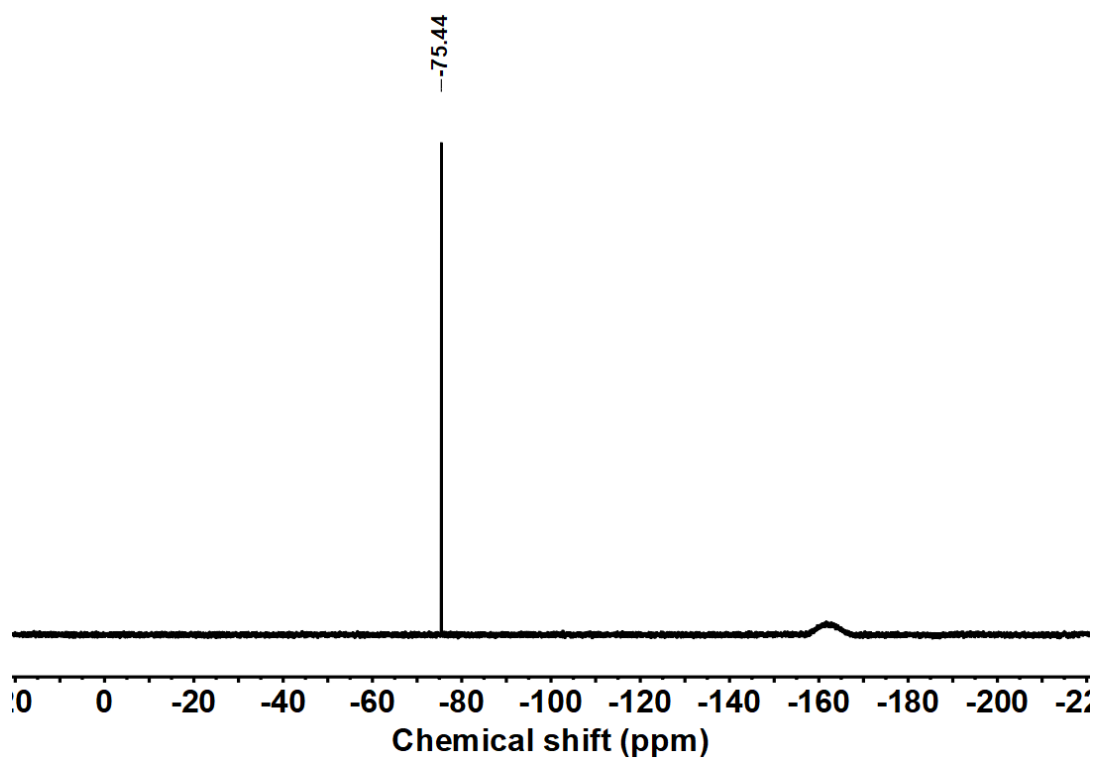


Figure S48. <sup>1</sup>H NMR spectra of photolysis product carbazole **Cb-2** (0.5 mM) in D<sub>2</sub>O (4.79 ppm) at 25 °C, 500 MHz.



**Figure S49.**  $^1\text{H}$ - $^1\text{H}$  COSY NMR spectra of photolysis product carbazole **Cb-2** (0.5 mM) in  $\text{D}_2\text{O}$  (4.79 ppm) at 25 °C, 500 MHz.



**Figure S50.**  $^{19}\text{F}$  NMR spectra of photolysis product carbazole **Cb-2** (0.5 mM) in  $\text{D}_2\text{O}$  at 25 °C, 470 MHz.

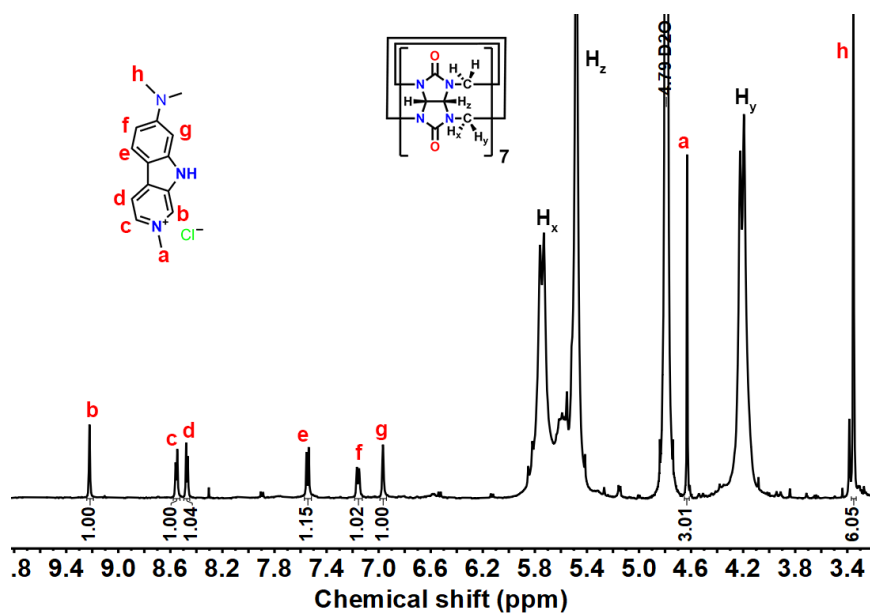


**Figure S51.**  $^1\text{H}$  NMR spectra of photolysis product carbazole **Cz-3•CB7** (0.5 mM) in  $\text{D}_2\text{O}$  (4.79 ppm) at 25 °C, 500 MHz.

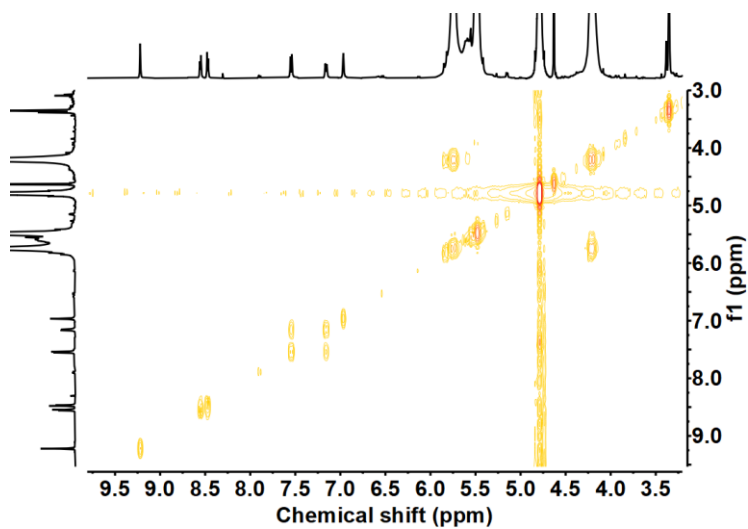


**Figure S52.**  $^1\text{H}$ - $^1\text{H}$  COSY NMR spectra of photolysis product carbazole **Cz-3•CB7** (0.5 mM) in  $\text{D}_2\text{O}$  (4.79 ppm) at 25 °C, 500 MHz.

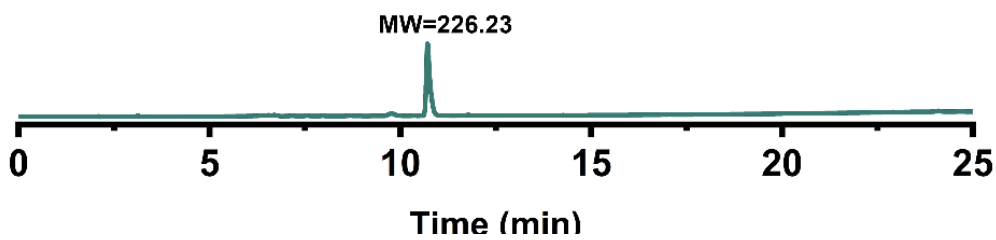


Figure S53. LC-MS of photolysis of aryl azide **Az-3**•CB7 after photoreaction.

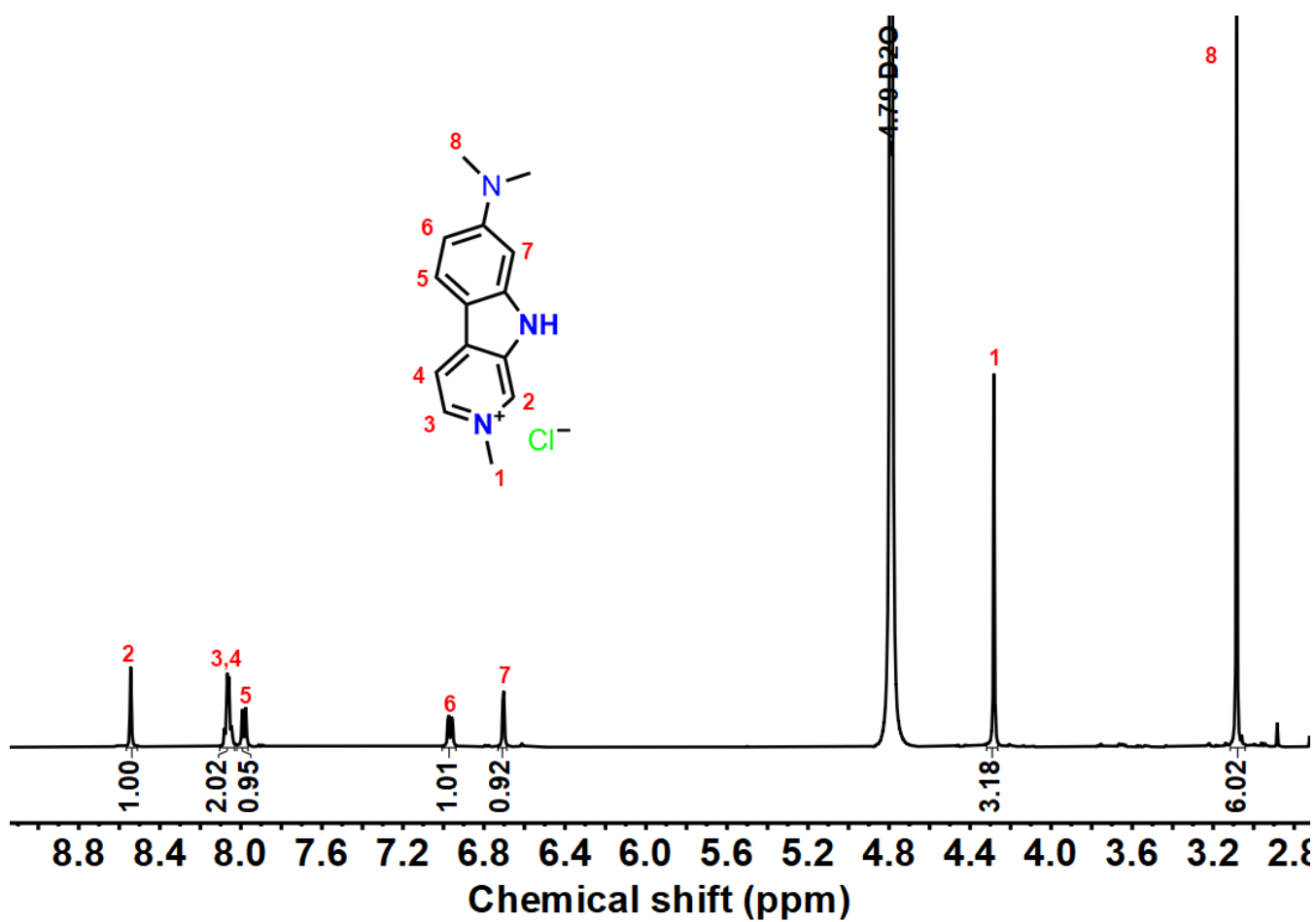
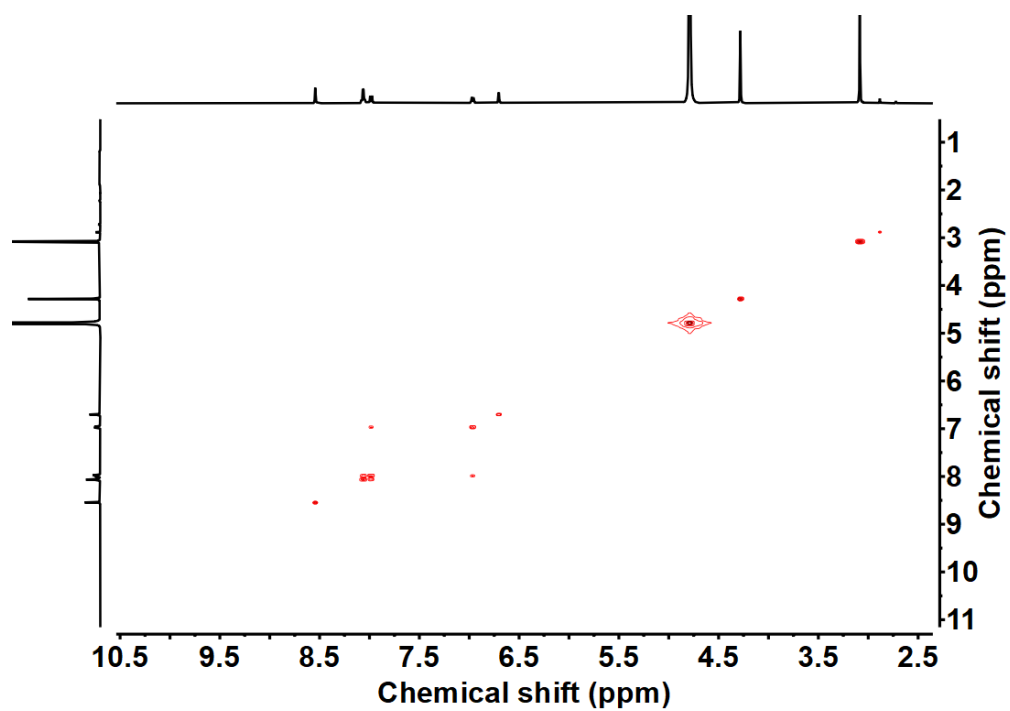
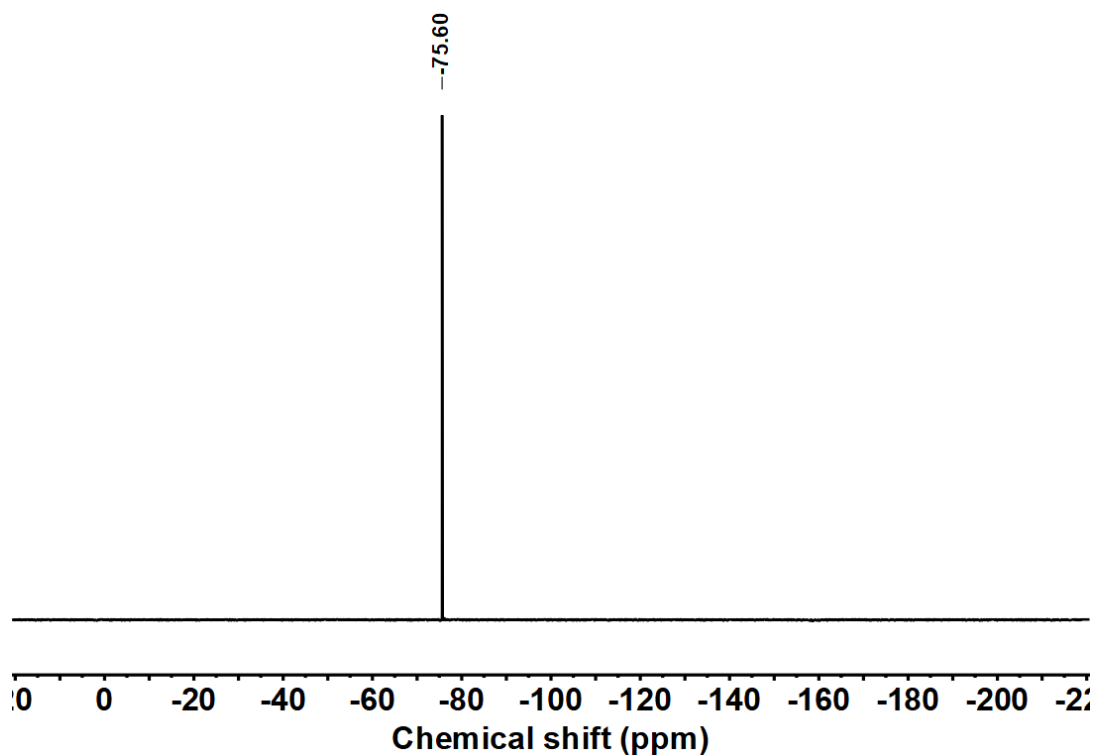


Figure S54.  $^1\text{H}$  NMR spectra of photolysis product carbazole **Cb-3** (0.5 mM) in  $\text{D}_2\text{O}$  (4.79 ppm) at 25 °C, 500 MHz.



**Figure S55.**  $^1\text{H}$ - $^1\text{H}$  COSY NMR spectra of photolysis product carbazole **Cb-3** (0.5 mM) in  $\text{D}_2\text{O}$  (4.79 ppm) at 25 °C, 500 MHz.



**Figure S56.**  $^{19}\text{F}$  NMR spectra of photolysis product carbazole **Cb-3** (0.5 mM) in  $\text{D}_2\text{O}$  at 25 °C, 470 MHz.

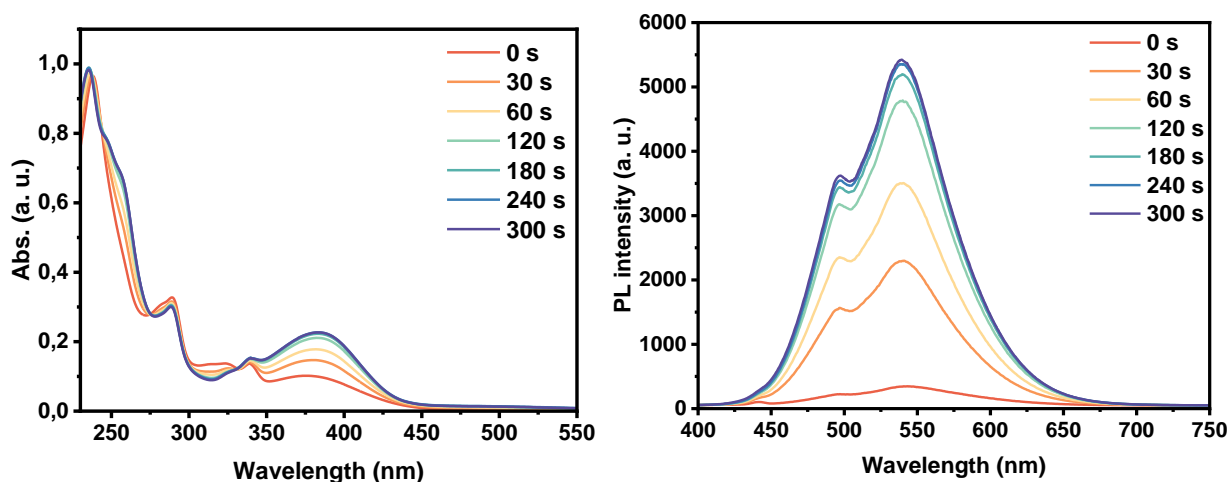


**Figure S57.** UV (left) and emission (right) spectra of photolysis of aryl azide **Az-1•CB7** (0.5 mM) after different reaction times in Milli Q water at 25 °C. The reaction mixture was diluted with Milli Q water to  $2 \times 10^{-4}$  M for UV and emission measurements ( $\lambda_{\text{ex}} = 383$  nm, Ex bandwidth = 5 nm, Em bandwidth = 5 nm).

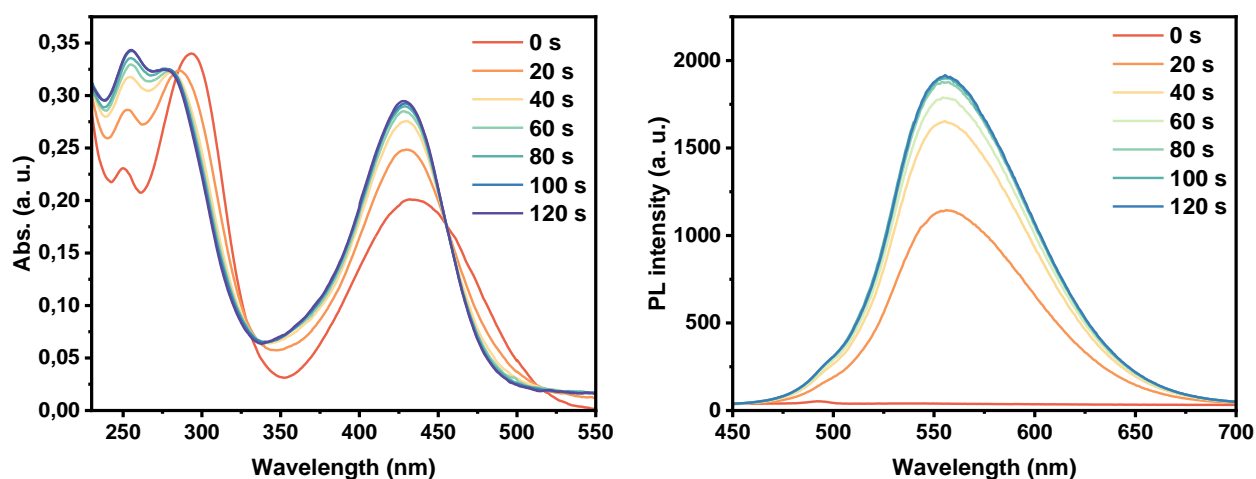


**Figure S58.** UV (left) and emission (right) spectra of photolysis of aryl azide **Az-2•CB7** (0.5 mM) after different reaction times in Milli Q water at 25 °C. The reaction mixture was diluted with Milli Q water to  $2 \times 10^{-4}$  M for UV and emission measurements ( $\lambda_{\text{ex}} = 433$  nm, Ex bandwidth = 5 nm, Em bandwidth = 5 nm).

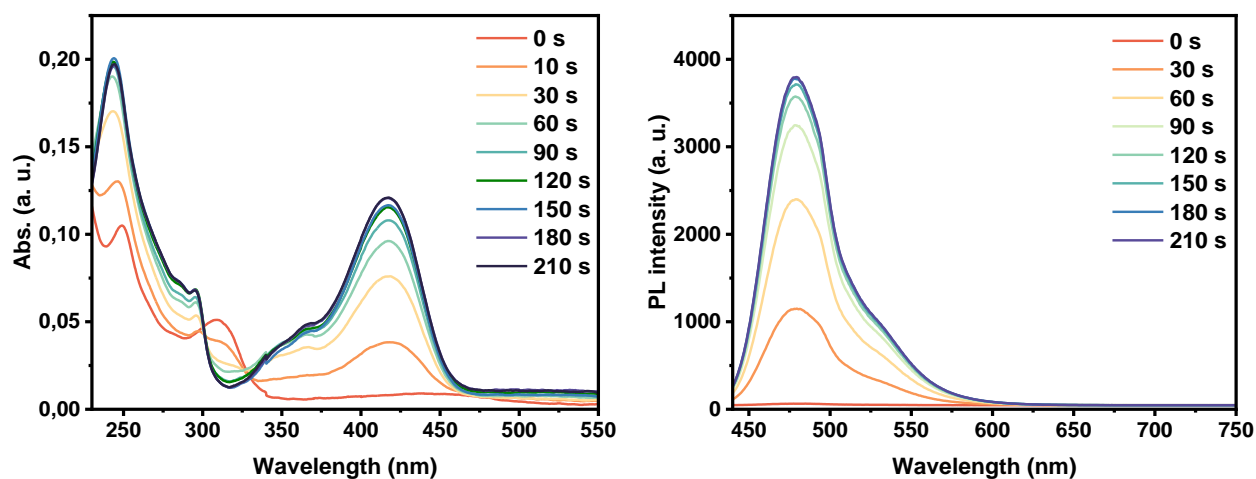


**Figure S59.** UV (left) and emission (right) spectra of photolysis of aryl azide **Az-3•CB7** (0.5 mM) after different reaction times in Milli Q water at 25 °C. The reaction mixture was diluted with Milli Q water to  $2 \times 10^{-4}$  M for UV and emission measurements ( $\lambda_{\text{ex}} = 417$  nm, Ex bandwidth = 2.5 nm, Em bandwidth = 2.5 nm).

**Table. S3.** Photophysical data for carbolines. (n. d. = not detected)

<i>Sample</i>	$\lambda_{\text{abs}}$ (nm)	$\lambda_{\text{em}}$ (nm)	PLQY (%)
<b>Cb-1</b>	375	n. d.	n. d.
<b>Cb-2</b>	410	n. d.	n. d.
<b>Cb-3</b>	400	456	17.2
<b>Cb-1•CB7</b>	383	539	11.8
<b>Cb-2•CB7</b>	433	556	6.7
<b>Cb-3•CB7</b>	417	480	43.1

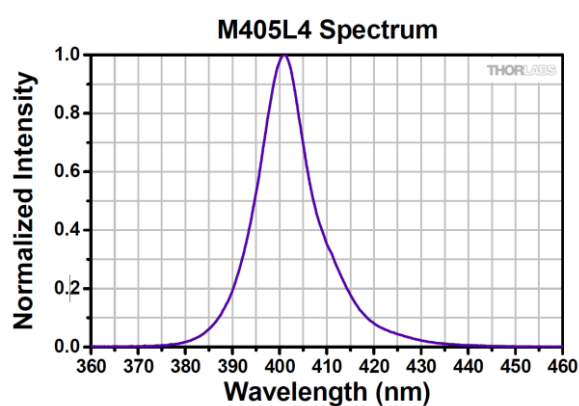


**Figure S60.** Emission spectra<sup>15</sup> of commercial LED used for the photoirradiation experiments.

### Photoreaction quantum yields of reaction within CB7

The photoreaction quantum yield was measured following a reported method.<sup>16, 17</sup> The samples were directly irradiated with an LED (M405L4 - 405 nm, 1000 mW (Min) Mounted LED, 1000 mA, THORLABS) while continuously tracking absorbance changes. The initial linear change in absorption during irradiation of the azides•CB7 was plotted against time to obtain the slope (m), see Fig. S61 as an example. The quantum yield was then calculated using the following equation:

$$\varphi = \frac{VN_Ahc}{P_{abs}\lambda_{ex}(\epsilon_{Cb\bullet CB7} - \epsilon_{Az\bullet CB7})d} m$$

Where h = Planck's constant ( $6.626 \times 10^{-34}$  Js), c = speed of light ( $2.9979 \times 10^8$  ms<sup>-1</sup>), N<sub>A</sub> = Avogadro constant, V = volume of sample, P = power of the laser,  $\lambda_{ex}$  = excitation wavelength,  $\epsilon_{Cb\bullet CB7}$  = extinction coefficient of carboline•CB7 at the probe wavelength,  $\epsilon_{Az\bullet CB7}$  = extinction coefficient of azide•CB7 at the probe wavelength, d = cuvette thickness, m = slope. The photoreaction quantum yields are calculated as 16.3% for **Az-1**•CB7, 31.4 % for **Az-2**•CB7, and 25.6 % for **Az-3**•CB7, respectively.

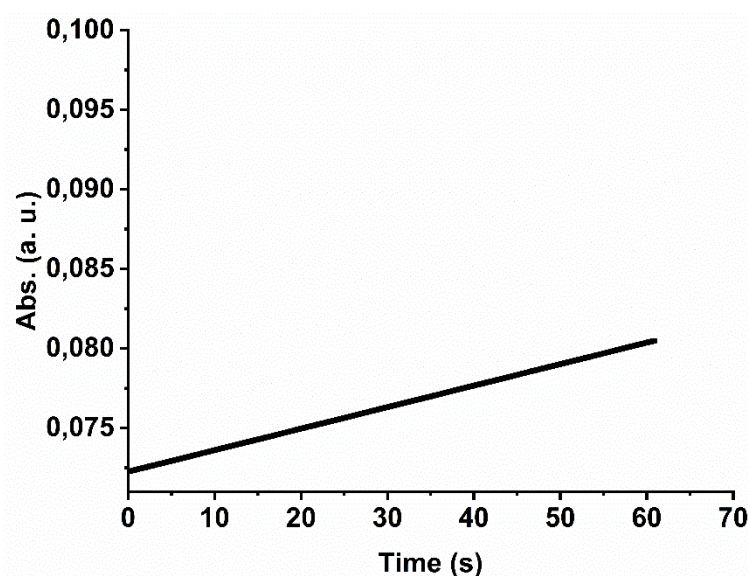


**Figure S61.** Change in the absorption of **Az-1**•CB7 at 383 nm during irradiation with 405 nm LED in different reaction time.

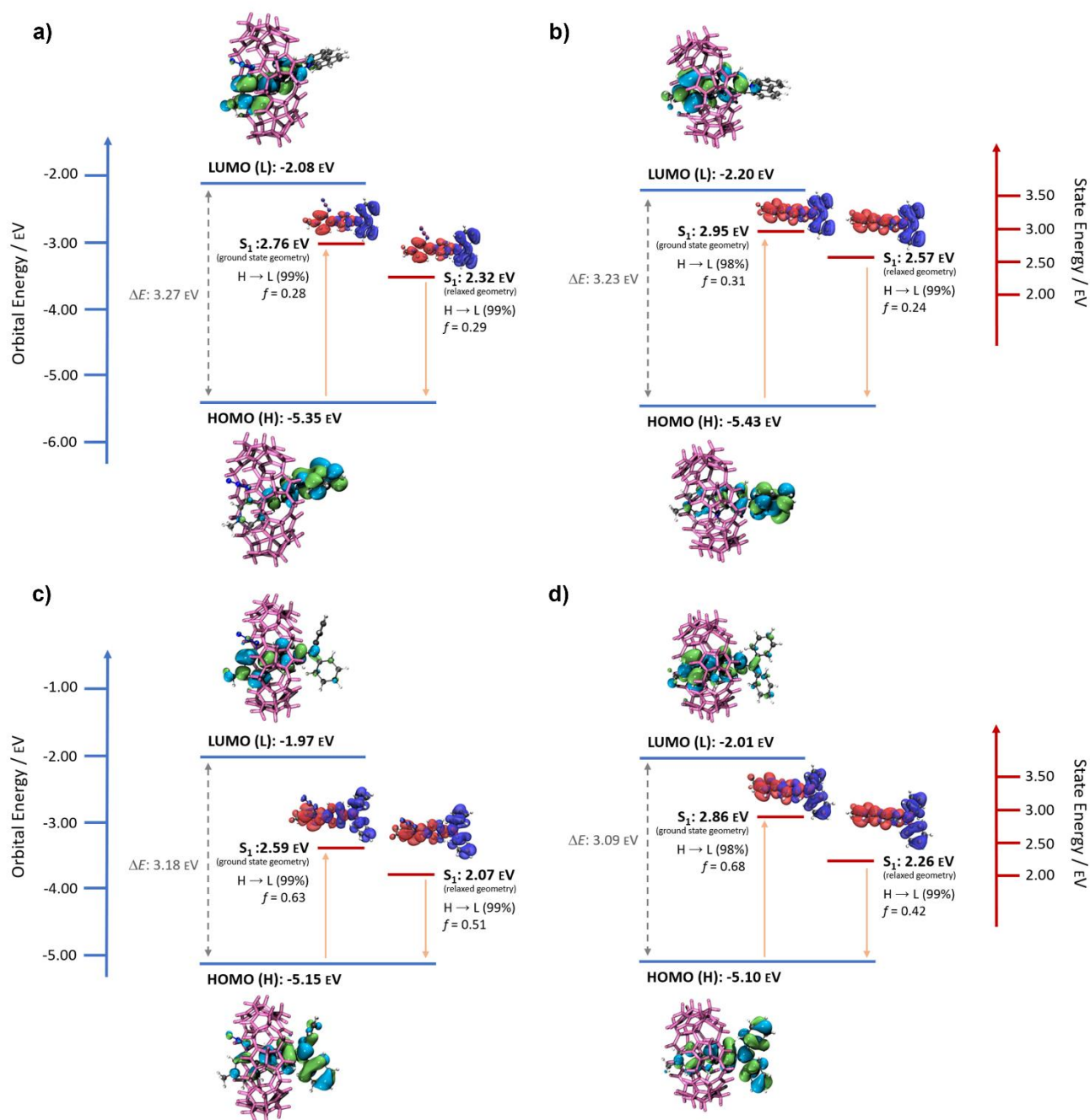


**Figure S62.** Computed frontier molecular orbitals (HOMO / LUMO) and difference density plots of the first excited singlet state at ground state and relaxed  $S_1$  geometry of a) **Az-1•CB7**, b) **Cb-1•CB7**, c) **Az-2•CB7**, b) **Cb-2•CB7** calculated at the (TD)-DFT PBE0 / 6-31+G\*\* level of theory in water (PCM). All density plots are rendered using an isovalue of 0.02. The red region of the difference density plots corresponds to an increase in electron density in the excited state; the blue to a decrease.

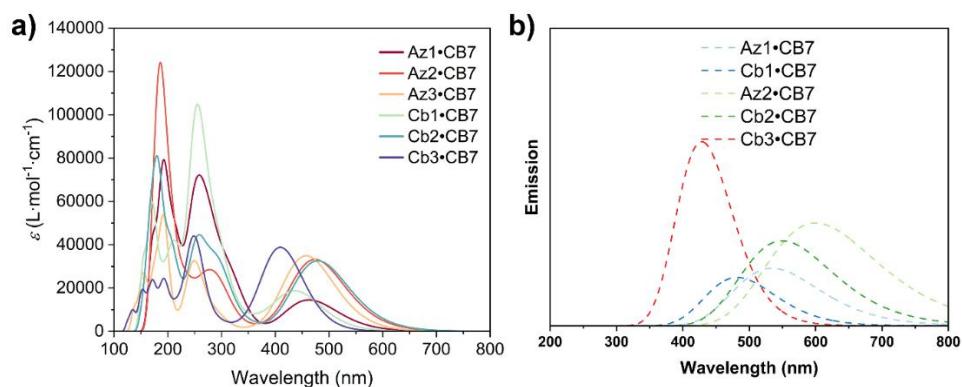


**Figure S63.** Simulated a) absorption and b) emission spectra of azides and carbolines, calculated at the TD-DFT PBE0 / 6-31+G\*\* level of theory in water (PCM). Emission spectrum of **Az-3•CB7** was not included due to insignificant oscillator strength  $f$  of the optimized  $S_1$  state.

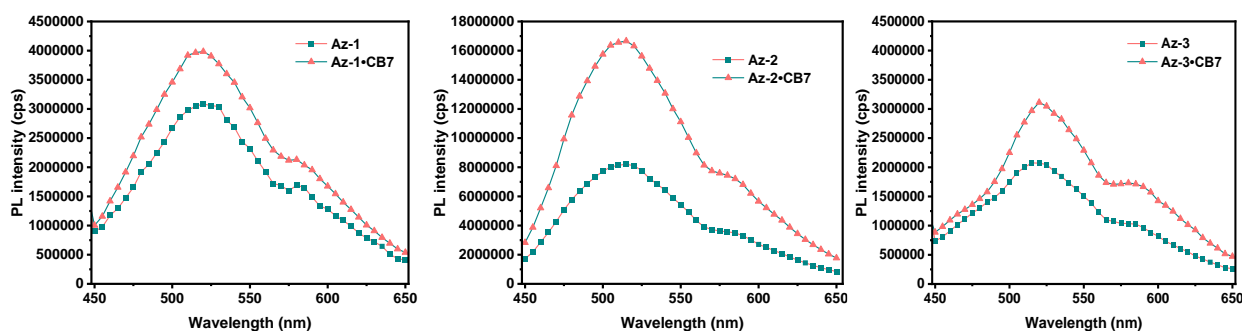


**Figure S64.** Emission spectra of aryl azide **Az-1**, **Az-1•CB7** (left), **Az-2**, **Az-2•CB7** (middle), **Az-3**, and **Az-3•CB7** (right) ( $5 \times 10^{-5}$  M) in cell media at 25 °C ( $\lambda_{ex} = 405$  nm).

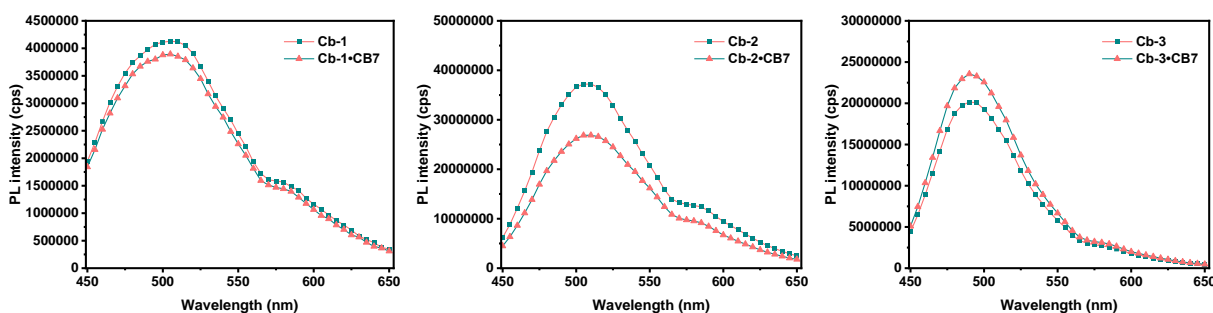


**Figure S65.** Emission spectra of carbolines **Cb-1**, **Cb-1•CB7** (left), **Cb-2**, **Cb-2•CB7** (middle), **Cb-3**, and **Cb-3•CB7** (right) ( $5 \times 10^{-5}$  M) in cell media at 25 °C ( $\lambda_{ex} = 405$  nm).

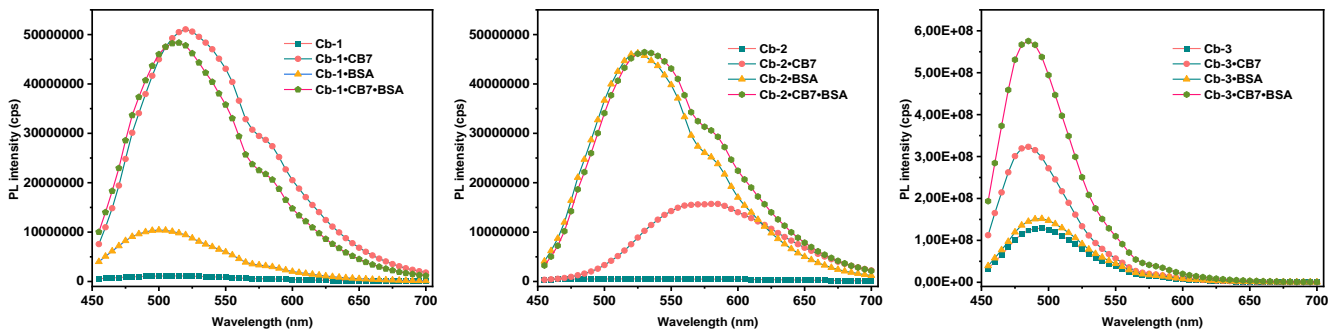


**Figure S66.** Emission spectra of carbolines **Cb-1**, **Cb-1•CB7**, **Cb-1•BSA**, **Cb-1•CB7•BSA** (left), **Cb-2**, **Cb-2•CB7**, **Cb-2•BSA**, **Cb-2•CB7•BSA** (middle), **Cb-3**, **Cb-3•CB7**, **Cb-3•BSA**, **Cb-3•CB7•BSA** (right) ( $5 \times 10^{-5}$  M) in water at 25 °C ( $\lambda_{ex} = 405$  nm).

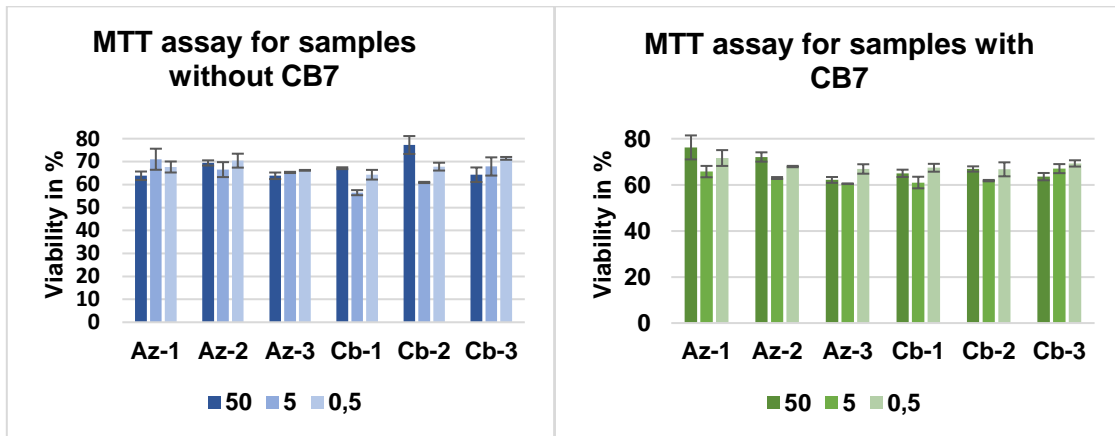


**Figure S67.** MTT Cytotoxicity assay, testing the effects of azides and carbolines samples with and without CB7 in different concentrations (50  $\mu$ M, 5  $\mu$ M, 0.5  $\mu$ M) on HeLa cells.

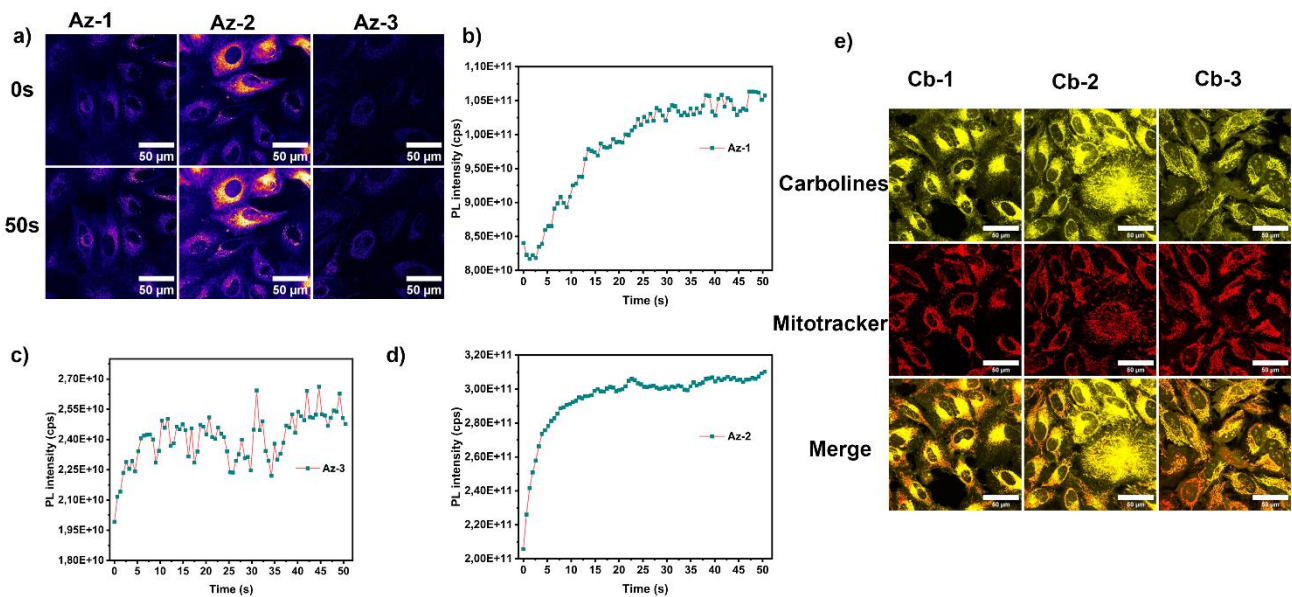


**Figure S68.** a) Confocal imaging of the photoactivation of **Az-1**, **Az-2**, and **Az-3** (5  $\mu$ M) in HeLa cells using the irradiation of 405 nm laser at different timepoints; b-d) Increase of the fluorescence intensity in HeLa cells at different timepoints of photoactivation; e) Confocal imaging of carbolines in HeLa cells.

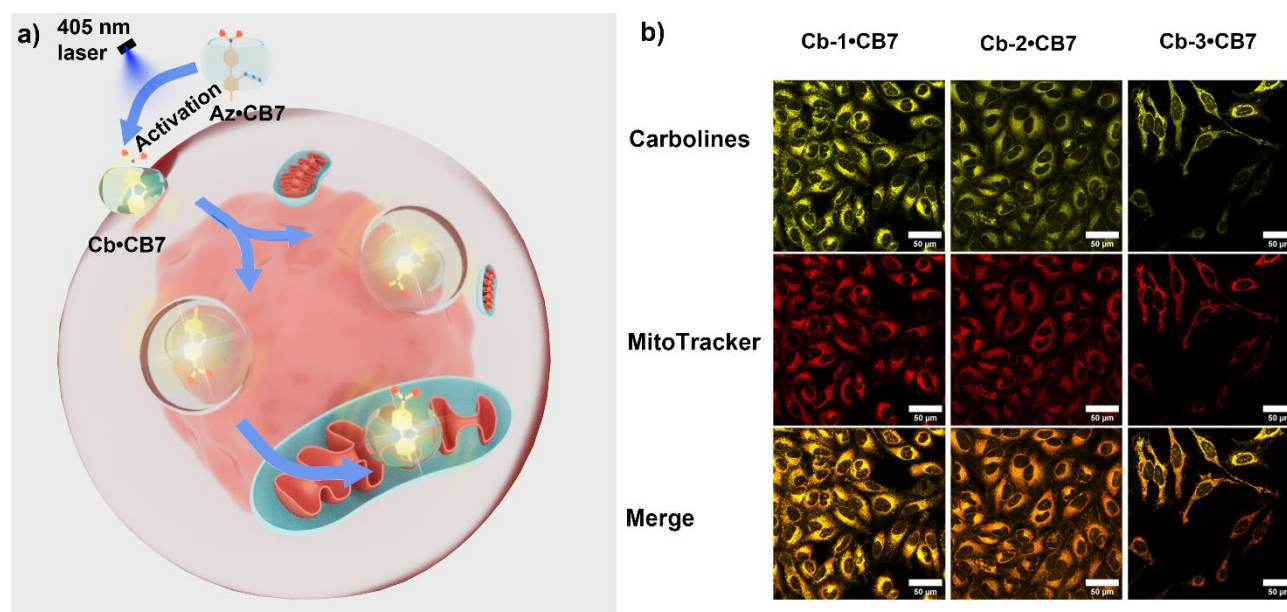


**Figure S69.** a) Schematic illustration of the preactivation of aryl azides-CB7 complex (5  $\mu$ M) before passing through the cell membrane; b) Confocal imaging of carbolines-CB7 complexes in HeLa cells.

### Interaction with FBS

To better understand how **Cb-1**, **Cb-2**, **Cb-3**, and their complexes with CB7 interact with serum proteins, we performed PL measurements using 5  $\mu$ M aliquots prepared in cell media containing different amounts of fetal bovine serum (FBS) (10 %, 5 %, 1 % and 0 %) For **Cb-1** and **Cb-2**, 0% FBS resulted in the lowest PL intensity. The increase in serum concentration up to 5% FBS was directly linked to an elevation of PL intensity. In contrast, when encapsulated in the CB7 cavity, both **Cb-1** and **Cb-2** exhibited significantly enhanced emission at 10% FBS, making them more suitable for cell imaging.

Interestingly, **Cb-3** showed peak emission at 1%, closely followed by 0%, while 5% and 10% FBS resulted in lower emissions. This can be explained by DFT calculations indicating that **Cb-3** is unaffected by water quenching and doesn't rely on protein pocket encapsulation. Thus, higher protein concentrations may limit its emission. Notably, CB7 increased **Cb-3** emission at both 10% and 5% FBS concentrations significantly (Figure S59, S60).

We then proceeded to incubate the cells using sample solutions containing different concentrations of FBS (0%, 1 %, 5 % and 10%) in cell media. Interestingly 1 % FBS displayed the highest PL emission for all samples

except **Cb-3**. This can be attributed to the upregulation of endosomal uptake. However for **Cb-3** these effects are neglected resulting strongly elevated PL for 0 % FBS (Figure S59, S60). Furthermore, CB7 mediated uptake displays a stronger PL for **Cb-1** and **Cb-3** proving the cavity's improvement of cellular uptake. The equal emission shown by **Cb-2** and **Cb-2•CB7** at 1 % can be explained by the significantly higher emission of **Cb-2** in the presence of FBS compared to **Cb-2•CB7** (Figure S61-72).

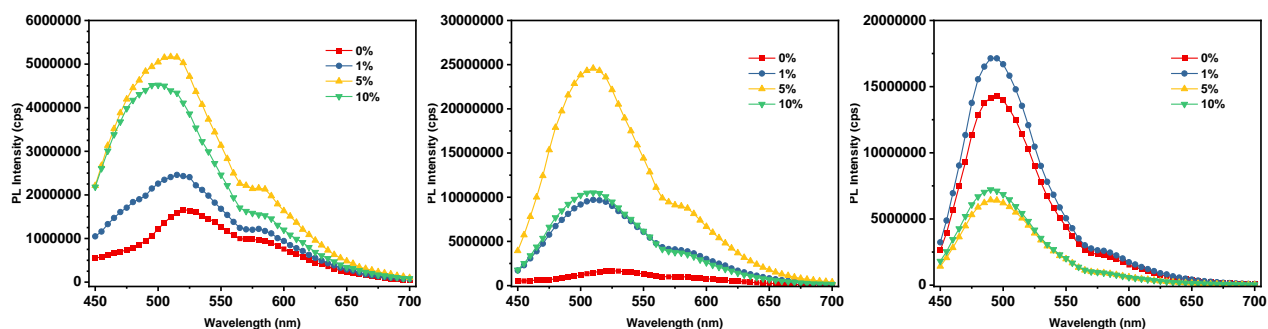


**Figure S70.** Emission spectra of carbolines ( $5 \times 10^{-5}$  M): **Cb-1** with different concentration of serum (left), **Cb-2** with different concentration of serum (middle), **Cb-3** with different concentration of serum (right) at 25 °C ( $\lambda_{\text{ex}} = 405$  nm).

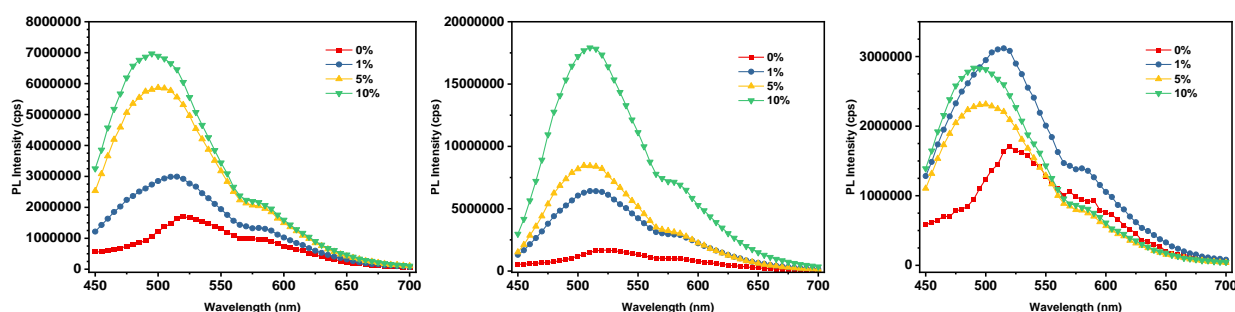


**Figure S71.** Emission spectra of carbolines-CB7 complex ( $5 \times 10^{-5}$  M): **Cb-1•CB7** with different concentration of serum (left), **Cb-2•CB7** with different concentration of serum (middle), **Cb-3•CB7** with different concentration of serum (right) at 25 °C ( $\lambda_{\text{ex}} = 405$  nm).

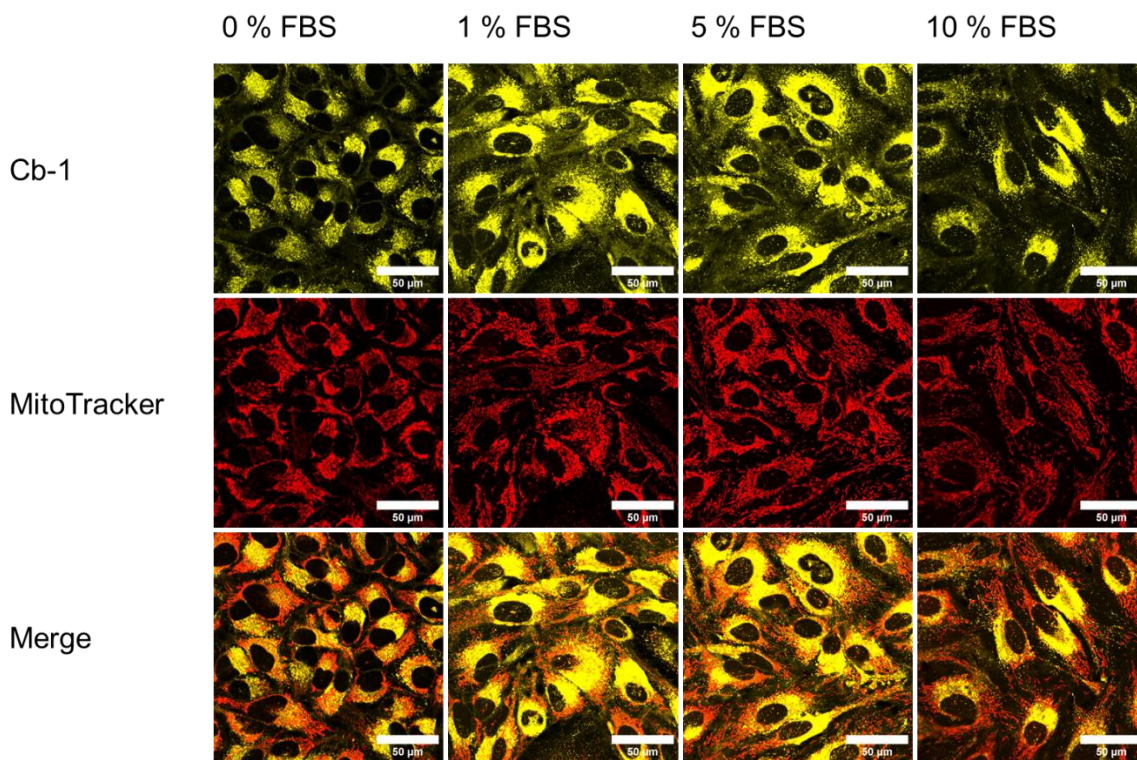


**Figure S72.** Confocal imaging of HeLa Cells treated with 5  $\mu\text{m}$  **Cb-1** diluted in cell media with different FBS concentrations (0 %, 1 %, 5 % and 10 %). Displayed are Images of Cb-1, Mitotracker and a merged image.

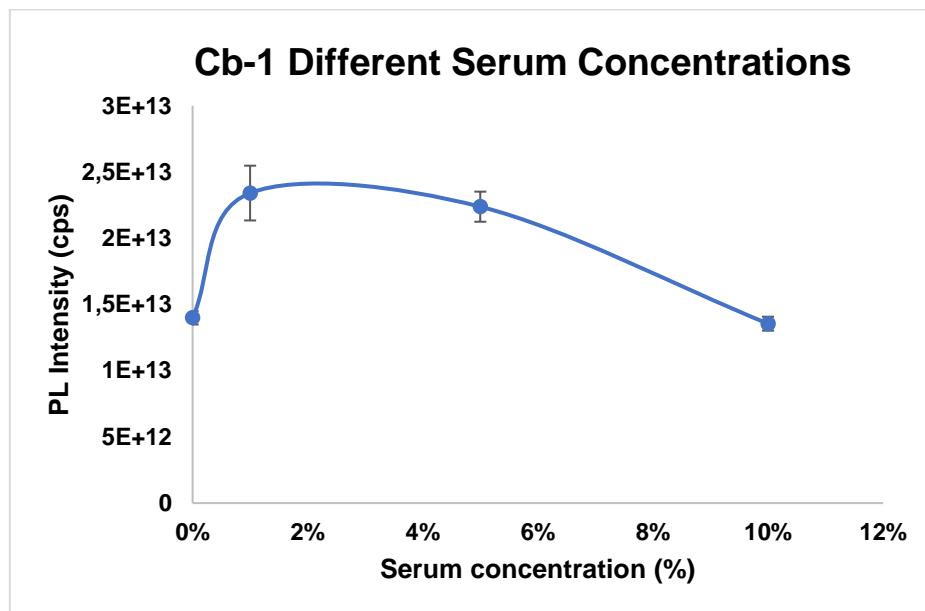


**Figure S73.** PL intensity of HeLa Cells treated with 5  $\mu\text{m}$  **Cb-1** diluted in cell media with different FBS concentrations (0 %, 1 %, 5 % and 10 %).

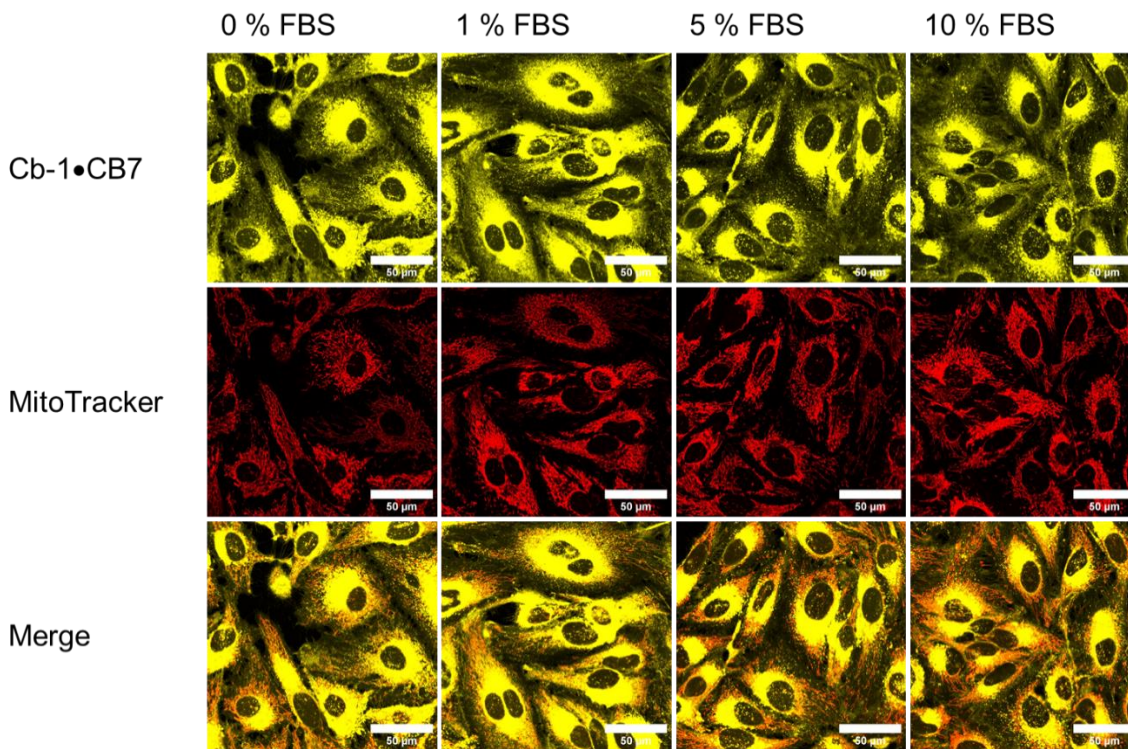


**Figure S74.** Confocal imaging of HeLa Cells treated with 5  $\mu\text{m}$  **Cb-1•CB7** diluted in cell media with different FBS concentrations (0 %, 1 %, 5 % and 10 %). Displayed are Images of **Cb-1•CB7**, Mitotracker and a merged image.

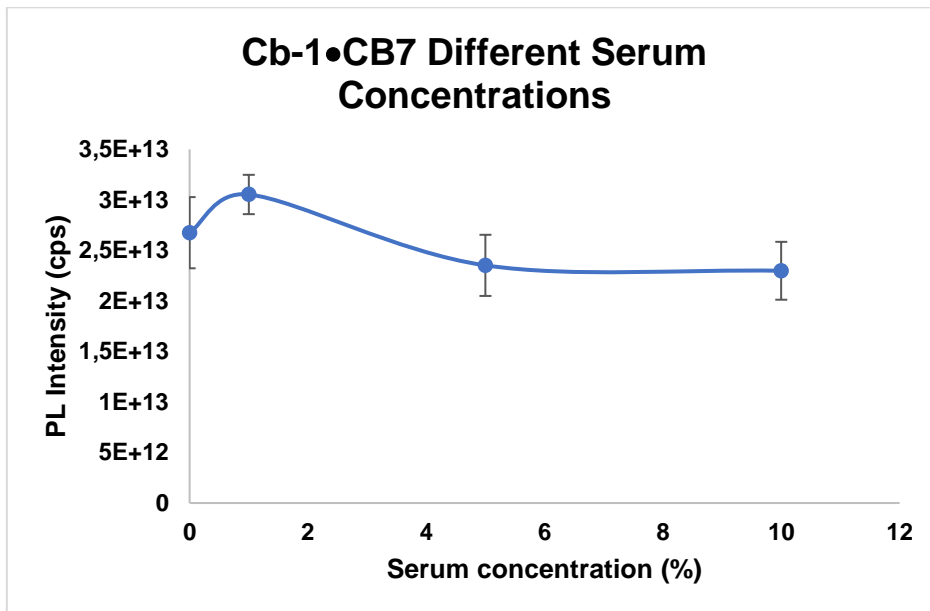


**Figure S75.** PL intensity of HeLa Cells treated with 5  $\mu\text{m}$  **Cb-1•CB7** diluted in cell media with different FBS concentrations (0 %, 1 %, 5 % and 10 %).

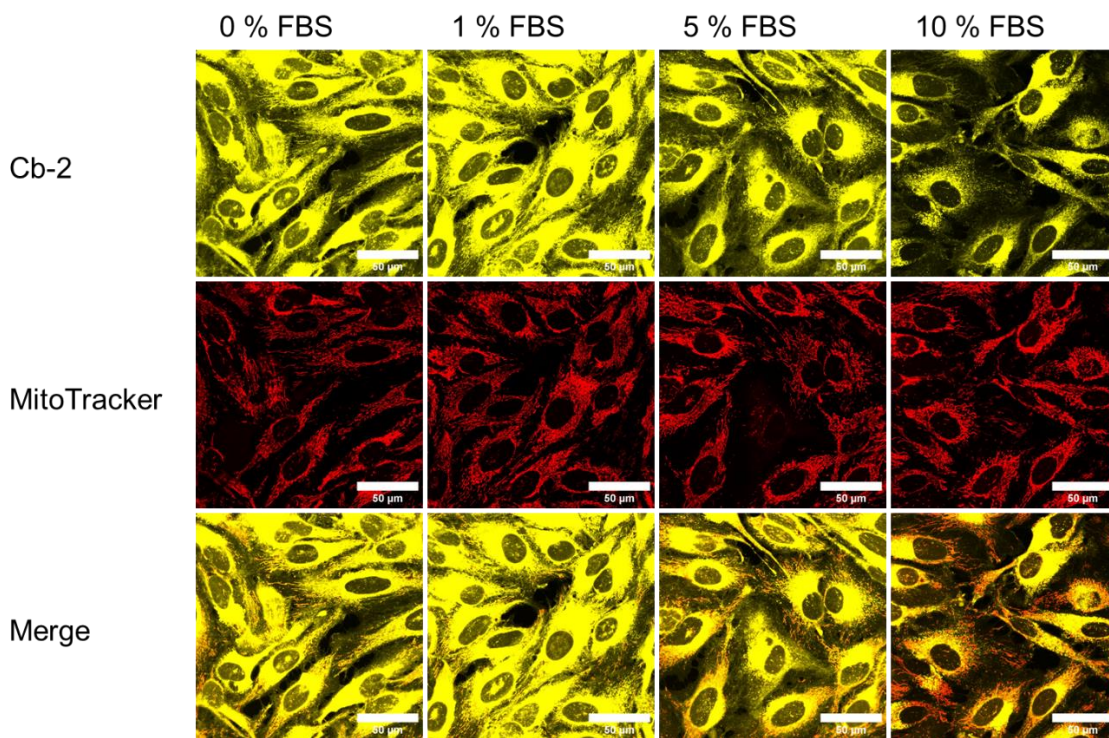


**Figure S76.** Confocal imaging of HeLa Cells treated with 5  $\mu\text{m}$  **Cb-2** diluted in cell media with different FBS concentrations (0 %, 1 %, 5 % and 10 %). Displayed are Images of Cb-2, Mitotracker and a merged image.

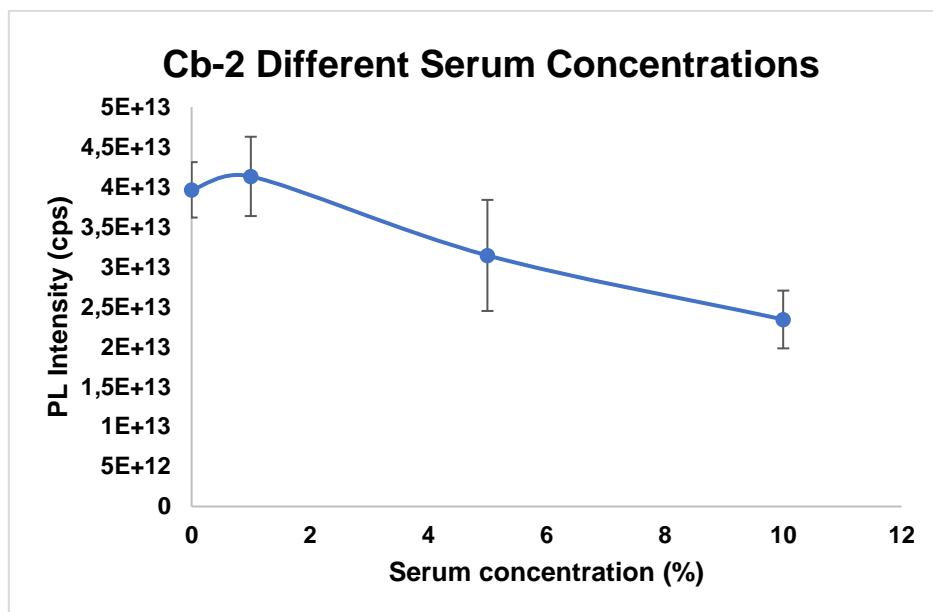


**Figure S77.** PL intensity of HeLa Cells treated with 5  $\mu\text{m}$  **Cb-2** diluted in cell media with different FBS concentrations (0 %, 1 %, 5 % and 10 %).

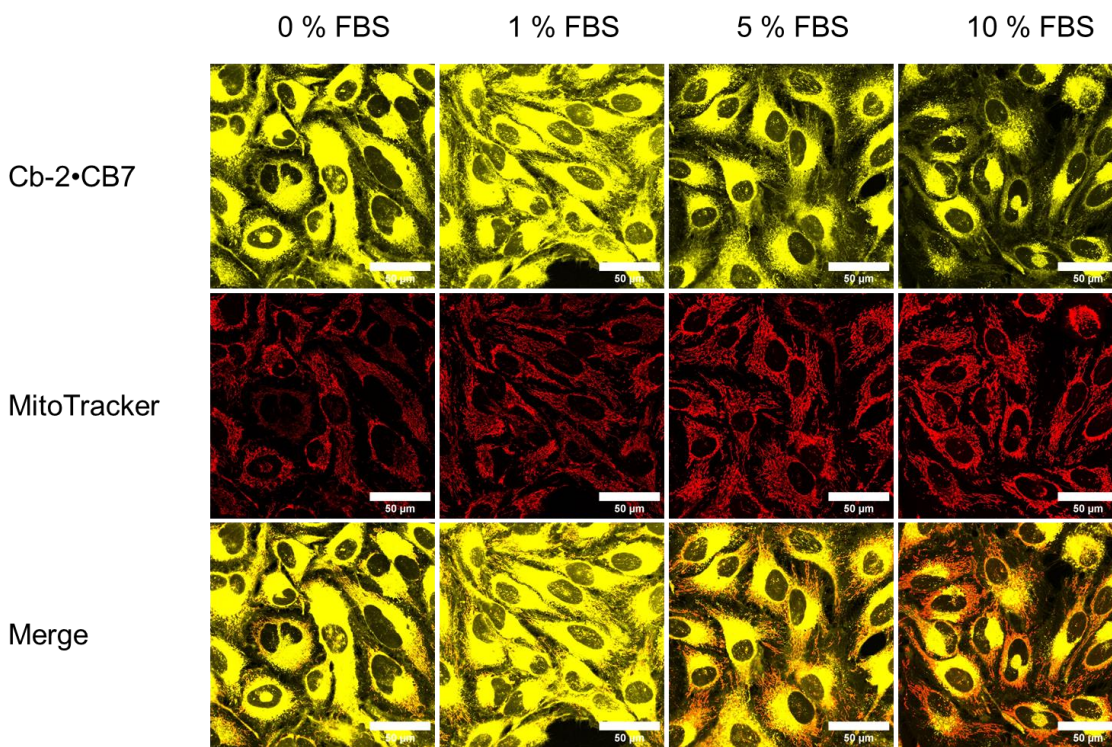


**Figure S78.** Confocal imaging of HeLa Cells treated with 5  $\mu\text{m}$  **Cb-2•CB7** diluted in cell media with different FBS concentrations (0 %, 1 %, 5 % and 10 %). Displayed are Images of **Cb-2•CB7**, Mitotracker and a merged image.

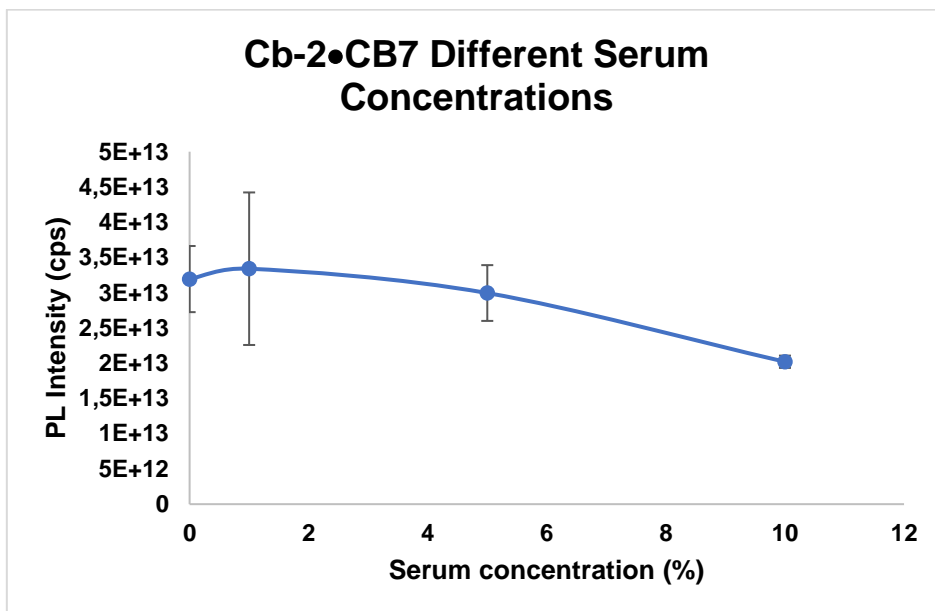


**Figure S79.** PL intensity of HeLa Cells treated with 5  $\mu\text{m}$  **Cb-2•CB7** diluted in cell media with different FBS concentrations (0 %, 1 %, 5 % and 10 %).

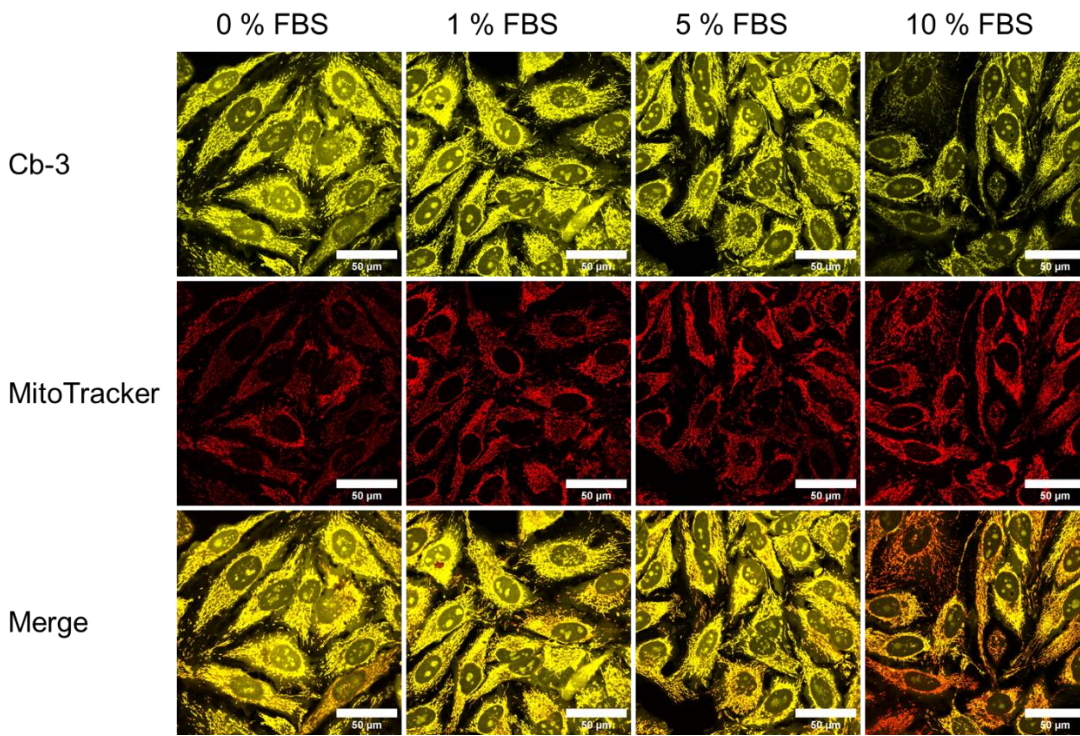


**Figure S80.** Confocal imaging of HeLa Cells treated with 5  $\mu\text{m}$  **Cb-3** diluted in cell media with different FBS concentrations (0 %, 1 %, 5 % and 10 %). Displayed are Images of **Cb-3**, Mitotracker and a merged image.

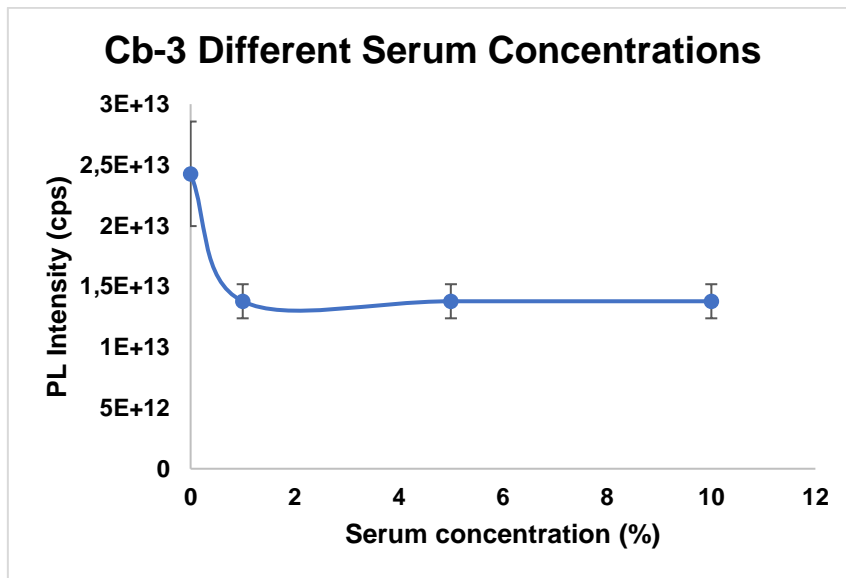


**Figure S81.** PL intensity of HeLa Cells treated with 5  $\mu\text{m}$  **Cb-3** diluted in cell media with different FBS concentrations (0 %, 1 %, 5 % and 10 %).

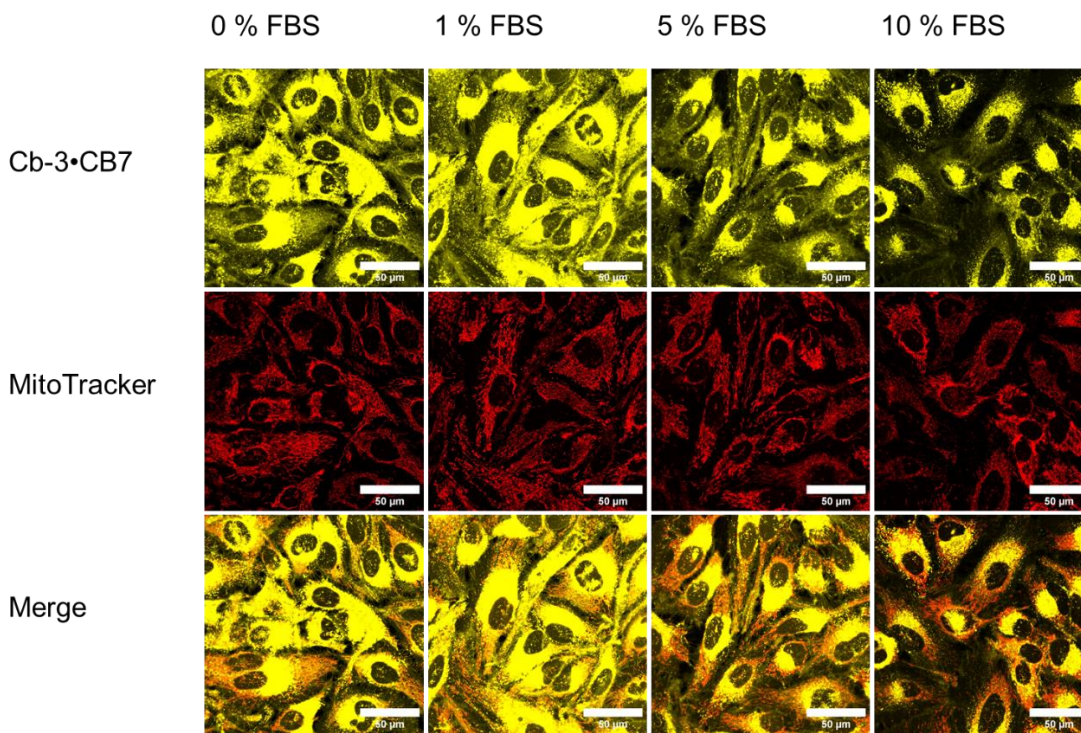


**Figure S82.** Confocal imaging of HeLa Cells treated with 5  $\mu\text{m}$  **Cb-3•CB7** diluted in cell media with different FBS concentrations (0 %, 1 %, 5 % and 10 %). Displayed are Images of **Cb-3•CB7**, Mitotracker and a merged image.

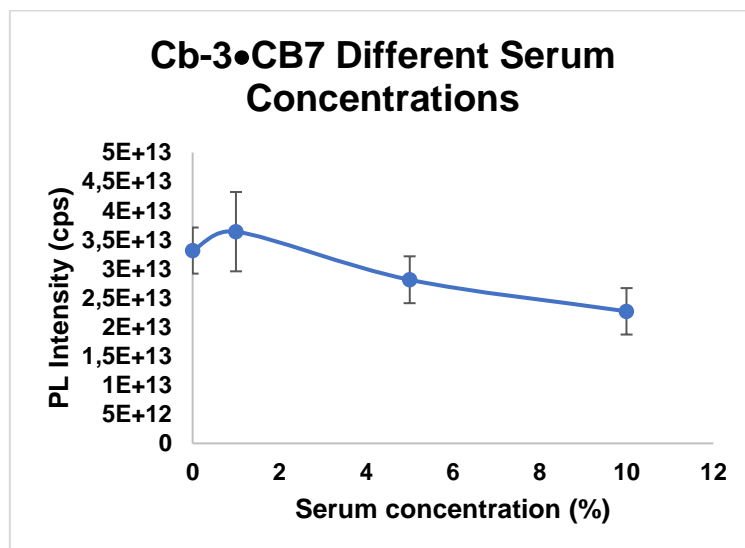


**Figure S83.** PL intensity of HeLa Cells treated with 5  $\mu\text{m}$  **Cb-3•CB7** diluted in cell media with different FBS concentrations (0 %, 1 %, 5 % and 10 %).

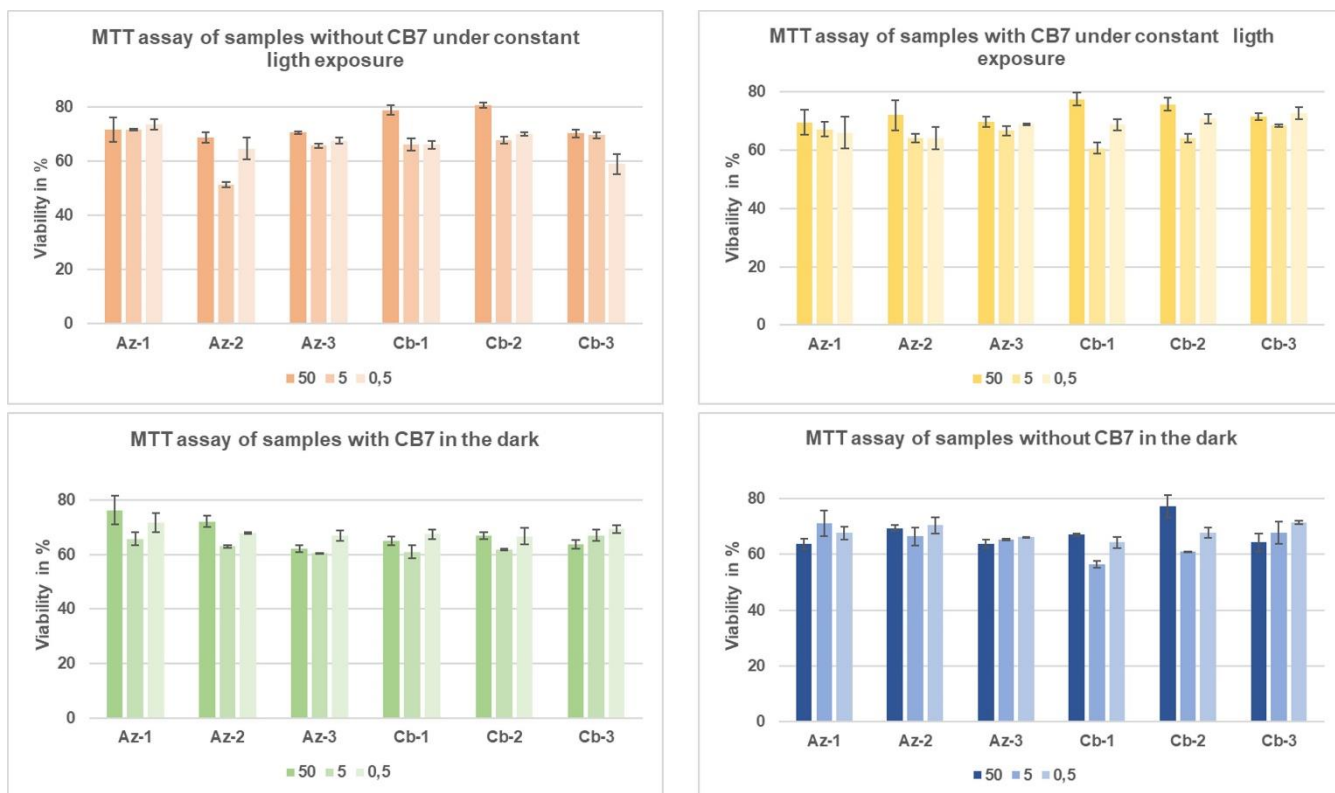


**Figure S84.** MTT Cytotoxicity assay, testing the effects of azides and carbolines samples with and without CB7 in different concentrations (50  $\mu\text{M}$ , 5  $\mu\text{M}$ , 0.5  $\mu\text{M}$ ) on Hela cells with and without light exposure.

## Additional Data and Characterization

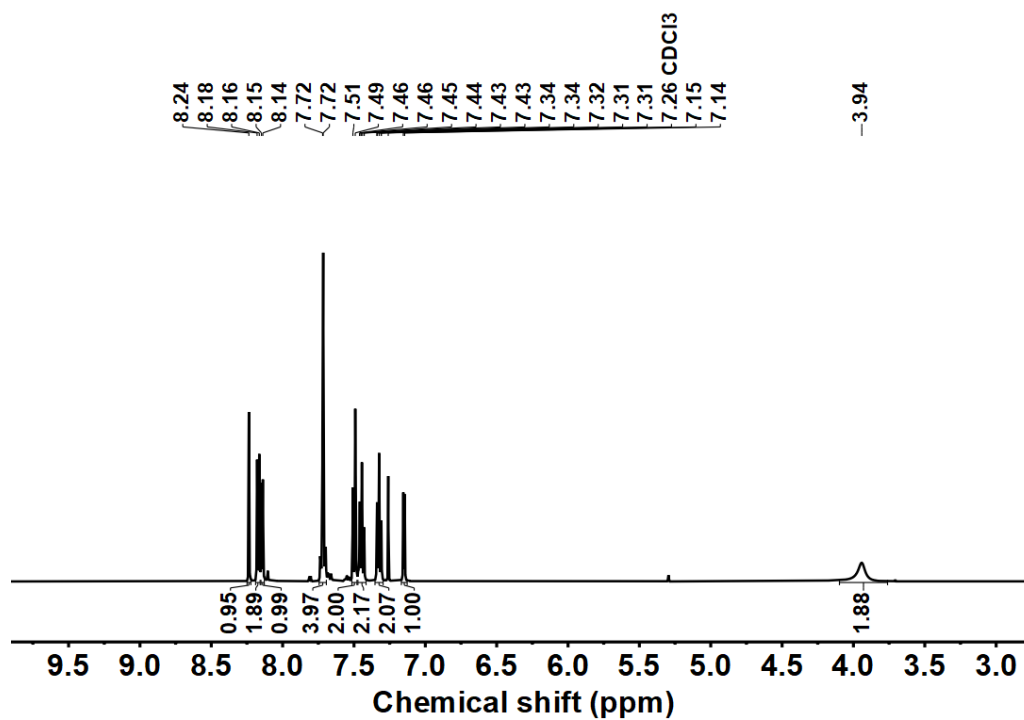


Figure S85. <sup>1</sup>H NMR of 4-(4-(9H-carbazol-9-yl)phenyl)pyridin-3-amine, 500 MHz, CDCl<sub>3</sub>.

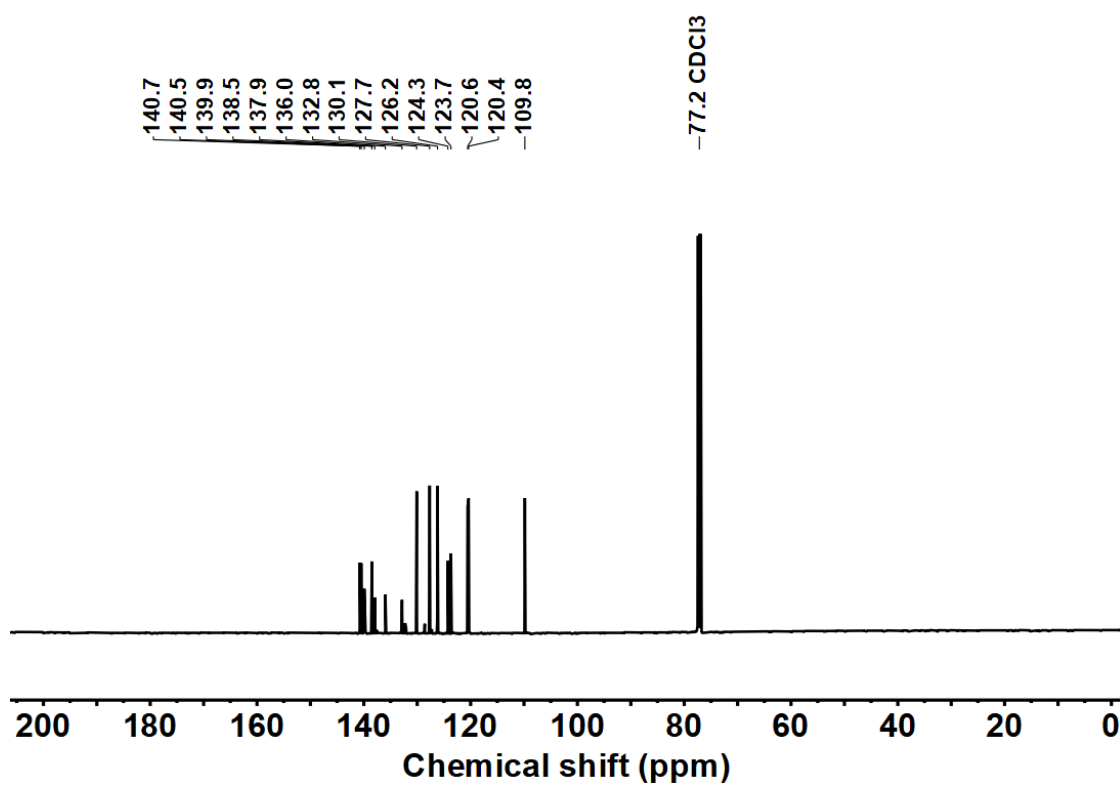


Figure S86. <sup>13</sup>C NMR of 4-(4-(9H-carbazol-9-yl)phenyl)pyridin-3-amine, 126 MHz, CDCl<sub>3</sub>.

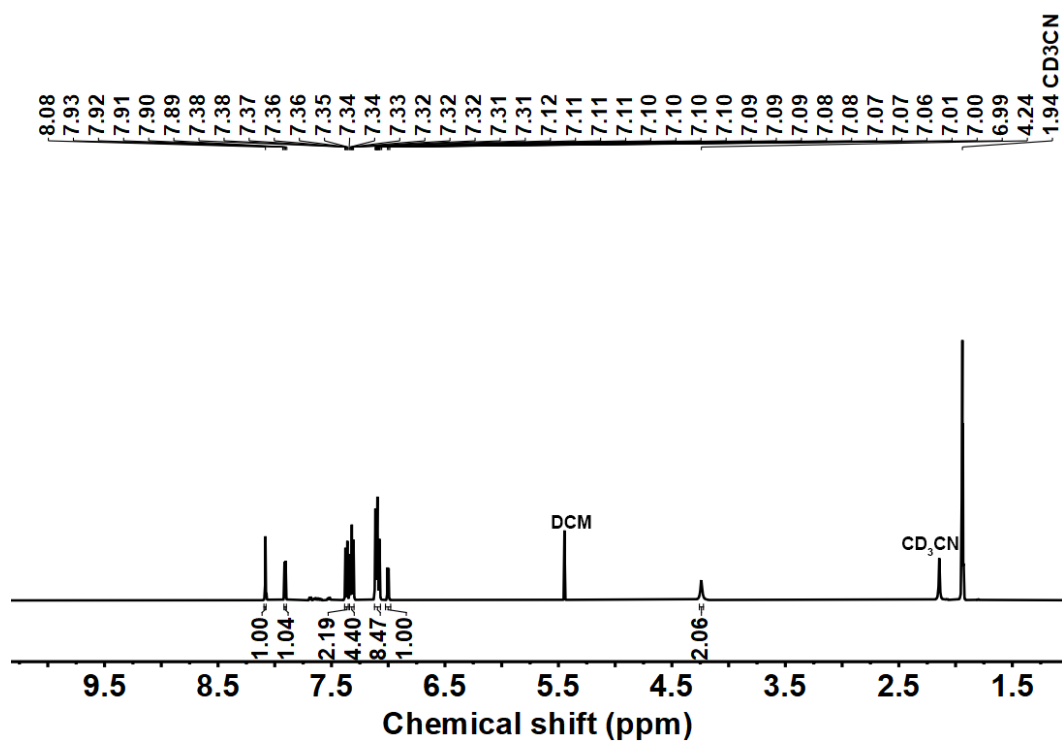


Figure S87. <sup>1</sup>H NMR of 4-(4-(diphenylamino)phenyl)pyridin-3-amine, 500 MHz, CD<sub>3</sub>CN.

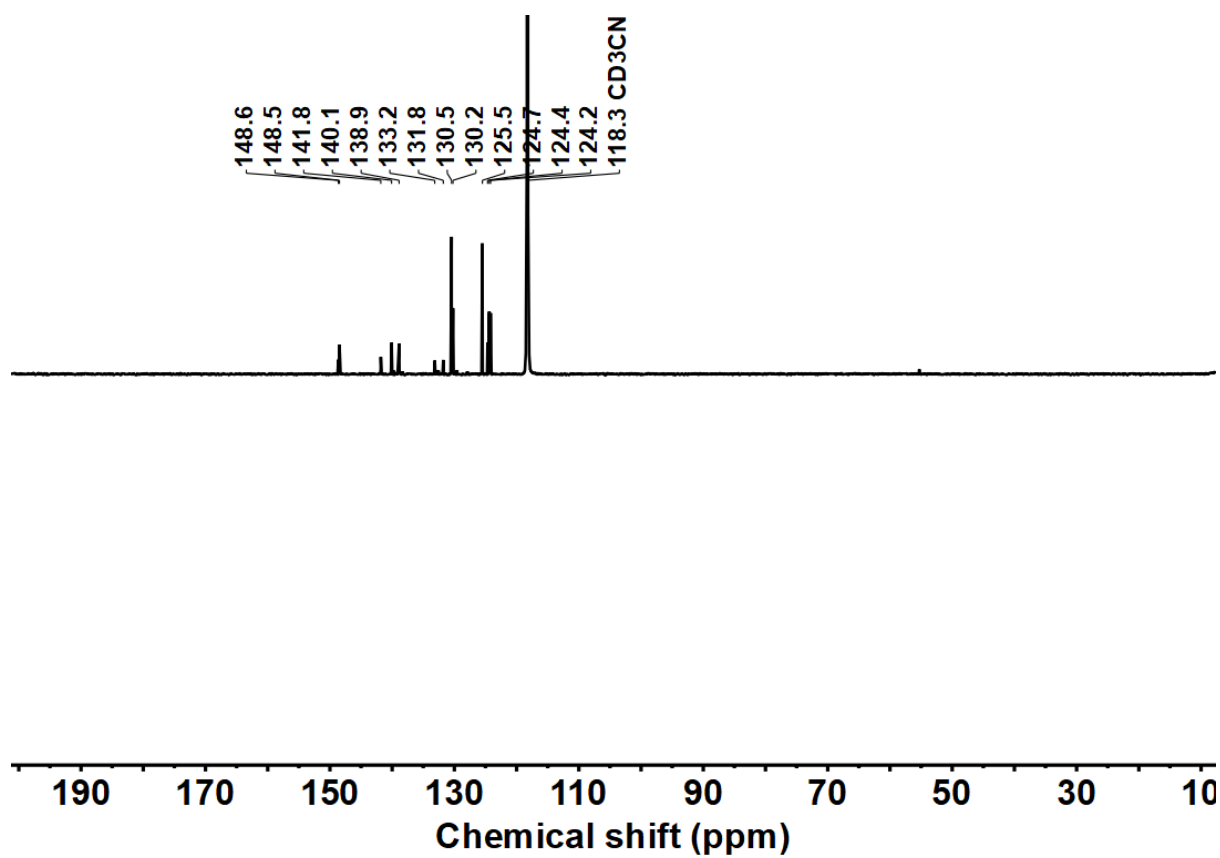


Figure S88. <sup>13</sup>C NMR of 4-(4-(diphenylamino)phenyl)pyridin-3-amine, 126 MHz, CD<sub>3</sub>CN

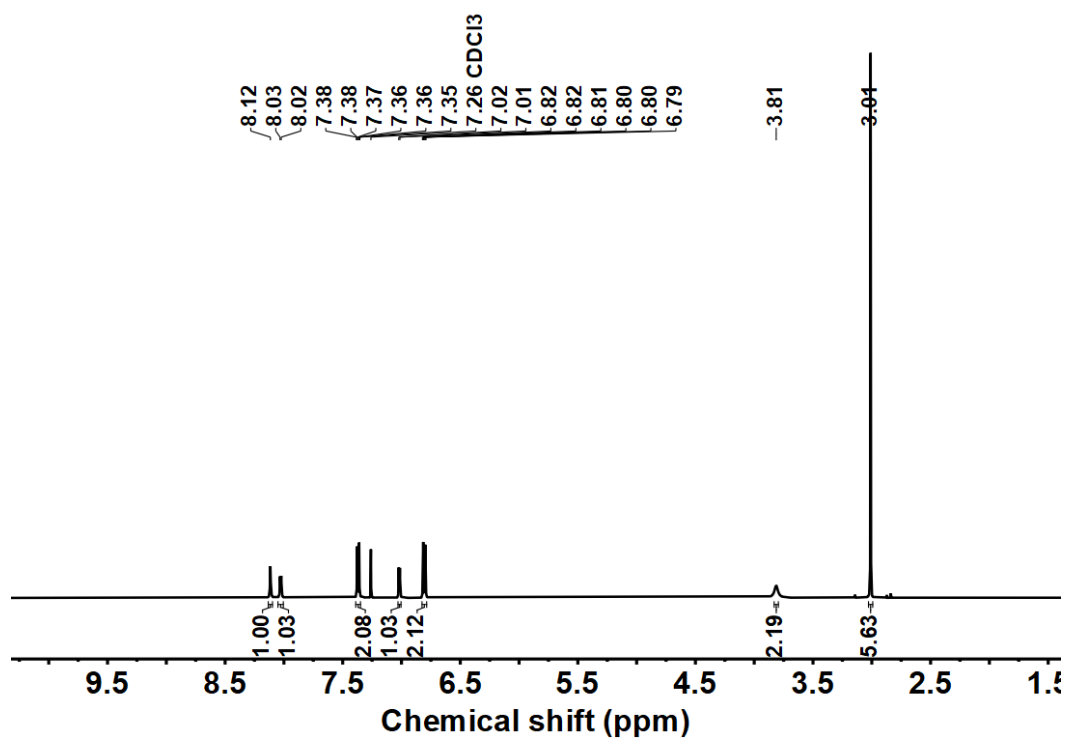


Figure S89. <sup>1</sup>H NMR of 4-(4-(dimethylamino)phenyl)pyridin-3-amine, 500 MHz, CDCl<sub>3</sub>.

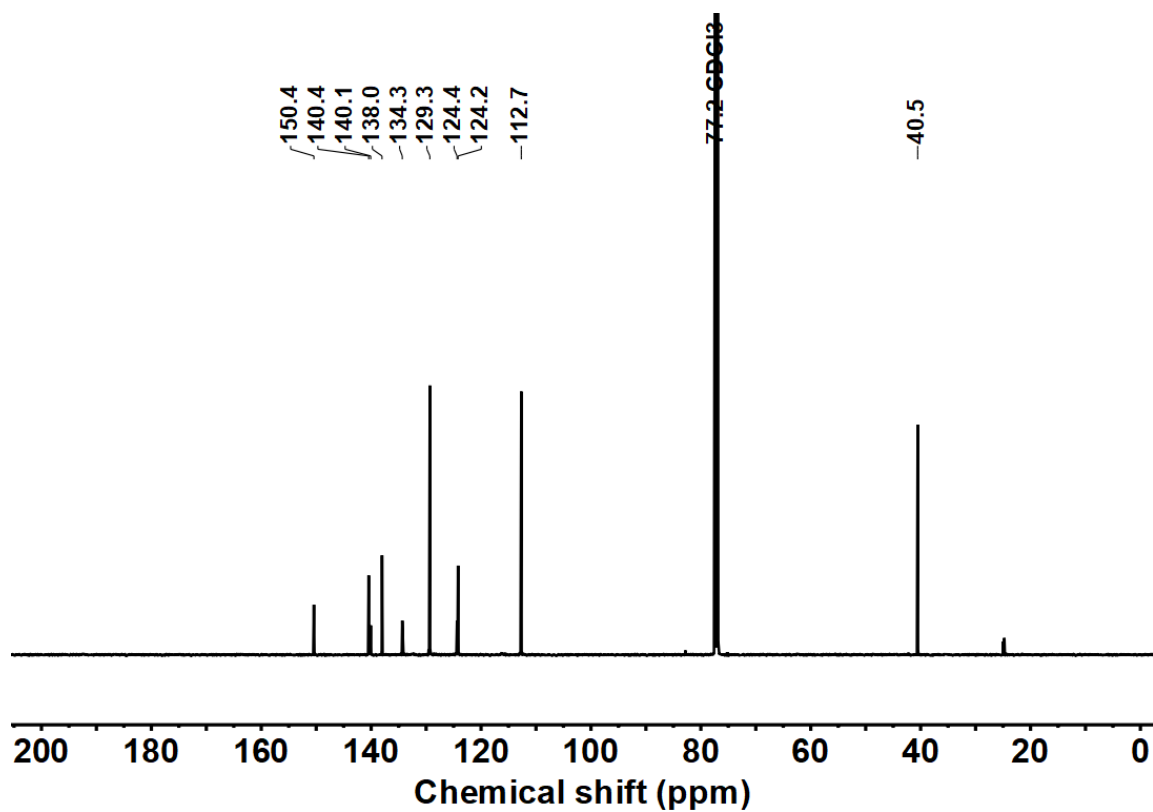


Figure S90. <sup>13</sup>C NMR of 4-(4-(dimethylamino)phenyl)pyridin-3-amine, 126 MHz, CDCl<sub>3</sub>.

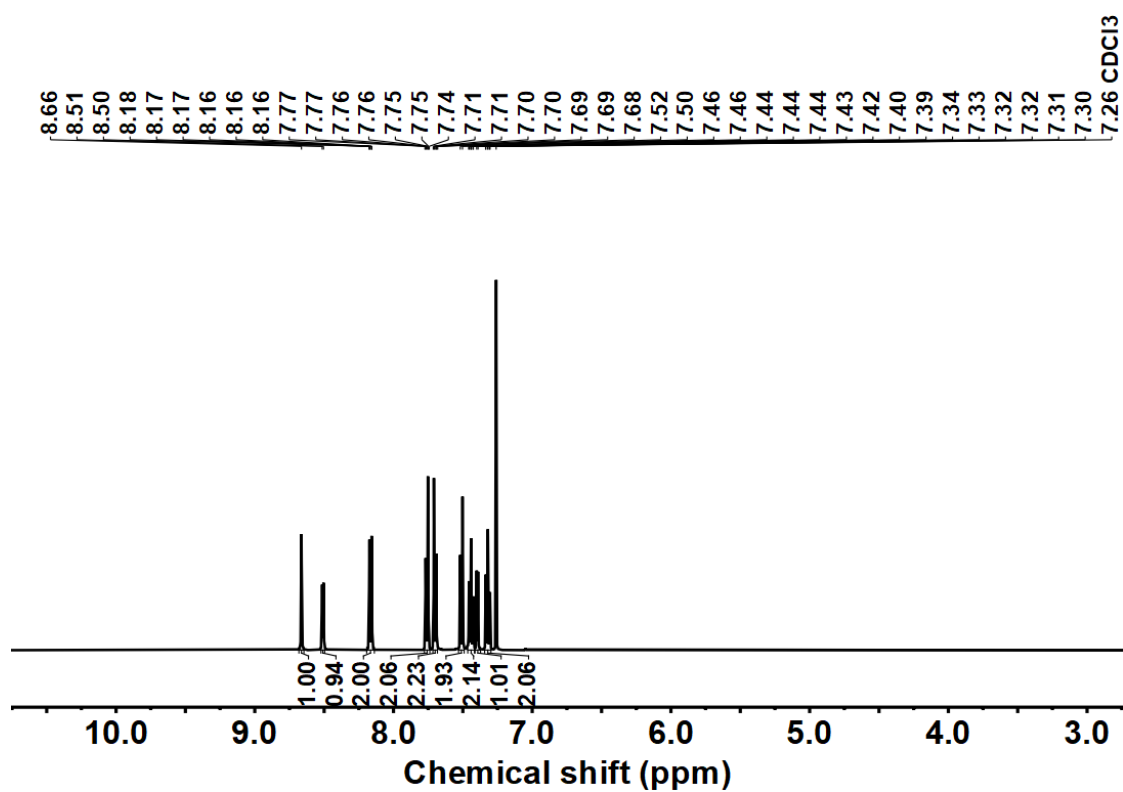


Figure S91. <sup>1</sup>H NMR of 9-(4-(3-azidopyridin-4-yl)phenyl)-9H-carbazole, 500 MHz, CDCl<sub>3</sub>.

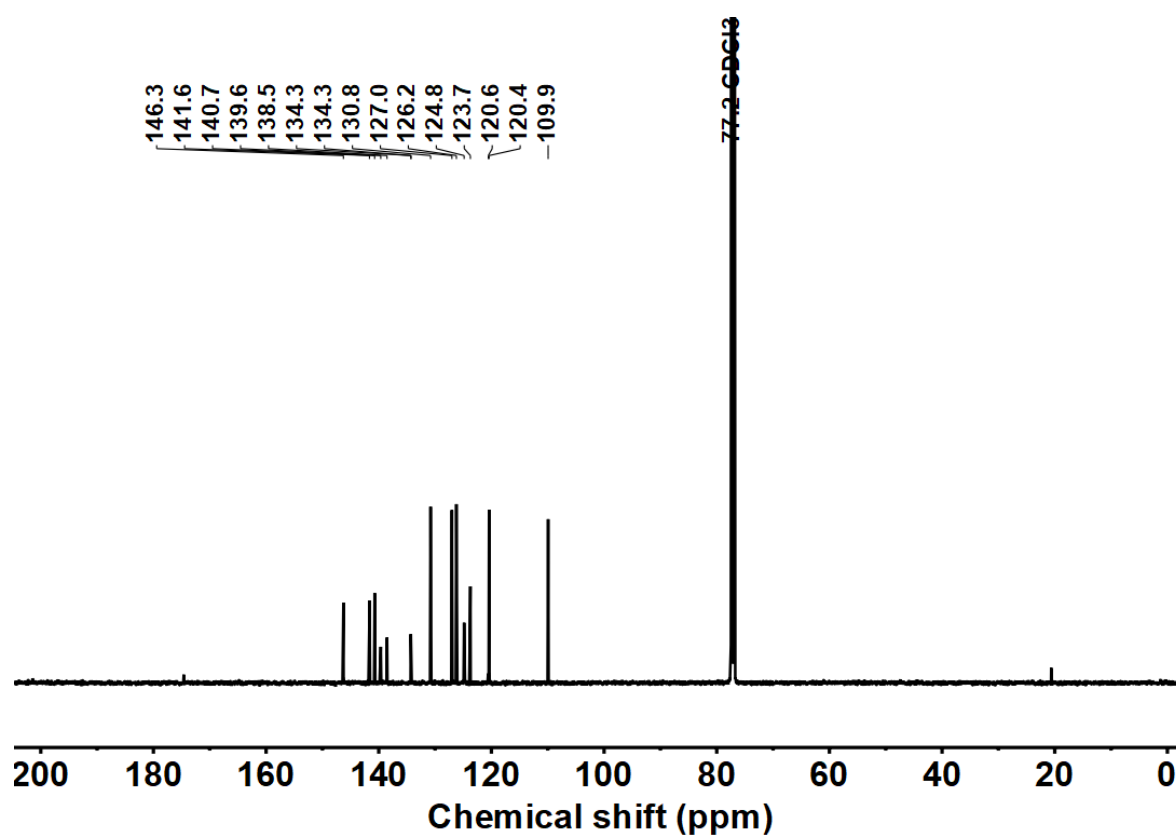


Figure S92. <sup>13</sup>C NMR of 9-(4-(3-azidopyridin-4-yl)phenyl)-9H-carbazole, 126 MHz, CDCl<sub>3</sub>.

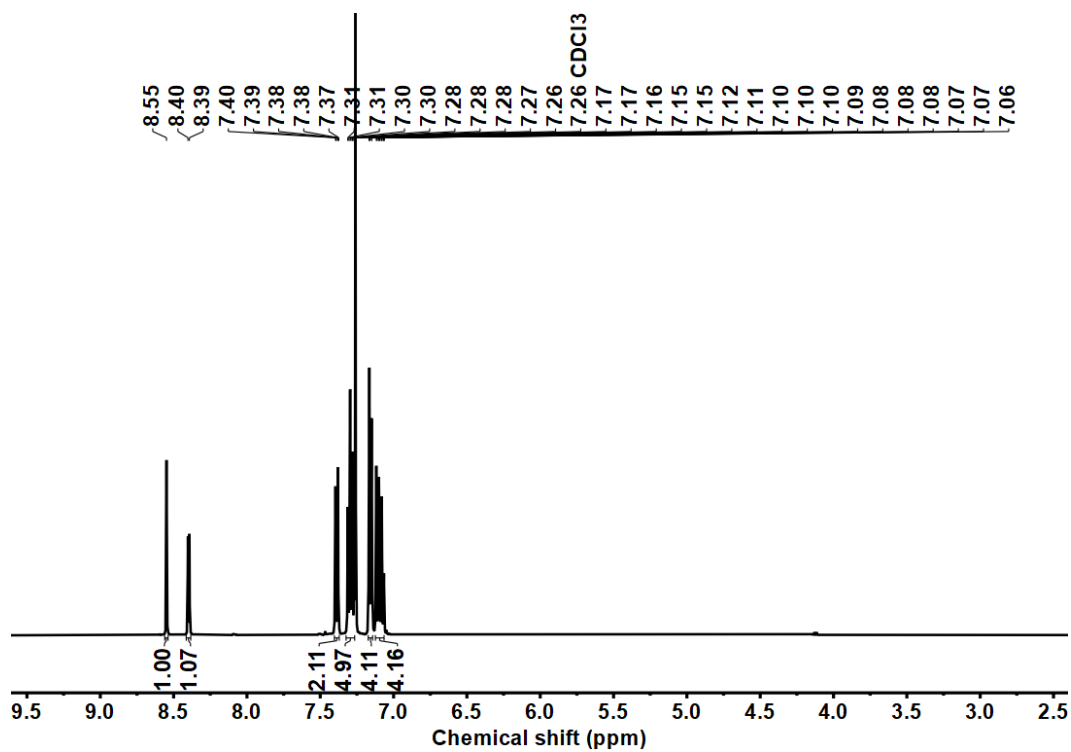


Figure S93.  $^1\text{H}$  NMR of 4-(3-azidopyridin-4-yl)-N,N-diphenylaniline, 500 MHz,  $\text{CDCl}_3$ .

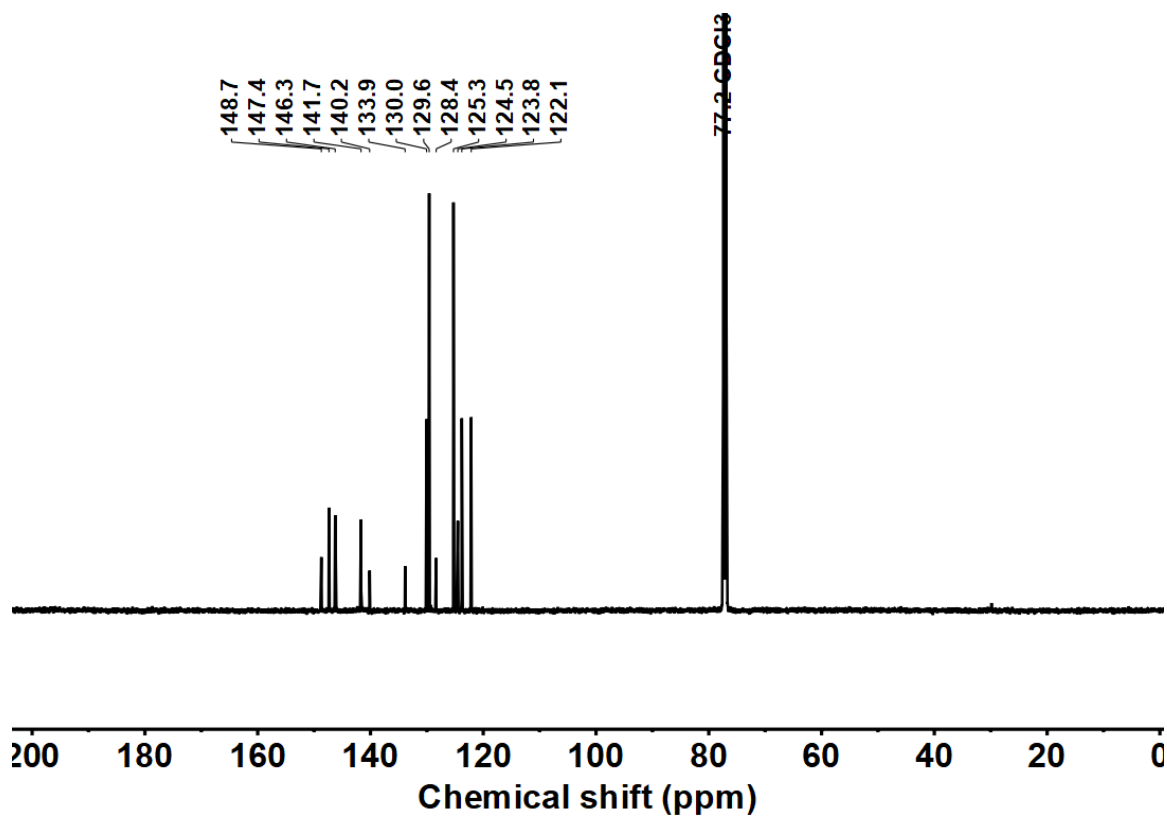


Figure S94.  $^{13}\text{C}$  NMR of 4-(3-azidopyridin-4-yl)-N,N-diphenylaniline, 126 MHz,  $\text{CDCl}_3$ .

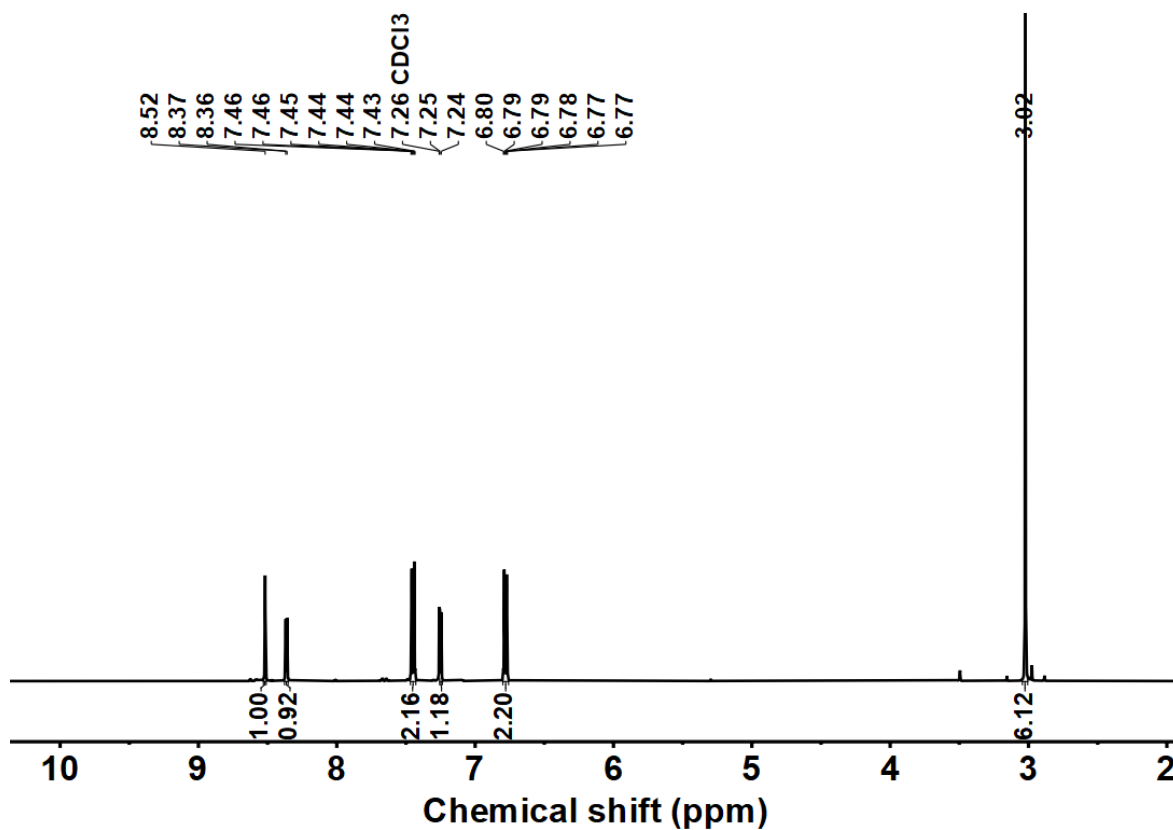


Figure S95.  $^1\text{H}$  NMR of 4-(3-azidopyridin-4-yl)-N,N-dimethylaniline, 500 MHz,  $\text{CDCl}_3$ .

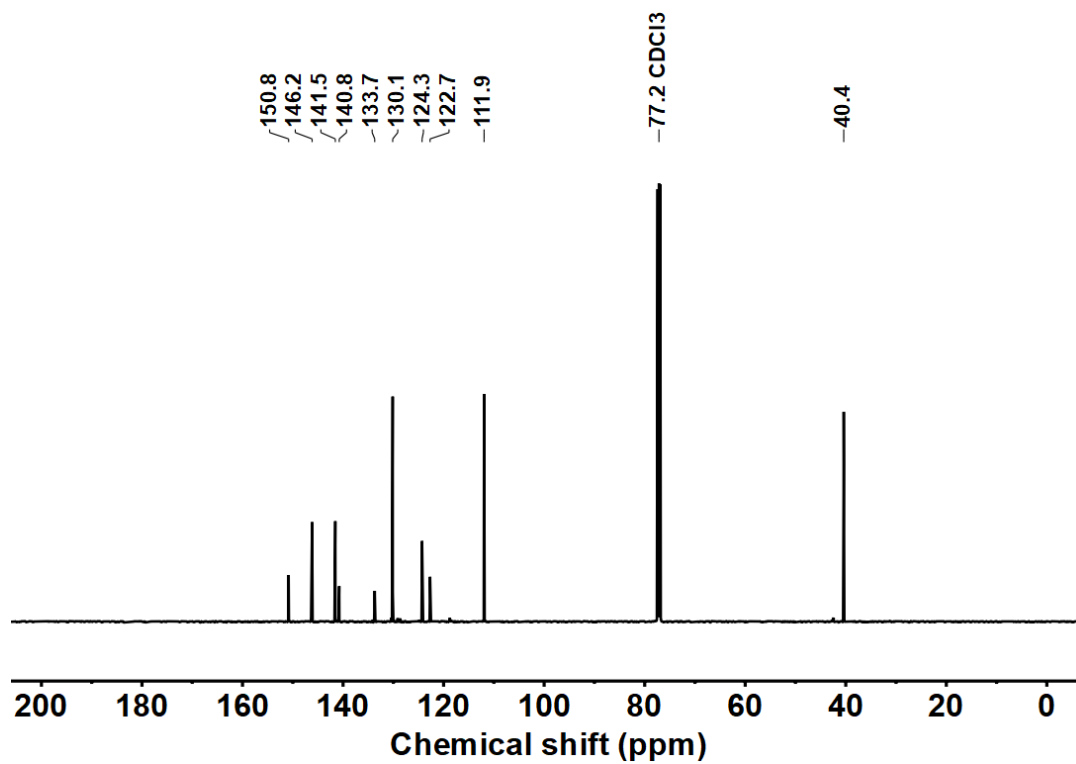
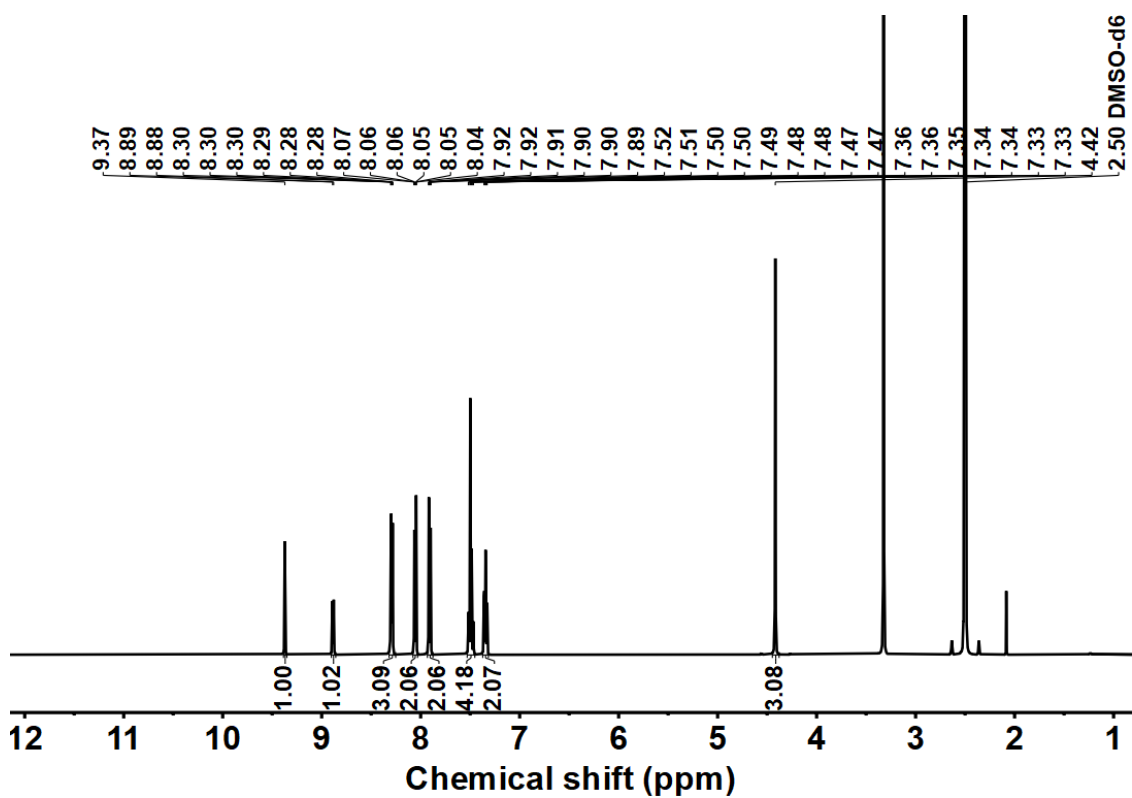
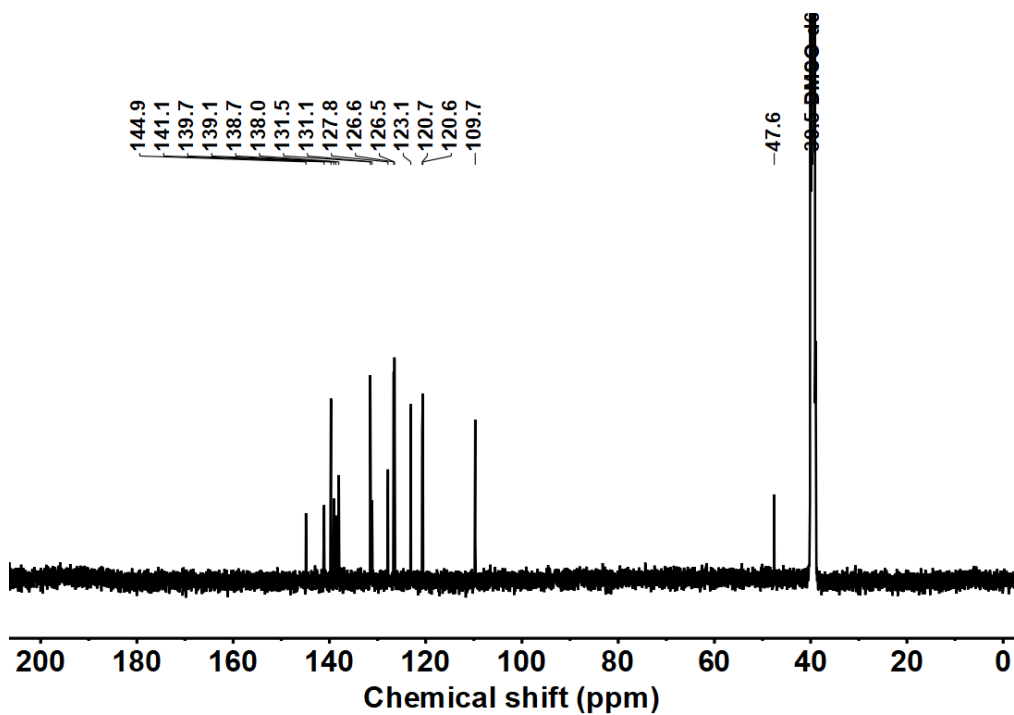


Figure S96.  $^{13}\text{C}$  NMR of 4-(3-azidopyridin-4-yl)-N,N-dimethylaniline, 126 MHz,  $\text{CDCl}_3$ .



**Figure S97.**  $^1\text{H}$  NMR of 4-(4-(9H-carbazol-9-yl)phenyl)-3-azido-1-methylpyridin-1-ium chloride (**AZ-1**), 500 MHz,  $\text{DMSO-}d_6$ .



**Figure S98.**  $^{13}\text{C}$  NMR of 4-(4-(9H-carbazol-9-yl)phenyl)-3-azido-1-methylpyridin-1-ium chloride (**AZ-1**), 126 MHz,  $\text{DMSO-}d_6$ .

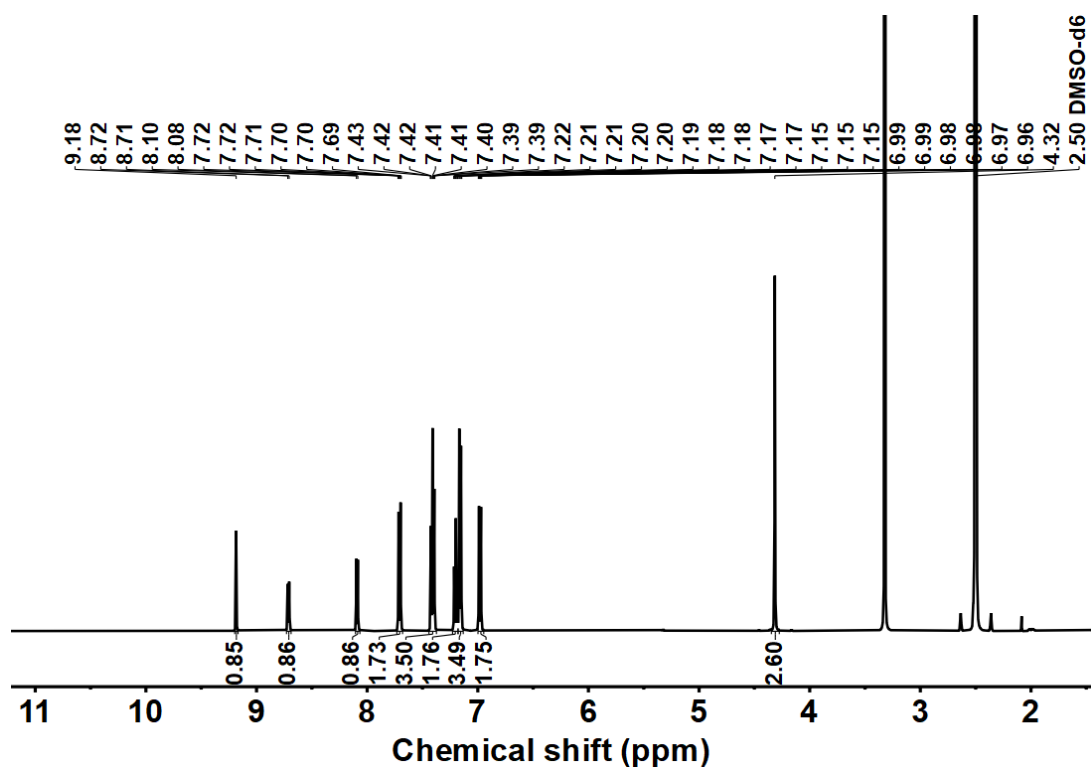


**Figure S99.**  $^1\text{H}$  NMR of 3-azido-4-(4-(diphenylamino)phenyl)-1-methylpyridin-1-ium chloride (**AZ-2**), 500 MHz,  $\text{DMSO-}d_6$ .

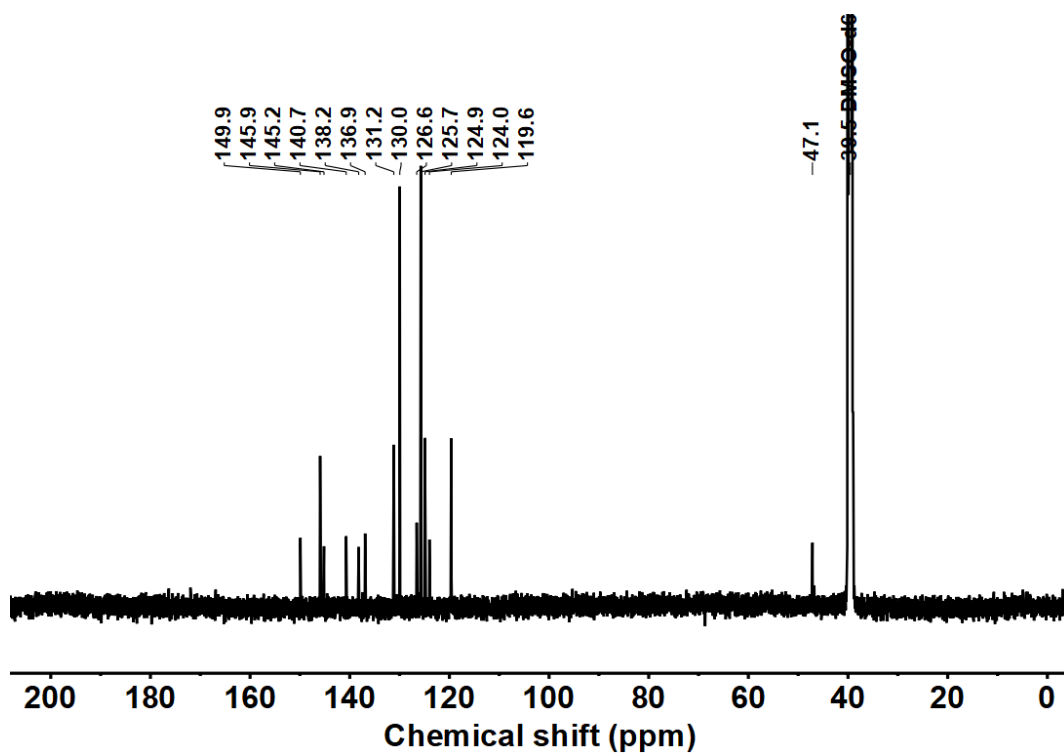


**Figure S100.**  $^{13}\text{C}$  NMR of 3-azido-4-(4-(diphenylamino)phenyl)-1-methylpyridin-1-ium chloride (**AZ-2**), 126 MHz,  $\text{DMSO-}d_6$ .

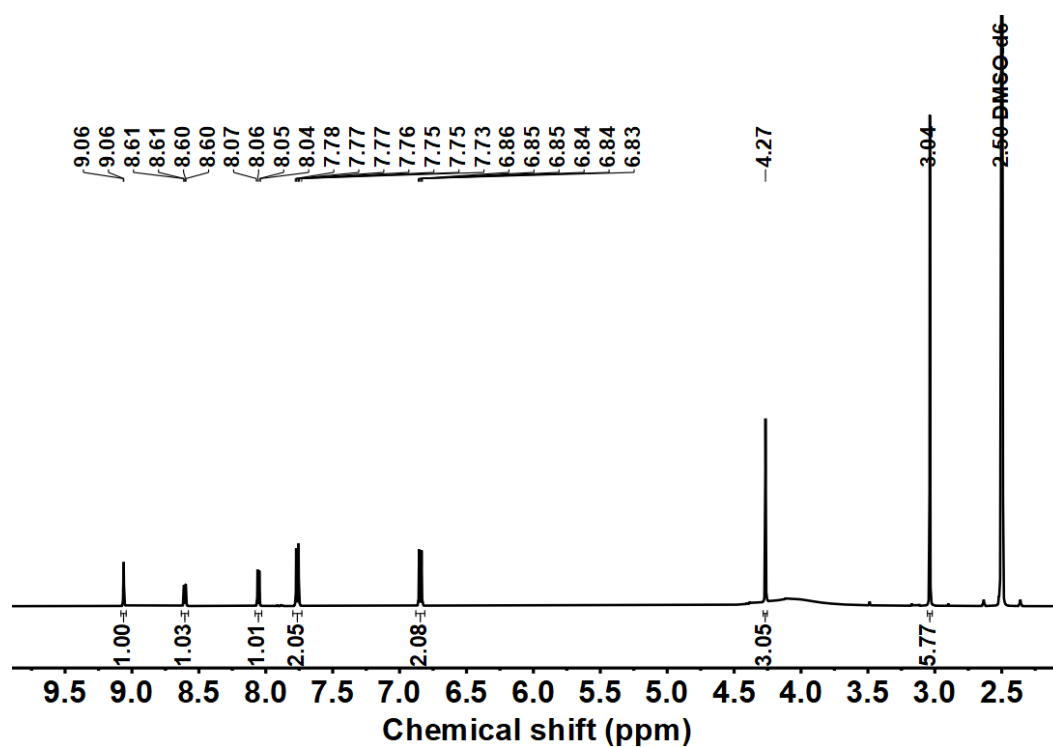


**Figure S101.**  $^1\text{H}$  NMR of 3-azido-4-(4-(dimethylamino)phenyl)-1-methylpyridin-1-ium chloride (**AZ-3**), 500 MHz,  $\text{DMSO-}d_6$ .

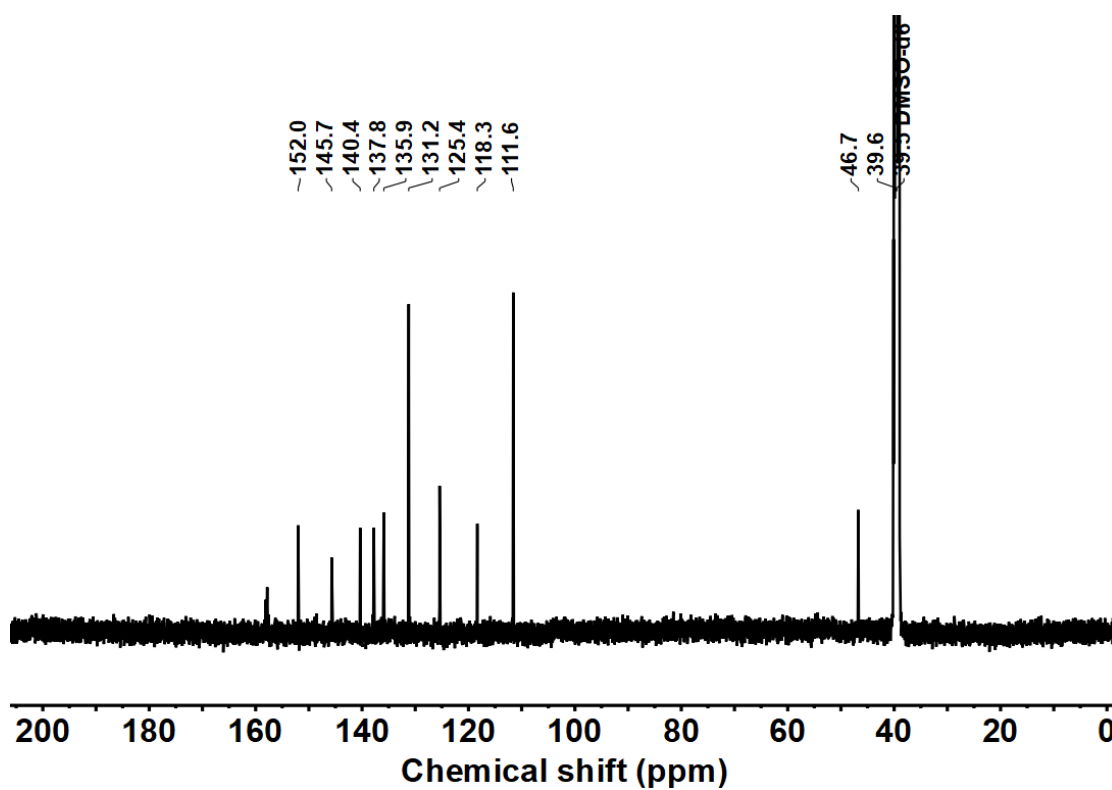


**Figure S102.**  $^{13}\text{C}$  NMR of 3-azido-4-(4-(dimethylamino)phenyl)-1-methylpyridin-1-ium chloride (**AZ-3**), 126 MHz,  $\text{DMSO-}d_6$

## References

- [1] Dolomanov, O.V., Bourhis, L.J., Gildea, R.J, Howard, J.A.K. & Puschmann, H. (2009), *J. Appl. Cryst.* 42, 339-341.
- [2] Sheldrick, G.M. (2015). *Acta Cryst.* A71, 3-8.
- [3] Sheldrick, G.M. (2015). *Acta Cryst.* C71, 3-8.
- [4] G. W. T. M. J. Frisch, H. B. Schlegel, G. E. Scuseria, M. A. Robb, J. R. Cheeseman, G. Scalmani, V. Barone, B. Mennucci, G. A. Petersson, H. Nakatsuji, M. Caricato, X. Li, H. P. Hratchian, A. F. Izmaylov, J. Bloino, G. Zheng, J. L. Sonnenberg, M. Hada, M. Ehara, K. Toyota, R. Fukuda, J. Hasegawa, M. Ishida, T. Nakajima, Y. Honda, O. Kitao, H. Nakai, T. Vreven, J. A. Montgomery Jr., J. E. Peralta, F. Ogliaro, M. Bearpark, J. J. Heyd, E. Brothers, K. N. Kudin, V. N. Staroverov, R. Kobayashi, J. Normand, K. Raghavachari, A. Rendell, J. C. Burant, S. S. Iyengar, J. Tomasi, M. Cossi, N. Rega, J. M. Millam, M. Klene, J. E. Knox, J. B. Cross, V. Bakken, C. Adamo, J. Jaramillo, R. Gomperts, R. E. Stratmann, O. Yazyev, A. J. Austin, R. Cammi, C. Pomelli, J. W. Ochterski, R. L. Martin, K. Morokuma, V. G. Zakrzewski, G. A. Voth, P. Salvador, J. J. Dannenberg, S. Dapprich, A. D. Daniels, Ö. Farkas, J. B. Foresman, J. V. Ortiz, J. Cioslowski, D. J. Fox, , Gaussian Inc., Gaussian 16 rev.C.01 Wallingford, CT, 2019.
- [5] C. Adamo, V. Barone, *J. Chem. Phys.* 1999, 110, 6158-6170.
- [6] T. H. Dunning Jr, *J. Chem. Phys.* 1989, 90, 1007-1023.
- [7] Lee, O. S.; Zysman-Colman, E. *Silico*, 2023.
- [8] O'Boyle, N. M.; Tenderholt, A. L.; Langner, K. M. *Cclib, J. Comput. Chem.* 2008, 29 (5), 839–845.
- [9] O'Boyle, N. M.; Banck, M.; James, C. A.; Morley, C.; Vandermeersch, T.; Hutchison, G. R, *J. Cheminformatics* 2011, 3 (1), 33.
- [10] O'Boyle, N. M.; Morley, C.; Hutchison, G. R, *Chem. Cent. J.* 2008, 2 (1), 5.
- [11] Humphrey, W.; Dalke, A.; Schulten, K, *J. Mol. Graph.* 1996, 14 (1), 33–38.

- [12] Stone, J. An Efficient Library for Parallel Ray Tracing and Animation, Computer Science Department, University of Missouri-Rolla, 1998.
- [13] Tian Lu, Feiwu Chen, J. Comput. Chem. 2012, 33, 580-592 (2012).
- [14] X. Qiu, J. Brückel, C. Zippel, M. Nieger, F. Biedermann, S. Bräse, *RSC Adv.* **2023**, 13, 2483-2486.
- [15] <https://www.thorlabs.com/thorproduct.cfm?partnumber=M405L4>.
- [16] C. Petermayer, S. Thumser, F. Kink, P. Mayer, and H. Dube, *J. Am. Chem. Soc.* **2017**, 139, 42, 15060–15067.
- [17] Wiedbrauk, S.; Maerz, B.; Samoylova, E.; Reiner, A.; Trommer, F.; Mayer, P.; Zinth, W.; Dube, H. *J. Am. Chem. Soc.* **2016**, 138, 12219– 12227.